NON-CANONICAL ROLES OF BCL-X_L IN REGULATING MITOCHONDRIAL FUNCTION AND MORPHOLOGY IN PANCREATIC β-CELLS

by

Rocky Qiushi Shi

B.Sc., The University of British Columbia, 2013

A THESIS SUBMITTED IN PARTIAL FULFILLMENT OF

THE REQUIREMENTS FOR THE DEGREE OF

MASTER OF SCIENCE

in

THE FACULTY OF GRADUATE AND POSTDOCTORAL STUDIES

(Experimental Medicine)

THE UNIVERSITY OF BRITISH COLUMBIA

(Vancouver)

April 2018

Abstract

Glucose-stimulated insulin secretion from pancreatic β-cells depends on mitochondrial oxidative metabolism. Mitochondrial dysfunction is believed to be a significant factor in the development of type 2 diabetes (T2D). Mitochondria exist as dynamic networks and the control of mitochondrial biomass and fusion/fission dynamics is essential for cellular health and function. The anti-apoptotic protein Bcl-x_L has recently been demonstrated to dampen β-cell mitochondrial metabolism and studies in other cell types suggest Bcl-x_L regulates mitochondrial biomass and dynamics. We hypothesize that Bcl-x_L is important for β-cell adaptation to metabolic stress by regulating mitochondrial dynamics and mass. To quantitatively study mitochondrial structural changes, we developed an image analysis pipeline for 2D/3D confocal imaging of mitochondria in FIJI. We applied the pipeline to primary islet cells and found that glucose stimulation is correlated with a more fragmented mitochondrial morphology. *In vitro* Bcl-x_L overexpression causes β-cell mitochondria to lose their tubular network structure and aggregate. These changes to network morphology and kinetics are associated with decreased total mitochondrial volume and a marked impairment of β-cell O_2 consumption. β-cell specific Bcl-x_L knockout islet cells demonstrated increased basal activity and decreased average mitochondrion size, suggesting that they behave more similarly to β-cells undergoing glucose stimulation. Challenging β-cells with prolonged high glucose culture increased the size and overall connectivity of their mitochondrial network. In Bcl-x_L knockout β-cells this increase in total mitochondrial mass and networking was significantly amplified, but was associated with reduced morphological and functional glucose-responsiveness of the individual mitochondrion. In conclusion, our *in vitro* data demonstrate that Bcl-x_L affects mitochondrial networking, function, and adaptation to stress in pancreatic β-cells.

Lay Summary

Diabetes is a major health concern affecting over 415 million people around the world. In diabetes, high levels of blood sugar (glucose) causes severe complication. Glucose levels are normally lowered by the hormone insulin, and diabetes arises, in large part, because insulin-producing β-cells fail and die. This is known to involve damage to mitochondria, the cellular "power plants" where essential metabolism takes place. Mitochondria are fascinating tubular structures that move and change shape by dividing and fusing within a network. Recent research suggests these dynamics are essential for normal mitochondrial function and quality-control. Bcl-x_L, an important protein for cell survival, has been recently shown to affect β-cell metabolism and insulin secretion. Using advanced cell microscopy and gene manipulation techniques, we found that Bcl-x_L can affect mitochondrial structure and function. Clarifying these complex mechanisms of mitochondrial function and failure in β-cells may help identify new means for diabetes prevention and treatment.

Preface

The work presented in this thesis was mostly completed and written by the author, Rocky Qiushi Shi. The sections on establishing 3D analysis pipeline and measurement of mitochondrial volume following Bcl-x_L overexpression were completed with the help and collaboration of Ahsen Chaudhry. The Seahorse oxygen consumption assay was completed with the help of Dr. Michal Aharoni-Simon.

All animal work was carried under approval by the University of British Columbia Animal Care Committee. The following training and certifications were completed:

- Canadian Council on Animal Care (CCAC) / National Institutional Animal User Training (NIAUT) Program (Certificate #: 7555-15)
- Introduction to Working with Rodents in Research (IWRR) (Certificate: IWRR-M-P-233-15)
- Restraint and Subcutaneous/Intraperitoneal (RSCIP) Injections Workshop (Certificate: RSCIP-M-P-147-15)
- Laboratory Rodent Anesthesia (Certificate: RA-136-15)

Table of Contents

List of Tables

List of Figures

List of Abbreviations

ADP	Adenosine diphosphate
APAF1	Apoptotic protease activating factor 1
AR	Aspect ratio
ATP	Adenosine triphosphate
BAD	Bcl-2-associated death promoter
BAK	BCL2 Antagonist/Killer 1
BAX	Bcl-2-associated X protein
Bcl	B cell lymphoma
Bcl-x_L	B-cell lymphoma-extra large
BclxWT	Bcl-x WT
BclxβKO	β-cell specific Bcl-x knockout
BH	Bcl-2 homology
BID	BH3 interacting-domain death agonist
BIM	Bcl-2 interacting mediator of cell death
BNIP3	BCL2/adenovirus E1B 19 kDa protein-interacting protein 3
bp	Basepair
C6	Compound 6
Ca^{2+}	Calcium ion
cAMP	Cyclic adenosine monophosphate
CD	Cluster of differentiation
cDNA	Complementary DNA

Cre	Cre recombinase
DNA	Deoxyribonucleic acid
DRP1	Dynamin-related protein 1
Dyn2	Dynamin 2
ER	Endoplasmic reticulum
ETC	Electron transport chain
FCCP	Carbonyl cyanide-4-(trifluoromethoxy)phenylhydrazone
FF	Form factor
FIS1	Mitochondrial fission 1 protein
FUNDC1	FUN14 Domain Containing 1
GIP	Glucose-dependent insulinotropic polypeptide
GLP-1	Glucagon-like peptide 1
Glut2	Glucose transporter 2
GTP	Guanosine triphosphate
GWAS	Genome-wide association studies
HG	High (25mM) glucose
HLA	Human leukocyte antigen
INS1	Insulin 1
INS2	Insulin 2
LDH	Lactate dehydrogenase
MafA	MAF BZIP Transcription Factor A
MCF	Metabolic coupling factor

MFF	Mitochondrial fission factor
MFN1/2	Mitofusin 1 and 2
MIN6	Mouse Insulinoma 6
MODY	Mature onset diabetes of the young
MOMP	Mitochochondria outer membrane permeabilization
MTG	MitoTracker Green FM
NADH	Nicotinamide adenine dinucleotide
NADPH	Nicotinamide adenine dinucleotide phosphate
NDM	Neonatal diabetes mellitus
NG	Normal (11mM) glucose
NRF1/2	Nuclear respiratory factor 1 and 2
OGTT	Oral glucose tolerance test
OPA1	Optic atrophy protein 1
OXPHOS	Oxidative phosphorylation
PAGFP	Photo-activatable green fluorescent protein
PCR	Polymerase chain reaction
Pdx1	Pancreatic and duodenal homeobox 1
PGC-1α	Peroxisome proliferator-activated receptor gamma coactivator 1-alpha
PINK1	PTEN-induced putative kinase 1
PP	Pancreatic polypeptide
PUMA	p53 upregulated modulator of apoptosis
RNA	Ribonucleic acid

ROS	Reactive oxygen species
RT-qPCR	Real-time quantitative polymerase chain reaction
SMAC	Second mitochondria-derived activator of caspases
SPADE	Spanning-tree progression analysis of density-normalized events
T1D	Type 1 diabetes
T2D	Type 2 diabetes
TCA	Tricarboxylic acid
TFAM	Transcription factor A, mitochondrial
TM	Transmembrane
TMRE	Tetramethylrhodamine, Ethyl Ester
tRNA	Transfer ribonucleic acid
UPR	Unfolded protein response
XIAP	X-linked inhibitor of apoptosis

Acknowledgements

I offer my enduring gratitude to my supervisor Dr. Dan S. Luciani for his mentorship that broadened my vision of science and deepened my understanding of physiology. I cannot thank him enough for the opportunity to work in his lab and learn confocal microscopy. I would also like to thank my committee members, Dr. James D. Johnson and Dr. Brad G. Hoffman, for their supervision and advice. I am grateful to Mitsuhiro Komba for his help with islet isolations and Dr. Jingsong Wang for training me on microscopy and deconvolution.

It has been a pleasure working with the other members of my lab. Particularly, I would like to thank Mei Tang for her help genotyping the mice; Michal Aharoni-Simon for teaching various laboratory and mouse handling techniques when I just started off; Ahsen Chaudhry for our fruitful collaboration; Peter and Daniel for our numerous discussions of science and philosophy; Margaret, Sophie, and Emma for their help as co-op students.

Special thanks to Canadian Institute of Health for their funding and offering me the Canada Graduate Scholarship Master's Award. I would like to express my thanks to University of British Columbia (UBC) and British Columbia Children’s Hospital Research Institute (BCCHRI) for their institutional support.

Lastly, I would like to thank my parents and family for my upbringing and unconditional support. Without them, I would not be the same person that I am today.

Dedication

I would like to dedicate this thesis to my parents.

Chapter 1: Introduction

1.1 Diabetes

1.1.1 Overview of diabetes

Diabetes Mellitus is a major health risk affecting 415 million people around the world and over 1/11 adults have the disease (1). These numbers have been projected to continue increasing. By 2040, 642 million people are predicted to have diabetes and its accompanying complications will make it one of most costly diseases (2). Physiologically, diabetes can be described as the loss of the body's ability to lower blood glucose concentration (3-7). Patients with diabetes have elevated glucose in their blood and chronic hyperglycemia is linked to damage and failure of various other biological systems; most notably the urinary system, cardiovascular system and nervous system (3, 7). Symptoms of diabetes include excessive thirst and urination, severe weight loss and blurred vision (3, 6). However, these symptoms worsen over time and can result in renal failure, vision loss, autonomic and peripheral neuropathy, and eventually death if left untreated (3, 8).

While there are rare monogenic forms of diabetes such as neonatal diabetes mellitus (NDM) and mature onset diabetes of the young (MODY), the two most prevalent forms are type 1 diabetes (T1D) and type 2 diabetes (T2D). Type 1 diabetes is an autoimmune disease where insulin-producing pancreatic β-cells are recognized as a threat by the immune system and become the target of destruction by the body's own CD8 killer T cells (5, 9). As a result, the number of functioning β-cells drastically decreases, leading to insufficient insulin production and secretion. Currently, the precise mechanisms underlying T1D have not been characterized but it is widely understood to be multi-factorial, involving both genetic and environmental factors (10). Genetic factors such as polymorphisms in HLA class II locus (important for immune recognition) incur

susceptibility to T1D (5, 11) while environmental factors such as diet, unfavorable gut flora, and viral infection are also linked to pathogenesis of T1D (5, 10).

Type 2 diabetes, on the other hand, is a metabolic disease where pancreatic β-cells fail due to the prolonged stress associated with increased demand for insulin production (4, 12). High levels of carbohydrates and fat in the diet stresses the β-cells to secrete excessive insulin. The elevated insulin levels in the blood (hyperinsulinemia) is a significant contributor to insulin resistance and obesity (13, 14). In turn, the build-up of insulin resistance and obesity increases the demand for insulin output. This vicious cycle makes the body increasingly glucose intolerant until full-scale diabetes results, where the insulin-producing β-cells become dysfunctional from the amplified stress and cannot secret sufficient insulin to meet the demand (4, 12). Consequently, hyperglycemia results. Similar to T1D, T2D is also recognized as a multi-factorial disease involving both genetic and environmental components. In addition to unhealthy diets and lack of physical activities, other environmental factors such as in-utero conditions and microbiota have been suggested to play a role (12). Moreover, Genome-Wide Association Studies (GWAS) have identified over 100 loci associated with increased risk for T2D (15), the majority of which have been associated with β-cell function (12, 16).

Overall, diabetes mellitus is a costly, painful, chronic disease with various etiologies that arise from distinct mechanisms. The various forms of the disease are highly complex, consisting of numerous factors that can influence their pathophysiology. We hope to understand more about the different types of diabetes so that novel fruitful interventions can be developed.

1.1.2 Physiology and regulation of glucose homeostasis

The control of glucose levels in the blood is crucial for physiological and metabolic functions in the body. While fatty acids can be used as a source of energy in most tissues and organs, the brain almost exclusively relies on glucose. The brain is also incapable of storing glucose as glycogen, resulting in the need of a constant glucose supply for the brain (17). Thus, blood glucose concentration is mostly controlled around 5mM, with some variations throughout the day (17-19). When glucose homeostasis is perturbed and blood glucose concentration falls under 3mM, cerebral function is disrupted (18) and prolonged hypoglycemia can cause permanent brain damage and death (17). On the other hand, elevated blood glucose concentration (i.e. diabetes) is associated with increased risks for nephropathy, neuropathy and cardiovascular morbidity (3, 17).

To maintain glucose homeostasis, the body must be able to alter the glucose flux by either increasing glucose uptake or release. The two primary hormones that control these biological functions, glucagon and insulin, are secreted by the islets of Langerhans in the pancreas (17). Glucagon is a peptide hormone secreted by the α-cells of the islets and functions mainly to increase blood glucose (17, 20). The primary target of glucagon is the liver where it can bind glucagon receptors and promote of glycogenolysis and gluconeogenesis. The breakdown of glycogen, in combination with synthesis of glucose, allows glucose to be released back into the bloodstream during times of fasting (17).

The opposing hormone, insulin, is a peptide hormone secreted by the β-cells of the islets. In contrast to glucagon, insulin decreases blood glucose levels (17, 19). Insulin signals the skeletal muscles and adipose tissues to begin uptake of glucose. In the liver, insulin inhibits glycogenolysis

and gluconeogenesis and promotes glycogen synthesis (13, 17, 19). In this manner, insulin is critical for glucose homeostasis by removing glucose from the blood after a meal.

The other cells in pancreatic islets also contain hormones that can fine-tune the secretion of insulin and glucagon. These include somatostatin secreted by the delta cells (21), pancreatic polypeptide secreted by PP cells (22), and ghrelin secreted by the epsilon cells (23). Other organs and systems, such as the intestines and brain, also play a role in regulating glucose homeostasis. The brain can increase its glucose uptake and indirectly regulate hepatic glucose production (24) and incretin hormones, such as glucagon-like peptide 1 (GLP-1) and glucose-dependent insulinotropic polypeptide (GIP) secreted from the gut, can also regulate hepatic glucose production and insulin secretion (25).

Overall, the regulation of glucose homeostasis is a highly organized whole-body effort. The control, however, is heavily weighted on the endocrine pancreas via its hormones. As such, dysfunctions in the endocrine pancreas can have devastating effects on blood glucose concentration, resulting in diabetes.

1.1.3 Current diagnosis and treatments of diabetes

In North America, the current clinical criteria serving as guidelines (3, 7) for the diagnosis of diabetes are as follows: 1) Glycated hemoglobin (A1C) levels are greater than 6.5%, 2) glucose concentration after 8 hours of fasting is greater than 7.0mM, 3) glucose concentration is higher than 11.1mM during a 75g oral glucose tolerance test (OGTT), and 4) random testing of glucose concentration is higher than 11.1mM. The diagnosis of diabetes is confirmed when a patient meets at least two of the criteria listed above.

While there are treatments to diabetes, there is currently no cure. In 1922, when Frederick Banting discovered the first treatment for diabetes, insulin, the disease transformed from being a death sentence to a manageable disease. Since then, the injection of exogenous insulin has been the primary treatment of T1D. However, insulin injections are not perfect as the dosage control is challenging to manage (26). Over the years, there have been numerous technological advancements to the traditional insulin therapy, including protein modification of insulin to improve efficacy and development of insulin pumps that have better control of the dosage (26). Moreover, alternative approaches are being actively explored including using immune-modulation (10, 27), islet transplantation (28), and artificial pancreas devices (29).

For the treatment of T2D, there are various strategies targeting different regulators of glucose homeostasis (12). Metformin is currently the primary treatment due to its tolerability and effectiveness in improving insulin sensitivity (30, 31). Mechanistically, metformin acts mostly on the liver and peripheral tissues, inhibiting complex I of the mitochondrial electron transport chain (ETC), resulting in decreased hepatic glucose production and increased uptake of glucose (32). On the other hand, therapies targeting the β-cells to improve insulin secretion have also been developed (e.g. sulfonylureas and GLP-1 receptor agonists) (12). More recently, a number of sodium-coupled glucose transporter type 2 (SGLT2) inhibitors were FDA approved for treatment of T2D. SGLT2 inhibitors target the nephrons and lower blood glucose by reducing renal reabsorption (33). Pramlintide (34) and Bromocriptine (35) are examples of drugs used to target the intestines and brain, respectively. Lifestyle changes, including controlled diet and exercise, are effective prevention strategies and can reverse pre-diabetes (36, 37). However, when T2D develops to the point where β-cells are failing and dying, exogenous insulin therapy is required (38).

1.2 Pancreatic β-cells

1.2.1 Characteristics and mechanism of insulin secretion

Pancreatic β-cells are located in islets of Langerhans of the pancreas and they are best known for their ability to secrete insulin to control glucose homeostasis. Mature β-cells are characterized by high expression of genes involved with glucose transport and insulin secretion (i.e. *Ins1/2*, *Glut2* and *Gck*) in addition to transcription factors that promote insulin expression (i.e. *Pdx1*, *MafA*) (39, 40).

The secretion of insulin in response to elevated glucose is the key function of β-cells. Preproinsulin is first synthesized into the endoplasmic reticulum (ER) and is processed via cleavage and folding into proinsulin, which is then subsequently packaged into insulin granules by the Golgi apparatus. Lastly, in the insulin granules, the proinsulin peptides are further cleaved, maturing them to insulin in preparation for secretion (41). When glucose enters the β-cell, glycolysis and oxidative phosphorylation in the mitochondria increases the ATP/ADP ratio. This change in ATP concentration closes the ATP-sensitive potassium channel, lowering the electrical potential difference across the plasma membrane (depolarization). Depolarization opens L-type voltage-gated calcium channels and the calcium influx then signals the insulin granule vesicles to fuse with the plasma membrane releasing their content into the bloodstream (4, 41-43). While changes in the ATP/ADP ratio is the “switch” that turns insulin secretion on or off, there are numerous metabolic by-products of glucose and mitochondrial metabolism, such as NADPH, GTP, cyclic AMP (cAMP), Glutamate and, reactive oxygen species (ROS), that are capable of amplifying and carefully “dialing” the amount of insulin secreted. These metabolites act as metabolic coupling factors (MCFs), helping to amplify the signal for insulin secretion (42, 44). Notably, glucose is not the only nutrient capable of inducing insulin secretion. Both metabolism

of fatty acids and amino acid produce ATP and other MCFs that can stimulate insulin secretion (44). As expected, genetic defects in various parts of the secretion pathway can result in diabetes (e.g. MODYs) and the mechanisms of insulin secretion have been drug targets for therapy (12).

1.2.2 Failure and death of β-cells in T2D

Failure and death of β-cells are important parts of the pathophysiology and progression of T2D. The most established insults to the well-being of pancreatic β-cells are being chronically exposed to high levels of circulating glucose (glucotoxicity) and fatty acids (lipotoxicity). Glucotoxicity and lipotoxicity push β-cells toward a state of "metabolic overload", inducing dysfunction and eventually death (4). Using rodent models, islets cultured for extended time in high glucose (30mM) resulted in lowered insulin secretion in response to glucose stimulation (45); while islets cultured in high levels of fatty acid also experience defects in glucose-stimulated insulin secretion (46).

Although the precise mechanisms of β-cell dysfunction and failure in T2D remain to be elucidated, numerous studies suggests it involves several intertwined factors including ER stress and oxidative stress (47-49). ER stress occurs when cell cannot adequately process proteins under conditions of functional demand. To cope with ER stress, cells initiate the unfolded protein response (UPR), which aims to decrease protein production to ease the ER stress and promote survival; but if the damage is unrecoverable, cells will undergo apoptosis (47). Under hyperglycemic conditions, the increased demand for insulin raises the processing of insulin in the β-cell ER, resulting in ER stress. However, in T2D under glucotoxicity and lipotoxicity, β-cells are unable to cope with the chronic ER stress and eventually, the cells undergo apoptosis.

Oxidative stress occurs when uncontrolled ROS production starts to damage cellular structures including DNA, protein and lipids (50, 51), which may eventually lead into apoptosis if the damage is severe. Cells adapt to oxidative stress by upregulating and activating anti-oxidant genes, thereby neutralizing the excessive ROS. However, β-cells have relatively low expression levels of anti-oxidant genes, making them especially susceptible to oxidative damage (52). When exposed to glucotoxicity and lipotoxicity, the β-cells experience higher levels of oxidative stress that are partially due to increased rate of ETC activity and oxidative metabolism that result in increased levels of ROS production in the mitochondria (53).

1.3 Mitochondrial physiology

1.3.1 Mitochondrial functions in the β-cell

Mitochondria have numerous functions within the cell. By far, the most well-known function of the mitochondria is to be the “powerhouse” of the cell and manage cellular energetics. To generate ATP from glucose, mammalian cells can use two metabolic pathways: 1) anaerobic fermentation or 2) aerobic respiration. The products of glycolysis, pyruvate and NADH, can either be used to make lactic acid without the use of oxygen, or transported into the mitochondria and more efficiently used by the tricarboxylic acid (TCA) cycle and electron transport chain (ETC) with the consumption of oxygen to generate additional ATP. The electron transport chain is a series of enzymes that actively use the energy from redox reactions to pump protons from the lumen of the mitochondria into the intermembrane space, creating a proton gradient. ATP synthase, the final complex of the ETC, uses the polarized proton gradient to synthesize ATP from ADP and inorganic phosphate (54-57). Comparing the two pathways, anaerobic fermentation produces 2 ATP molecules per molecule of glucose, while aerobic respiration generates 30-32 ATP molecules per glucose molecule, further demonstrating the importance of mitochondria in bioenergetics in the cell.

The same pathways for ATP production happens in β-cells. However, β-cells are more dependent on the mitochondria than most other cell types. β-Cells are unable to effectively use anaerobic fermentation as a crucial enzyme in this pathway, lactate dehydrogenase (LDH), is highly downregulated (58, 59). As mentioned previously, the ATP/ADP ratio is central for regulating insulin secretion. The lack of anaerobic fermentation directs pyruvate almost exclusively towards the mitochondria (60), allowing for more efficient and consistent ATP production to glucose consumption ratio. This has been proposed to be important for β-cell’s

ability to link glucose sensing to insulin secretion. Indeed, overexpression of LDH reduces mitochondrial metabolism and insulin secretion in response to glucose stimulation (61).

In addition to being the “powerhouse” of the cell, mitochondria are also important players in cellular metabolism. The ETC of the mitochondria serves as the redox hub of the cell, where numerous metabolites are synthesized and processed (57). Not counting the various key members of the TCA cycle, mitochondria are, for instance, the site of amino acid synthesis (e.g. aspartate and glutamate) and the site of fatty acid breakdown as well as production (62). These metabolic processes produce metabolic coupling factors (MCFs) that act as amplifying signals to further regulate insulin secretion in pancreatic β-cells (43, 44). Taken together, β-cells are highly dependent on mitochondria not only for its importance in energy balance, but also for its primary function.

Importantly, the mitochondria are major contributors of reactive oxygen species (ROS) in the cell. Complexes of the ETC produce ROS as a by-product of their usual function and this physiological level of ROS production is important for cellular signaling and mitochondrial functions (63, 64). These physiological functions ROS extend to being MCFs in β-cells (44) and have been demonstrated to be important for insulin secretion (65, 66). However, when ROS generation becomes dysfunctional, elevated pathological levels of ROS become damaging for the cell, resulting in oxidative stress (64).

The mitochondria are also important for calcium homeostasis in the cell and intracellular Ca^{2+} storage. Together with the endoplasmic reticulum (ER), mitochondria actively regulate the cytoplasmic levels of calcium. Simultaneously, mitochondrial calcium levels also affect mitochondrial function, including efficacy of ATP synthesis and ROS production (64, 67). In β-cells, mitochondrial calcium homeostasis is especially important in the pathway of insulin

secretion. Following glucose stimulation, the increase in cytosolic calcium concentration promotes the uptake of calcium into the β-cell mitochondria. In turn, this has been suggested to improve the efficiency of ATP synthesis and create a feed-forward mechanism for insulin secretion (68). Damaging alterations to mitochondrial calcium levels have been associated with pathophysiology of aging, cardiovascular diseases, and, if in β-cells, diabetes (69).

Mitochondria are also critical for apoptosis, a form of programmed cell death. Permeabilization of the mitochondrial outer membrane and subsequent release of cytochrome C, a component of the ETC, into the cytosol is the regulatory key and the rate-limiting step in the apoptosis pathway (70, 71). The specific process of apoptosis and the role mitochondria play in β-cells will be further described in Section 1.4.1.

1.3.2 Mitochondrial dynamics and networking

Mitochondria are not static, anchored organelles in the cell. Rather they exist as a dynamic network and are constantly moving. The cell provides molecular motors and the cytoskeleton frameworks to help move the mitochondria (72-74). In the mitochondrial outer membrane a protein complex containing the GTPase Miro and the adaptor protein Milton recruits and binds kinesin and dynein motor systems on microtubules, allowing the mitochondria to move along the microtubules. Kinesin drives the mitochondria towards the plus (+) end of microtubules while dynein pushes the mitochondria towards the minus (-) end (72, 74). There is also evidence in non-mammalian cells that suggests filamentous actin contributes to mitochondrial movement between microtubule filaments (72-74). The basic protein movement machinery allows the mitochondria to participate in more complex dynamics in the cell.

The dynamics of mitochondria do not only involve movements around the cell, they are also constantly undergoing fusion and fission events. These networking processes are imperative for the mitochondria quality control, normal mitochondrial functions, as well as stress and survival of the cell (75-77). Mitochondrial fusion is mediated by Mitofusin 1 and 2 (MFN1/2) for the fusion of outer membrane followed by Optic atrophy protein 1 (OPA1) for fusion of the inner mitochondrial membrane. While the precise metabolic conditions for which mitochondrial fusion occurs are not yet completely understood, there is evidence suggesting that mitochondrial fusion is important for oxidative phosphorylation (OXPHOS) activity and oxidative stress (76, 77). An elongated mitochondria morphology has been associated with increased OXPHOS activity (78) and increased levels of oxidized glutathione (79). Notably, mitochondrial fusion is also linked to a pro-survival state in the cell by allowing stress and damage to be shared and distributed across the organelle network (80), possibly as an adaptive response. Inducing cells towards an increased mitochondrial fusion results in delayed apoptosis (81), but also decreased autophagosomal degradation of mitochondria (82), which suggests that excessive fusion can also be maladaptive for cellular and mitochondrial quality control purposes.

On the other hand, mitochondrial fission is mediated by Dynamin-related protein 1 (DRP1). The activation of DRP1 relocates it to the mitochondrial fission receptors (e.g. FIS1 and MFF) on the mitochondrial outer membrane. DRP1 oligomerizes to form a ring like structure, constricting around the mitochondrion (75-77). A recent study discovered another protein in the fission machinery, DYN2, that further constricts the mitochondria and delivers the final pinch off, splitting a mitochondrion in two (83). Mitochondrial fission serves two main functions in the cell: 1) replicative fission for mitosis and 2) asymmetrical fission in response to stress (70). Replicative fission serves mainly to divide and produce additional mitochondria for growth and cellular

division (80). Replicative fission is also sometimes called symmetric fission as it mostly produces mitochondria of similar sizes. Alternatively, mitochondrial asymmetrical fission produces mitochondria of unequal sizes and functions mainly for quality control of the network by removing damaged parts (70, 76, 77). In this way, mitochondrial fission also plays an important role as an adaptive response to stress and the loss of functional fission machinery results in the accumulation of damaged mitochondria (84, 85) that would normally have been removed by a process known as mitophagy (refer to Section 1.3.3). However, excessive mitochondrial fission can be maladaptive and has been associated with stress and eventual death of the cell (81, 86). Similar to mitochondrial fusion, there is also evidence suggesting a metabolic role for fission (76). Mitochondrial fission has been associated with decreased efficiency of OXPHOS (87) and bioenergetic stress (88). In all, mitochondrial dynamics of both fission and fusion are important for cellular control of survival and death, function and failure, stress and adaptation.

Despite the known importance of mitochondria for β-cell function, the current literature on mitochondrial fission and fusion, and its effect on mitochondrial metabolism and function in β-cells remains limited. Studies in islets from Type 2 diabetic patients and diabetic rats reported that mitochondria in the β-cells were small, round, and had lost their cristae structure (89, 90). These studies have led to the hypothesis that inhibition of mitochondrial fission may prevent progression towards β-cell failure and death. Indeed, inhibition of fission has been demonstrated to be able to delay the onset of β-cell apoptosis (81). Recent studies have demonstrated that the roles of mitochondrial dynamics in β-cells may be more nuanced. Contrary to studies in other cell types that suggest mitochondrial fission is linked to decreased efficiency of OXPHOS (87), mitochondrial fission, more specifically DRP1 function, in β-cells has been demonstrated to be important for increased ATP levels and insulin secretion following glucose stimulation (91, 92).

Downregulation of fission receptor, FIS1, impaired respiratory function and glucose-stimulated insulin secretion (93). Adding to the complexity, overexpression of FIS1 in β-cells did not improve glucose stimulated insulin secretion, rather, it promoted LDH expression and lactic acid production. Moreover, a fragmented morphology attained from dominant-negative MFN1 overexpression did not promote apoptosis or affect insulin secretion (94). Ultimately, more studies of mitochondrial dynamics in β-cells are needed for a better understanding of the nuanced roles these dynamics have in metabolism and insulin secretion.

1.3.3 The mitochondrial life cycle

The mitochondrial life cycle involves both the creation of new mitochondria (i.e. biogenesis) and clearance of old and damaged mitochondria. The intricate balance of biogenesis and degradation controls mitochondrial mass and quality. Mitochondrial biogenesis can be a misleading term because it suggests cells are capable of *de novo* synthesis of mitochondria. However, new mitochondria cannot be synthesized and must come from existing mitochondria through division and growth. Biogenesis occurs when newly synthesized mitochondrial lipids and proteins are incorporated into existing mitochondria. This process is tightly controlled by the transcription co-factor PGC-1α, commonly referred to as the master regulator of mitochondrial biogenesis (95-97). The activation of PGC-1α increases transcription of nuclear respiratory factors (NRF1/2) which promotes the transcription of proteins in the ETC complexes. PGC-1α also increases levels of TFAM (Transcription Factor A, Mitochondrial) which activates mitochondrial DNA replication and mitochondrial gene transcription machineries (95, 96, 98, 99).

Over time, the functioning mitochondria accumulate damage, such as from ROS, and become dysfunctional. The clearance and removal of damaged mitochondria is especially

important as dysfunctional mitochondria are a source of cellular failure and death. The main mechanism for mitochondrial clearance is through orchestrated mitochondrial fission (refer to Section 1.3.2) and mitophagy. Mitophagy describes the process for which mitochondria are specifically targeted for lysosomal degradation by autophagy (70, 76, 77, 95, 97, 100-102). The most well studied mitophagy mechanism is the PINK1-Parkin pathway where PINK1 and Parkin are recruited to areas of the mitochondria that has lost its membrane potential, an indicator of dysfunction. Alternatively, in hypoxia-induced mitophagy, is regulated by the BNIP3 and/or FUNDC1 pathways, where they become activated in low oxygen conditions (100, 102, 103). After recruitment and activation of these key mitophagy proteins, autophagy initiators are recruited to the mitochondria, leading ultimately to the formation of the autophagosome, which engulfs the mitochondria and fuse with lysosomes, delivering the damaged organelles for degradation.

In the context of diabetes, mitochondria in β-cells are critical for β-cell function and, by extension, maintenance of sufficient mitochondrial quantity and quality is essential. However, mitochondrial biogenesis and mitophagy in β-cells has been relatively unexplored. Studies on PGC-1α, the master regulator of mitochondrial biogenesis, have suggested that acute glucose stimulation promotes PGC-1α expression (104) and PGC-1α help control insulin secretion (105) and lipid metabolism (104). Surprisingly, however, deletion of PGC-1α did not appear to affect mitochondrial mass in β-cells (104). TFAM has been demonstrated to be a downstream target of PDX1, a key transcription factor that maintains β-cell identity; overexpression of TFAM was able to rescue the functional defects associated with PDX1 deficiency (106). Moreover, loss of TFAM was associated with decreased mitochondrial metabolism and insulin secretion in response to glucose stimulation (107, 108). It has also been demonstrated that islets from diabetic rats have decreased mitochondrial DNA and decreased expression of *Pgc-1α* and *Tfam,* suggesting a defect

in mitochondrial biogenesis (109). Mitophagy has been demonstrated to be important for β-cell mitochondrial quality control (93) and adaptation to nutrient stress (81, 110). Taken together, the studies to date strongly suggest that mitochondrial biogenesis and mitophagy play important roles in pancreatic β-cells, and that these processes should be studied further to determine their regulation and involvement in β-cell mitochondrial quality control.

1.3.4 Mitochondrial failure in β-cells and T2D

Given the importance of mitochondria for β-cell function, it is perhaps not surprising that there is evidence to suggest that mitochondrial failure is an important contributor to the pathophysiology of type 2 diabetes. First of all, there is a rare genetic form of diabetes involving a mutation within the mitochondrial genome, giving the carriers dysfunctional mitochondrial tRNA. These patients show decreased insulin secretion upon a glucose challenge (111-113), presenting a genetic example of how mitochondrial failure can lead to diabetes.

Second, there is evidence for dysregulated mitochondrial structure in β-cells of T2D patients. In T2D, mitochondria cristae structure is lost, and normally tubular mitochondria become round and bloated. This is associated with a defect in insulin secretion and mitochondrial metabolism, where ATP levels and mitochondrial hyperpolarization was lowered (90). In accordance with this, studies in rodent insulin-producing cells also showed altered mitochondrial morphology and loss of movement following exposure to nutrient stress; whereas dynamic networking protects these cells from apoptosis (81).

Lastly, defects in mitochondrial biogenesis may also play a role in the pathophysiology of T2D. In mice, β-cell-specific knockout of TFAM resulted in development of diabetes that was accompanied by severe loss of mitochondrial DNA, as well as altered mitochondrial morphology

and OXPHOS function (108). Moreover, deficient levels of PDX1 and NKX6.1 are associated with decreased expression levels *Tfam* and *Pgc-1α* (106, 109).

Overall, there are numerous pieces of evidence suggesting that defects in mitochondrial structure and function may have significant roles in the pathogenesis of T2D, which is perhaps no surprise, considering the many roles these dynamic organelles have in controlling β-cell function and health.

1.4 Bcl-x_L and apoptosis

1.4.1 Canonical roles of Bcl-x_L and other Bcl-2 family proteins in apoptosis

Apoptosis, the most well-known form of programmed cell death, is a mechanism by which cells "commit suicide" for the well-being of whole organism. Apoptosis is important for normal development where it is necessary for proper limb formation and prevention of autoimmunity. It is also important for the elimination of damaged and harmful cells. Inability to undergo apoptosis leads to diseases such as developmental defects and cancer (114). However, excessive and inappropriate activation of apoptosis can also lead to harmful diseases, such as apoptosis of β-cells leading to diabetes.

Apoptosis can be separated into two different pathways, the extrinsic and the intrinsic (or mitochondrial), depending on the source of the initiation signal. The intrinsic pathway is controlled by the Bcl-2 family of pro-apoptotic and anti-apoptotic proteins, of which Bcl-x_L is an important anti-apoptotic member (see also 1.4.2, below). Bcl-2 family proteins share so-called Bcl-2 homology (BH) domains, of which four have been identified (115). Based on structure and function, the Bcl-2 proteins have been categorized into 3 groups: Pro-apoptotic initiators, pro-apoptotic effectors, and pro-survival (anti-apoptotic) members. Pro-apoptotic effectors include BAX and BAK. They have 4 BH domains and function as the "executioners" of apoptosis (114, 115). Once activated, they translocate to the mitochondrial outer membrane where they homooligomerize and permeabilize the membrane. This mitochondrial outer membrane permeabilization (MOMP) causes release of cytochrome C and SMAC and is generally considered the point of no return in the process of apoptosis. In the cytosol, cytochrome C binds APAF1 and activates caspase 9 while SMAC obstructs the function of the caspase inhibitor, XIAP. This leads to the activation of the effector caspases, including caspase 3, 6, 7 that cleave DNA and other

important cellular structural components. The pro-apoptotic initiators include BAD, BIM, BID, PUMA, and NOXA. Structurally, they only have the BH-3 domain and thus referred to as "BH-3 only" proteins. Some BH3-only proteins (activators) promote apoptosis by binding and directly activating BAX and BAK, other BH3-only proteins (sensitizers) do so indirectly by binding and antagonizing pro-survival members of the family (114, 115). The pro-survival proteins include Bcl-2, MCL-1, as well as Bcl-x_L which is the protein studied in this thesis. Similar to BAX and BAK, the anti-apoptotic proteins have 4 BH domains and counteract MOMP mainly by binding and restraining the pro-apoptotic effectors (BAX and BAK), as well as the subset of BH3-only proteins that activate them (114-116). Consequently, the relative abundance and mutual interactions of the pro- and anti-apoptotic Bcl-2 protein family members are critical for controlling cell fate towards survival or apoptosis under stress.

The extrinsic apoptotic pathway, also called death receptor-mediated pathway, involves the binding of the death receptor ligand (e.g. Fas ligand) to the death receptor (e.g. Fas receptor), leading to the activation of Caspase 8, which can further activate the effector caspases and apoptosis. In β-cells, activation of death receptors can also result in activation of Bcl-2 family-regulated mitochondrial apoptosis because caspase 8 can cleave the pro-apoptotic BH3-only protein BID to form tBID, which then activates BAX and BAK, resulting in MOMP (117).

1.4.2 Structure and functions of anti-apoptotic Bcl-x_L

Bcl-x_L was the first protein of the Bcl-2 family to be characterized by x-ray crystallography and NMR spectroscopy. Structural analyses of Bcl-x_L identified 9 alpha-helices, 4 BH domains and a transmembrane (TM) domain that Bcl-x_L shares with other members of the Bcl-2 family. Importantly, the TM domain allows the docking of Bcl-x_L to the mitochondrial outer membrane,

where it can effectively perform its functions (115, 118). As a pro-survival Bcl-2 family member, Bcl-x_L is classically known for its ability to inhibit apoptosis by binding to BAX and BAK, preventing them from oligomerizing and forming pores in the mitochondrial outer membrane. Thus, Bcl-x_L can indirectly prevent the release of cytochrome c and the subsequent activation of the caspases (114).

Bcl-x_L has been shown to not be necessary for normal β-cell development as β-cell-specific deletion of Bcl-x_L did not alter islet morphology (119). However, the Bcl-x_L deficient β-cells were more susceptible to apoptotic stimuli and insults (e.g. ER stress and Fas ligand), suggesting its importance in protecting β-cells from stress (119). In addition to its anti-apoptotic functions, Bcl-x_L has more recently been shown to have metabolic functions. When Bcl-x_L is moderately overexpressed (2 to 3 times more than control) in transgenic mouse β-cells, these β-cells were protected from ER stress without metabolic defects. However, in mice where β-cell Bcl-x_L was overexpressed to levels that were 10 times higher than the control, the transgenic mice became glucose intolerant and their islets secreted significantly less insulin in response to glucose stimulation. This decrease in function was associated with a decrease in mitochondrial OXPHOS and metabolism (120). On the other hand, when Bcl-x_L was specifically knocked out in the β-cells, mice exhibited better glucose tolerance, increased calcium response to stimulation by glucose, and increased mitochondrial metabolism (121). Overall, this suggest that Bcl-x_L helps balance β-cell survival and death with metabolic function and failure, but the mechanisms by which Bcl-x_L performs its metabolic roles are largely unknown.

In other cell types, Bcl-x_L has been demonstrated to interact with the mitochondrial dynamic machinery and directly regulate mitochondrial fission and fusion. Immuno-precipitation studies of Bcl-x_L demonstrated that Bcl-x_L interacts with DRP1 (122) as well as MFN1/2 (123) to

regulate their activity. This is further supported by CED-9, the Bcl-x_L homologue in *C. elegans*, which has been shown to interact with FZO-1 (MFN1/2 homolog) and EAT-3 (OPA1 homolog) (124). Bcl-x_L is also known to inhibit the autophagy and mitophagy machinery via binding to Beclin-1 (125) and PGAM5 (102, 126). However, these interesting and novel roles for Bcl-x_L have not been explored in β-cells, and it remains unknown if, and how, they may relate to its involvement in β-cell metabolism and insulin secretion.

1.5 Thesis proposal

Rationale:

Mitochondria are very important for β-cell function and insulin secretion, but also for the regulation of β-cell death by apoptosis. As a result, mitochondrial dysfunction leads β-cell failure and can contribute to the development of T2D. An important aspect of mitochondrial physiology is their dynamic fusion and fission, which help maintain their function, quality control, adaptation to stress and cellular health. The anti-apoptotic protein Bcl-x_L was recently found to have non-canonical functions in mitochondrial metabolism. Studies in other non-β-cell types suggest that these metabolic roles may extend to the control of mitochondrial dynamics. Thus, understanding the involvement of Bcl-x_L in β-cell mitochondrial physiology may help clarify the mechanisms that promote healthy mitochondria in pancreatic β-cells under T2D-related stress, which may eventually lead to the development of innovative therapies for diabetes intervention.

Hypothesis: Bcl-x_L is important for β-cell adaptation to metabolic stress by regulating mitochondrial dynamics.

Specific aims:

AIM 1: Establish a method to quantify mitochondrial morphology and volume in β-cells.

AIM 2: Determine if Bcl-x_L regulates mitochondrial mass and morphogenesis in β-cells.

AIM 3: Determine the importance of Bcl-x_L for β-cell mitochondrial adaptation to a prolonged high-glucose challenge.

Chapter 2: Material and Methods

2.1 Reagents

Collagenase type XI (#C7657), corn oil (#C8267), tamoxifen (#T5648), tetramethylrhodamine (TMRE, #87917), D-glucose (#G7528), rotenone (#R8875), FCCP (#C2920), antimycin-A (#A8674), and oligomycin (#75351) were purchased from Sigma-Aldrich (St. Louis, Missouri). MitoTracker Deep Red FM (#M224726), MitoTracker Green FM (#M7514), Hoechst 33342 (#H3570) were purchased from Thermo Fisher Scientific/Life Technologies (Carlsbad, California). Dimethyl sulfoxide (DMSO, #BP231) was purchased from Fisher Scientific (Waltham, Massachusetts). Compound 6 was purchased from Calbiochem (San Diego, California). The plasmids for expression of mitochondria-targeted YFP (Mito-YFP) and mitochondria-targeted photoactivatable GFP (mito-PAGFP) were kind gifts from Dr. Mark Cookson (127) and Dr. Richard Youle (Addgene plasmid #23348) (128), respectively.

2.2 Cell culture

MIN6 cells, a mouse pancreatic β-cell line, were cultured in DMEM (Dulbecco's Modified Eagle's Medium, Life Technologies #11995) supplemented with 10% Fetal Bovine Serum (FBS, Life Technologies #10438) and 2% Pen Strep (Penicillin-Streptomycin at 10,000U/mL, Life Technologies #15140) under 37ºC and 5% CO_2. Culture media was changed every 2 days and the cells were passaged when they reach 70-80% confluency. Briefly, the cells were washed with Dulbecco's Phosphate-Buffered Saline (DPBS, Life Technologies #14190) before Trypsin-EDTA (0.25%, Life Technologies #25200) was added for 3 minutes to detach the cells. The cell suspension was then diluted with complete DMEM, spun down at 500×*g* and the supernatant

replaced with fresh media to re-plate the cells. HEK293T cells were similarly cultured in complete DMEM under 37ºC and 5% CO_2 and passaged when they reached 70-80% confluency.

2.3 MIN6 transfection

Lipofectamine® 2000 (Life Technologies #11668) was used to introduce the plasmids (mito-eYFP and mtPA-GFP) into MIN6 cells. Briefly, 1×10^5 MIN6 cells were seeded on 25 mm glass coverslips (VWR #102097) in complete DMEM and cultured overnight. The next day, DMEM was replaced with Opti-MEM (Life Technologies #31985). Meanwhile, 1µg plasmid DNA in Opti-MEM was mixed with 2µL Lipofectamine Reagent in Opti-MEM and were incubated at room temperature for 30 min. Subsequently, the plasmid-Lipofectamine mixture was added to the cells and they were incubated for 5 hours before transfection media was replaced with complete DMEM. The plasmid was allowed to be expressed for at least 24 hours before transfection was confirmed by confocal microscopy.

2.4 Animals and genotyping

To study Bcl-x_L knockout in adult islets, we used a β-cell specific inducible Bcl-x KO mouse model previously generated by Luciani *et al*. (121). Genotyping was done by digesting ear notch samples in 40µL lysis buffer (25mM NaOH, 0.5mM EDTA) for 15 min at 80ºC. The samples were then quickly neutralized with 40µL 40mM Tris-HCl buffer (pH=8.0) and the supernatant containing the DNA was collected for PCR amplification. Briefly, the 10µL PCR reaction (95ºC-120s; 30 cycles: 95 ºC-30s, 55ºC-30s, 68ºC-60s; Hold: 4ºC) was prepared by mixing 5µL of DreamTaq Green PCR Master Mix (2X) (ThermoFisher #K1082) with 1µL DNA and 0.75µM of each primer pair (*CreER F: AACCTGGAAGTGAAACAGGGGC and R:*

TTCCATGGAGCGAACGACGAGACC; *Tcrd F: CAAATGTTGCTTGTCTGGTG and R: GTCAGTCGAGTGCACAGTTT*). PCR products were visualized after agarose gel electrophoresis (2% agarose gel stained with 1× RedSafe, 130V for 30min) under UV (BioSpectrum 310 Imaging System, UVP). The presence of CreER transgene in BclxβKO mice was recognized by the 410bp amplicon product and the 200bp Tcrd amplicon product served as the internal positive control for the PCR reaction.

2.5 Tamoxifen injections

Tamoxifen (Sigma-Aldrich #T5648) was dissolved in corn oil (Sigma-Aldrich #C8267) at 10mg/mL and was subsequently vacuum filtered through a 0.22µm membrane (Millipore #SCGP00525). Intraperitoneal injections were performed daily on both $Bclx^{flox/flox}$:$Pdx1CreER^{Tamoxifen}$ (BclxβKO) mice and their littermate $Bclx^{flox/flox}$ (BclxWT) controls at 75µg per gram body weight (7.5µL oil per gram body weight) for 4 consecutive days.

2.6 Islet isolation

Islets from C57BL/6, BclxβKO and BclxWT mice were isolated via enzymatic digestion and mechanical agitation. Collagenase (Sigma-Aldrich #C7657) was dissolved in 1× HBSS (Life Technology #14185) at 1000U/mL and kept on ice until ready to use. The mice were anesthetized by isoflurane prior to euthanasia and surgical dissection, revealing common bile duct and the sphincter of Oddi. To prevent the flow of collagenase into the intestines, the sphincter of Oddi was clamped with haemostat prior to injecting 3mL collagenase into common bile duct, inflating the pancreas. The inflated pancreas was then removed and incubated at 37ºC in an additional 2mL of collagenase solution for 15min. Afterwards, the pancreas was shaken by hand until most of the

visible tissues had disintegrated (usually between 3 to 6 minutes). The homogenized tissues were washed two times with 1×HBSS supplemented with 1mM $CaCl_2$ and filtered through a 70µm cell strainer (Fisher Scientific #352350). Subsequently, the islets were washed off the strainer with complete RPMI (RPMI 1640 supplemented with 10% FBS and 2% Pen Strep) and were hand-picked under a dissection microscope.

2.7 Islet culture and dispersion

Islets and dispersed islet cells were cultured in complete RPMI (RPMI 1640 supplemented with 10% FBS and 2% Pen Strep) at 37ºC and 5% CO_2. 3mM, 17mM, and 25mM glucose RPMI was prepared by diluting the appropriate amount of 2M stock glucose solution in no glucose RPMI 1640 media (Life Technologies #11879).

To make the single cell dispersions, intact islets were first washed 3 times with Minimum Essential Media (MEM, Corning cellgro #15-015-CV) by centrifugation and re-suspending the islet pellets. The islets were then pipetted up and down vigorously in 0.01% Trypsin-EDTA (0.05%, Life Technologies #25300) for 1 min. The dispersed cells were then washed in MEM and further dispersed by pipetting for approximately 10 seconds. Lastly, the dispersed cells were re-suspended with complete RPMI. For confocal imaging, cells were seeded as a 50µL droplet on 25mm glass coverslips (0.13-0.16mm thickness, VWR #16004-310) and allowed to adhere in culture at 37 ºC for 3-5 hours before topping up with 2mL of complete RPMI.

2.8 Adenovirus amplification, purification and transduction

HEK293T cells were cultured in complete DMEM until 70-80% confluency. Adenovirus carrying eYFP-tagged Bcl-x_L (Ad.Bcl-x_L-YFP) or EGFP (Ad.GFP) was added to the cells at an

approximate MOI of 10 pfu/cell. After 3 to 4 days, when over 95% of the cells have detached, both cells and media were collected in a 50mL tube and then lysed by 3 freeze-thaw cycles. The cells debris was then pelleted by centrifugation at 239×g for 5 min and supernatant containing the virus collected.

To purify the virus, the lysates were treated with 10 U/mL of Benzonase (Sigma #E1014-SKU). Subsequently, the same volume of dilution buffer (20 mM Bicine, 0.6 M NaCl, pH=8.4) as the lysate was added to stop the digestion reaction. Diluted lysate purified through a Sartobind Q15 anionic exchange filter (Sartorius Stedim #93IEXQ42GB-12--A), washed with wash buffer (10 mM Bicine, 0.4 M NaCl, pH=8.4) and eluted with elution buffer (10 mM Bicine; 0.61 M NaCl; pH=8.2) supplemented with glycerol. Purified virus were stored at -80 ºC.

To determine the concentration of virus, HEK-293T cells were seeded in a 96-well plate at 10,000 cells per well. Serial dilutions of purified adenovirus from 10^{-3} to 10^{-10} were transduced along with negative controls. Cells in the same row were transduced at the same concentration and were subsequently cultured at 37 ºC in 5% CO_2. Two to four days after transduction, the number of wells displaying fluorescent signal per row was counted under a florescent wide-field microscope. Viral titer was calculated using the following equation:

$$Virus\ concentration\ (pfu/mL) = 10^{(x + 2.8)}$$

, where x is the sum of the fraction of fluorescent wells in each row.

For adenovirus transduction, the Multiplicity of Infection (MOI) was determined using the following equation:

$$Volume\ of\ virus\ added\ (mL) = \frac{MOI\ \times\ Number\ of\ Cells\ (estimated)}{Concentration\ of\ Virus\ (pfu/mL)}$$

The estimated number of MIN6 cells was the initial number of cells that were seeded. To estimate the number of primary islet cells, every dispersed islet was assumed to yield 1000 cells. The adenovirus was left in the media overnight and replaced with complete media the next day.

2.9 Identification and measurement of mitochondrial morphology in 2D

Image acquisition

Cells were imaged using Leica SP8 Confocal Microscope (Concord, Ontario) with a 63X HC Plan Apochromatic water immersion objective (NA=1.2). I digitally zoomed in on the cells to increase the structural detail and allow me to better focus; acquisition resolution (*x* and *y* dimensions) were adjusted using suggested "Optimize" function in the Leica LASX Software; laser power, detector filtering/gating and gain were adjusted appropriately to maximize signal without saturating the detector and to minimalize background and cross-fluorescence.

Activation of photo-activatable-green-fluorescent-protein (PAGFP)

MIN6 cells were co-transfected with mito-PAGFP (Addgene plasmid #23348) (128) and mito-dsRed plasmids for 24 hours prior to imaging. The "Bleach Point" function (time = 150ms) was used with 405nm laser for activation of mito-PAGFP and images were acquired as described above. Regions with lower mitochondria density were preferred as points of activation.

Processing, thresholding, and measurement of images

In ImageJ/FIJI (129), the images were processed using the "Subtract Background" (Radius = 25 pixels) command and the "Sigma Filer Plus" plugin (130) (Radius = 2.0 pixels; Sigma = 2.0; Minimum Pixel Fraction = 0.2). Different thresholding strategies for mitochondria identification

were performed as follows: 1) Global threshold using “Auto Threshold” (Method = Default) command. 2) Local threshold using “Auto Local Threshold” (Method = Mean, Radius = 5). 3) Combination Threshold using both “Auto Threshold” (Method = Li) and “Auto Local Threshold” (Method = Mean, Radius = 5) on the same image; the resultant 2 binary images were then combined with the “AND” operation under the “Image Calculator…” command. The final combined image was then cleaned up with the “Despeckle” command.

To measure the morphology of each mitochondrion, the “Analyze Particles…” (Size = 10-Infinity pixel^2, Circularity = 0.00-1.00) command was used on the threshold image and measurements were set to include “Area”, “Perimeter”, and “Shape Descriptors”. Form factor was calculated afterwards using the following equation:

$$Form\ Factor\ (FF) = \frac{1}{Circularity}$$

Lastly, mitochondria network characteristics were quantified by first skeletonizing the network structure using the “Skeletonize 2D/3D” command on the threshold image. The skeleton map was analyzed using the “Analyze Skeleton” command to calculate the number of branches, branch length, and branch points of the network.

Simultaneous detection of mitochondrial morphology and function on a per-mitochondrion basis

Dispersed islet cells were transferred to either 3mM glucose or 17mM glucose completed RPMI for 60 min. Cells were then stained 0.1µg/mL Hoescht 33342 (ThermoFisher # H3570), 50nM MitoTracker Green FM (MTG) (ThermoFisher # M7514), and 25nM Tetramethylrhodamine, ethyl ester (TMRE) (Sigma-Aldrich #87917) for 30 min prior to imaging. Images were acquired and processed as described above. Using the MTG signal, mitochondria in

the images were identified using the combination threshold approach. Morphology was then measured using the "Analyze Particles…" (Size = 10-Infinity pixel^2, Circularity = 0.00-1.00) command with the "Add to Manager" option checked to create regions of interest (ROIs). These ROIs were then superimposed onto raw images of MTG and TMRE signals and the MTG and TMRE intensities of each mitochondrion was measured as the "Mean gray value" using the "Analyze Particles…" command. Network characteristics were calculated as described above.

2.10 Mitochondrial 3D volume analysis

Image acquisition

Image stacks of cells were acquired using the Resonance confocal imaging mode (scan speed 8000hz) of Leica SP8 Confocal Microscope (Concord, Ontario) under 63X oil objective (NA = 1.4). Image stacks were taken from the bottom of the cell (where there is no fluorescent signal yet) to the top of the cell (where fluorescent signal disappears); pinhole size was reduced 0.5 AU; acquisition resolution (*x*, *y*, and *z* dimensions) settings were adjusted based on optimal Nyquist standard (131) (often each pixel dimensions less than 56nm×56nm and a z-step less than 170nm); laser power, detector filtering/gating and gain were adjusted to maximize signal without saturating the detector and minimize background signal and cross-fluorescence.

Image deconvolution

Deconvolution was performed using Huygens Essential (Scientific Volume Imaging B.V., Hilversum, Netherlands). Raw image stacks were loaded in to Huygens Essential and image properties/parameters were verified. Subsequently, "Deconvolution Wizard" was used and a theoretical Point Spread Function (PSF) was used to compute out-of-focus signals. Estimation of

background was automatically determined (Mode = Lowest, Area radius = 0.7µm). Deconvolution was done with the following settings: maximum iterations = 100, quality threshold = 0.001, iteration mode = optimized, brick layout = Auto. The signal-to-noise ratio was calculated as follows:

$$Signal\ to\ Noise\ Ratio = \sqrt{\frac{Highest\ intesity\ value}{Lowest\ nonzero\ intensity\ value}}$$

Processing, thresholding, and quantification of image stacks

In ImageJ/FIJI, the images were processed as described for 2D, above. The plugin "Adaptive Threshold" (132) available as a plugin for FIJI/ImageJ (129) was used to identify positive mitochondrial signal from each 2D slice. The final images were then cleaned up using the following commands: "Despeckle", "Remove Outliers", and "Fill 3D Holes" (available with the 3D ROI Manager Plugin) (133). The quantification of mitochondrial structure is separated in two steps. First, volume, surface area, mitochondrial count were measured using the "3D Object Counter" command, producing a labelled object map. Second, the "Skeletonize 2D/3D" command was used to calculate a 3D skeleton for the image stack. The skeleton map was analyzed using the "Analyze Skeleton" command to quantify the number of branches, branch length, and branch points of the network.

2.11 Unsupervised categorization of mitochondrial morphology

Spanning-tree Progression Analysis of Density-normalized Events (SPADE) (134) was used to automatically classify the mitochondrial images into 3 different categories based on their calculated morphological parameters (Average area, average perimeter, form factor, aspect ratio, branches per mito, branch length per mito, and branch junctions per mito). Briefly, mitochondrial

morphology data was stored as comma-separated values (CSV) file and transformed into Flow Cytometry Standard (FCS) file using FlowJo V10. Then, SPADE V3.0 (135) was used to create a SPADE tree; *Settings*: Ignore compensation, No arcsinh transformation, neighbourhood size = 5, local density approximation factor = 1.5, 0^{th} percentile outlier, fixed number of cells remain = number of images used, clustering parameter = K-means, number of desired clusters = number of images used. The "Auto Suggest Annotation" function was then used to partition the SPADE tree into 2 subgroups and the larger of these was subsequently auto-partitioned again, resulting in 3 subgroups in total. The 3 subgroups were then individually exported back as 3 FCS files and CSV files afterwards for analysis.

2.12 Seahorse Mitostress assay

Oxidative respiration levels of dispersed islet cells were determined using the Seahorse XFe96 Extracellular Flux Analyzer (Agilent / Seahorse Bioscience, Santa Clara, California), as previously described (136). Briefly, 40 dispersed islets seeded per well in Seahorse XF96 Cell Culture Microplates and cultured at 37ºC at 5% CO_2 for 2 days before the experiment. Adenovirus were transduced one day before the experiment. Before loading plates into the Analyzer, cells were washed with XF Basic Medium supplemented with 3mM glucose, 2mM glutamine, and 2mM sodium pyruvate and incubated at 37°C in a 0% CO2 chamber for 60 minutes. After measuring the basal oxygen consumption rate (OCR), each well was injected sequentially with 25mM glucose, 1µM Oligomycin, 0.5µM FCCP, and finally a mixture of 1µM rotenone and 1µM Antimycin A (137).

2.13 RNA isolation, cDNA synthesis, and real-time quantitative PCR (RT-qPCR)

Total RNA was isolated from MIN6 cells and islets using the RNEasy Mini Kit (Qiagen #74106). For islets, 30 to 40 islets were preserved in 40µL RNAlater (Qiagen #76104) at -80ºC before RNA isolation. Yield and concentration of RNA isolated were measured by NanoDrop™ 2000 (ThermoFischer, Carlsbad, California). Afterwards, 100ng RNA was reverse transcribed using qScript cDNA synthesis kit (Quanta Bioscience #95047-500) and stored at -20ºC until use. SYBR RT-qPCR was run in 8µL reaction: 4µL PerfeCTa SYBR green Fastmix (Quanta Biosciences #95072), 0.5µL 5µM forward and reverse primer mix (sequences summarized in Table 1), 1µL cDNA, and 1.5µL ddH_2O. Relative expression levels were assayed in triplicates on 384-well microplates (Life technologies #4309849) in a ViiA7 Real-Time PCR machine (Applied Biosystems, Foster City, California). Actin was used as the housekeeping gene. Primers are summarized in Table 1. The following formulas were used to calculate relative expression levels (experimental group over control):

$$Relative\ expression = \frac{2^{-\Delta CT_{Exp}}}{2^{-\Delta CT_{Ctrl}}} \qquad \Delta CT = CT_{Gene\ of\ Interest} - CT_{Actin}$$

Table 1. Summary of primers used for gene expression analysis

Gene (reference if applicable)	Primers (from 5' to 3')
Actb	**F:** GATCTGGCACCACACCTTCT
	R: GGGGTGTTGAAGGTCTCAAA
Bcl-x$_L$	**F:** GACAAGGAGATGCAGGTATTGG
	R: TCCCGTAGAGATCCACAAAAGT
Drp1 (138)	**F:** GCGCTGATCCCGCGTCAT
	R: CCGCACCCACTGTGTTGA
Fis1 (138)	**F:** GCCCCTGCTACTGGACCAT
	R: CCCTGAAAGCCTCACACTAAGG
Mfn1 (138)	**F:** TCTCCAAGCCCAACATCTTCA
	R: ACTCCGGCTCCGAAGCA
Mfn2 (139)	**F:** ACGTCAAAGGGTACCTGTCCA
	R: CAATCCCAGATGGCAGAACTT
Opa1 (140)	**F:** AAGTGGATTGTGCCTGACTTT
	R: CAACCCGTGGTAGGTGATCT
Pgc-1α	**F:** CAAACCCTGCCATTGTTAAG
	R: TGACAAATGCTCTTCGCTTT
Tfam (141)	**F:** GATGGCGCTGTTCCGG
	R: TGGATAGCTACCCATGCTGGA
Nfe2l2	**F:** AGTGGATCCGCCAGCTACT
	R: TCTCTGCCAAAAGCTGCAT
Ucp2 (142)	**F:** CAGCCAGCGCCCAGTACC
	R: CAATGCGGACGGAGGCAAAGC
MnSod	**F:** CACACCATTTTCTGGACAAACCT
	R: TTCTCAAAAGACCCAAAGTCACG
Hmox	**F:** CAGAAGGGTCAGGTGTCCA
	R: CTTCCAGGGCCGTGTAGAT

2.14 Western blot

Western blot detection of proteins was performed as previously described (121). Briefly, MIN6 cells and islets were lysed using radioimmunoprecipitation assay buffer supplemented with protease inhibitors (Fermentas #R1321) and protein concentration was quantified using the Pierce BCA Protein Assay Kit (ThermoFisher #23225). Equal amounts of protein was loaded and resolved on 12% SDS-PAGE gels. Subsequently, proteins were transferred onto polyvinylidene difluoride membranes (Bio-Rad #1620177) and probed with the following primary antibodies

overnight at 4ºC: Bcl-x_L (Cell Signaling Technology #2762), TOM20 (Santa Cruz #sc-11415), and β-actin (Novus Biologicals #NB600-501). Subsequently, secondary antibodies linked to horseradish-peroxidase and Pierce ECL Western Blotting Substrate (ThermoFisher #32106) were used to visualize the protein bands. Band densitometry was quantified using FIJI/ImageJ.

2.15 Statistical analysis

All data were represented as mean ± standard error of the mean (SEM). Data were analyzed in GraphPad Prism software (La Jolla, California) using Student's t-test, Paired Ratio t-test, One-way ANOVA followed by Sidak multiple comparison test, or Two-way ANOVA, as appropriate. Statistical significance was set at a threshold of $p < 0.05$.

Chapter 3: Results

3.1 Establishing a pipeline for accurate quantification of mitochondrial properties by 2D and 3D confocal microscopy

3.1.1 Accurate identification of fluorescently labeled mitochondria

To accurately measure the potential roles of Bcl-x_L in both physiological and pathophysiological mitochondrial dynamics, it is essential to have a robust and sensitive method for measuring small changes in the network morphology and complexity. We aimed to do so using the widely available laser scanning confocal microscopy technique and the image analysis shareware, FIJI/ImageJ (129).

Prior to identification of mitochondria, raw confocal images were uniformly processed to reduce background noise and smooth edges, thereby reducing artifacts and improving edge detection. Accurate mitochondrial identification for analysis requires that 2 fundamental goals are achieved: (1) the ability to distinguish the fluorescently labelled mitochondria from the background in the processed confocal images, and (2) the ability to precisely separate individual mitochondrial units within the networks from each other. The most often used method for distinguishing fluorescently labelled structures from background is the global threshold in ImageJ, which identifies only pixels above a certain intensity. When using the “Default” global thresholding algorithm (for details see Chapter 2.9) on our dispersed pancreatic islet cells stained with MitoTracker Green FM (MTG), we found that we were able to accomplish goal (1) and distinguish mitochondria from the background, but generally failed to accomplish goal (2) to accurately separate one mitochondrial network unit from another. As illustrated in Figure 1A, which shows a representative cluster of 3 cells, this was an issue particularly in areas of the cells with high mitochondrial density (lower left corner). In this cluster of cells, global thresholding

identified 64 mitochondria, a likely underestimation of mitochondria count given the apparent lack of detail in the identified network. As a result, we realized the global threshold method might be able to detect major changes in mitochondrial morphology, but was unlikely to allow accurate quantification of subtle changes in mitochondrial morphology and number.

Local threshold algorithms, on the other hand, base the thresholding on the relative pixel intensities in a local neighborhood. When a local threshold algorithm (for details see Chapter 2.9) was applied to the same image (Figure 1A), we observed the opposite effect of the global thresholding. Local thresholding accomplished goal (2) and successfully separated one mitochondrial network unit from another, but also included background noise in the mask. This resulted in the detection of 808 mitochondrial units, a clear overestimate due to the background signal. To overcome the weakness of each thresholding method, we established an approach in which the global and local masks were combined by a Boolean 'AND' function (Figure 1B). This combination approach uses a less stringent global thresholding algorithm (for details see Chapter 2.9) as a "mold" that allows the local mask to "carve" out the detailed structure of the mitochondria, thus maintaining both the accurate background elimination from the global mask and the structural details of the local mask. In the representative 3 cell cluster this resulted in the identification of 121 mitochondria (Figure 1A). By visual inspection this appeared to be a much more accurate separation and identification of mitochondria, and we next verified this using a more stringent approach.

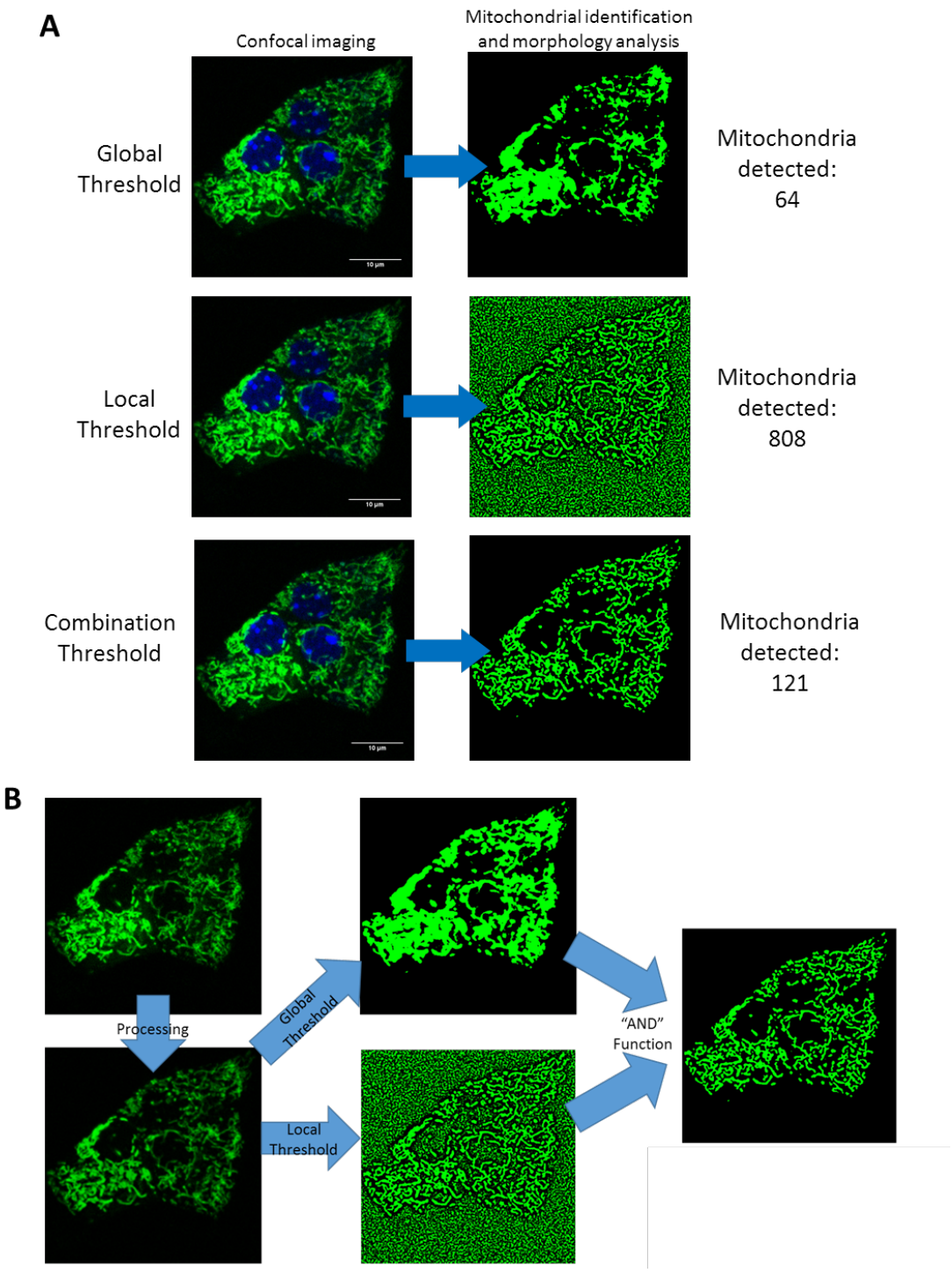

Figure 1. Establishing a pipeline for accurate identification and analysis of mitochondrial morphology using FIJI. Mitochondria of primary islet cells were fluorescently labeled with MitoTracker Green and confocal images acquired for further processing and analysis. (A) Representative images of the mitochondrial identification achieved using the "Default" FIJI global threshold algorithm, the FIJI local threshold algorithm, and our combination threshold approach. (B) Schematic of the steps involved in the combination threshold approach for mitochondrial identification. The global threshold here uses the less stringent "Li" algorithm to ensure full coverage of the network.

3.1.2 Verification of correct mitochondrial identification using mito-PAGFP

To verify whether we were correctly identifying the mitochondria of β-cells within a confocal image, we transfected MIN6 cells with mitochondria-targeted photoactivatable GFP (mito-PAGFP), which allows selective photo-labeling of a single mitochondrion (143). After mito-PAGFP is activated by a 405 nm laser pulse (see details in Chapter 2.9), the fluorescence quickly spreads throughout the entire single mitochondrial network unit, thus distinguishing it from the neighbouring networks (Figure 2A). This unambiguous identification of a mitochondrial unit allowed us to more rigorously compare the accuracy of our threshold algorithms. As illustrated in Figure 2B, global thresholding would often merged un-connected parts of the network (labeled white) and miss other connected pieces (labeled in blue). On the other hand, our combination thresholding approach more closely matched the PAGFP signals (Figure 2C). In summary, these results support that our combined thresholding method is superior for identification and separation of mitochondria within a confocal image, and we used this approach for all analysis of their morphological properties such as size and shape, as well as the connectivity/complexity of the whole network.

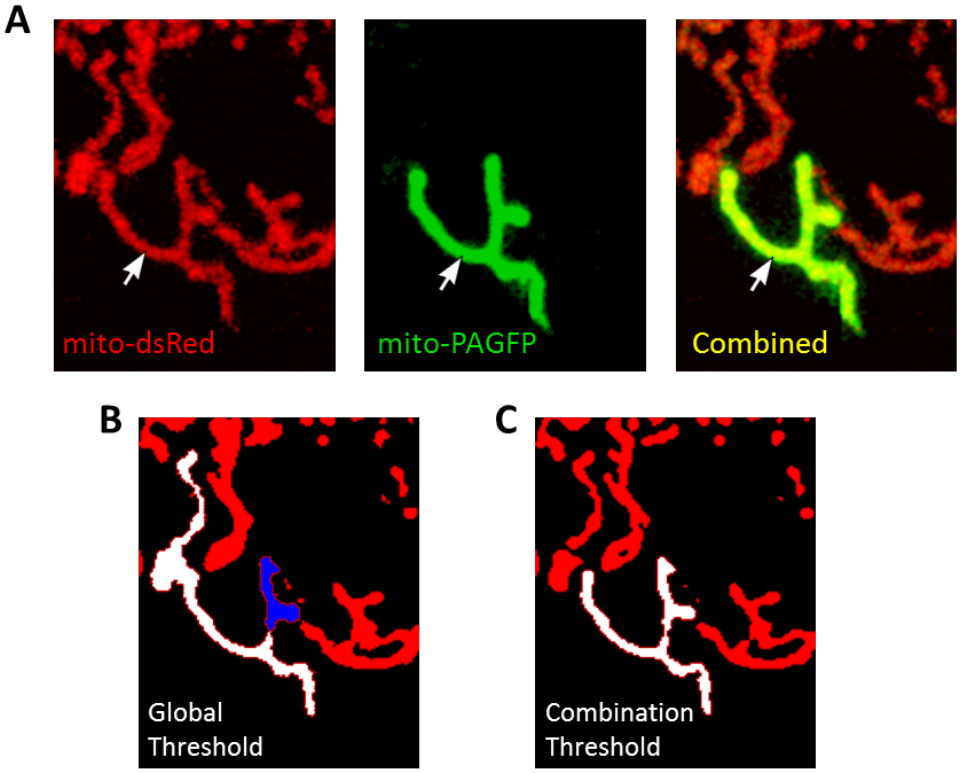

Figure 2. Use of mito-PAGFP to verify the accuracy of mitochondria identification. MIN6 cells were co-transfected with mitoPA-GFP plasmid and mito-dsRED plasmid 24 hours prior to imaging. Mito-PAGFP was activated using a 405nm laser (refer to Chapter 2.9 for details). (A) A region within the cell where a single mitochondrial unit (green) of the total mitochondrial network (red) was photo-labeled by mito-PAGFP activation. The white arrow denotes the activation point. (B) Identification of mitochondria by the global threshold method applied to the mito-dsRed image. The white area illustrates how the global threshold algorithm mistakenly merges adjacent mitochondrial units. The blue area represents a region that was erroneously missed. (C) Identification of mitochondria by our combination threshold approach applied to the mito-dsRed image. The white area illustrates how the photo-painted mitochondrial unit was correctly distinguished from the neighbouring mitochondria. (Representative of n=16 replicates).

3.1.3 Establishing an approach for quantification of mitochondrial morphology in 2D

After establishing a method to accurately identify mitochondria within a confocal image, we aimed to mathematically describe and quantify their morphology. Further skeletonization of the identified mitochondria permits analysis of their network characteristics (Figure 3A). Based on previous studies (144, 145), we identified suitable parameters for quantifying mitochondrial morphology in pancreatic β-cells (summarized in Figure 3B). For 2D analysis, we used area and

perimeter to mathematically describe mitochondrion size, their shape was described by form factor (FF) and aspect ratio (AR), and network connectivity and/or complexity was determined by the number of branches, the number of branch junction, as well as total branch lengths of each mitochondrion. Figure 3C illustrates how these factors change with different morphologies.

To evaluate our ability to quantify and distinguish different mitochondrial morphologies using these parameters, we obtained a set of 84 2D image slices of MIN6 cells expressing a mitochondria-targeted yellow fluorescent protein (Mito-YFP; Figure 4A). Based on visual assessment of the mitochondrial morphology we manually categorized the images into 3 groups: (1) “fragmented”, characterized by small, round mitochondria with little branching; (2) “filamentous”, characterized by highly connected networks of long and tubular mitochondria; and (3) an “intermediate” group, which are morphologically between the 2 other groups (Figure 4A). Analysis of these three image sets showed that we were capable of distinguishing the morphologies based on the parameters related to size, shape and network complexity. Moving from filamentous to intermediate to fragmented, we detected significant decreases in average mitochondrion area and perimeter between each group (Figure 4B). Moreover, we also detected significant changes in mitochondria shape across the 3 morphological groups, as represented by significant changes in FF and AR (Figure 4C). This was further supported by our connectivity/complexity analysis of the mitochondria skeleton, which showed significant changes in number of branches, branch lengths, and number of branch junctions (Figure 4D). These results demonstrate that our analysis pipeline can quantitatively distinguish mitochondrial morphological sub-types that are evident by eye. We next wanted to further validate these analysis results and our morphological classifications using an unbiased machine-based approach.

A

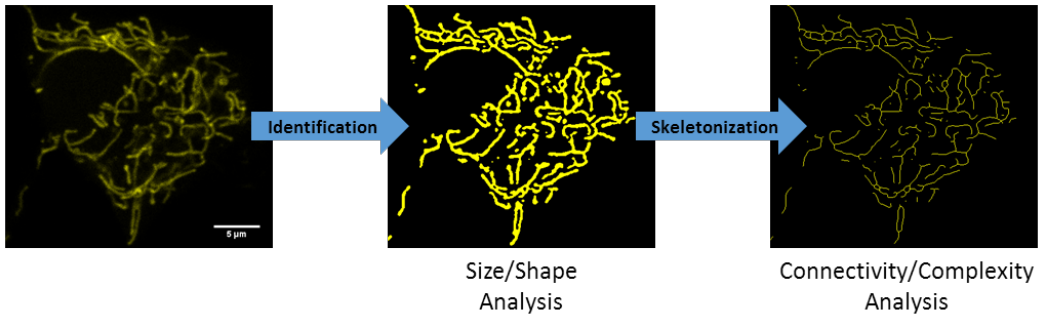

B

Mitochondrial Morphology Quantification Parameters		
SIZE (2D/3D)	**SHAPE (2D/3D)**	**CONNECTIVITY/COMPLEXITY**
Area/Volume	Form Factor/Sphericity	Branches
Perimeter/Surface Area	Aspect Ratio	Total Branch Length
		Branch Junctions

C

Figure 3. Parameters used to quantify mitochondrial morphology and networking. (A) Schematic flow chart of the analysis pipeline. From the raw confocal image, mitochondria were identified using our combination threshold approach for morphological analysis. The mask was then further skeletonized for a quantitative description of network connectivity. (B) Table summarizing the 2D and 3D parameters we used to describe mitochondrial morphology and networking in terms of size, shape and connectivity/complexity. (C) Schematic diagrams illustrating how changes in mitochondrial size, shape and connectivity are reflected in the quantified parameters.

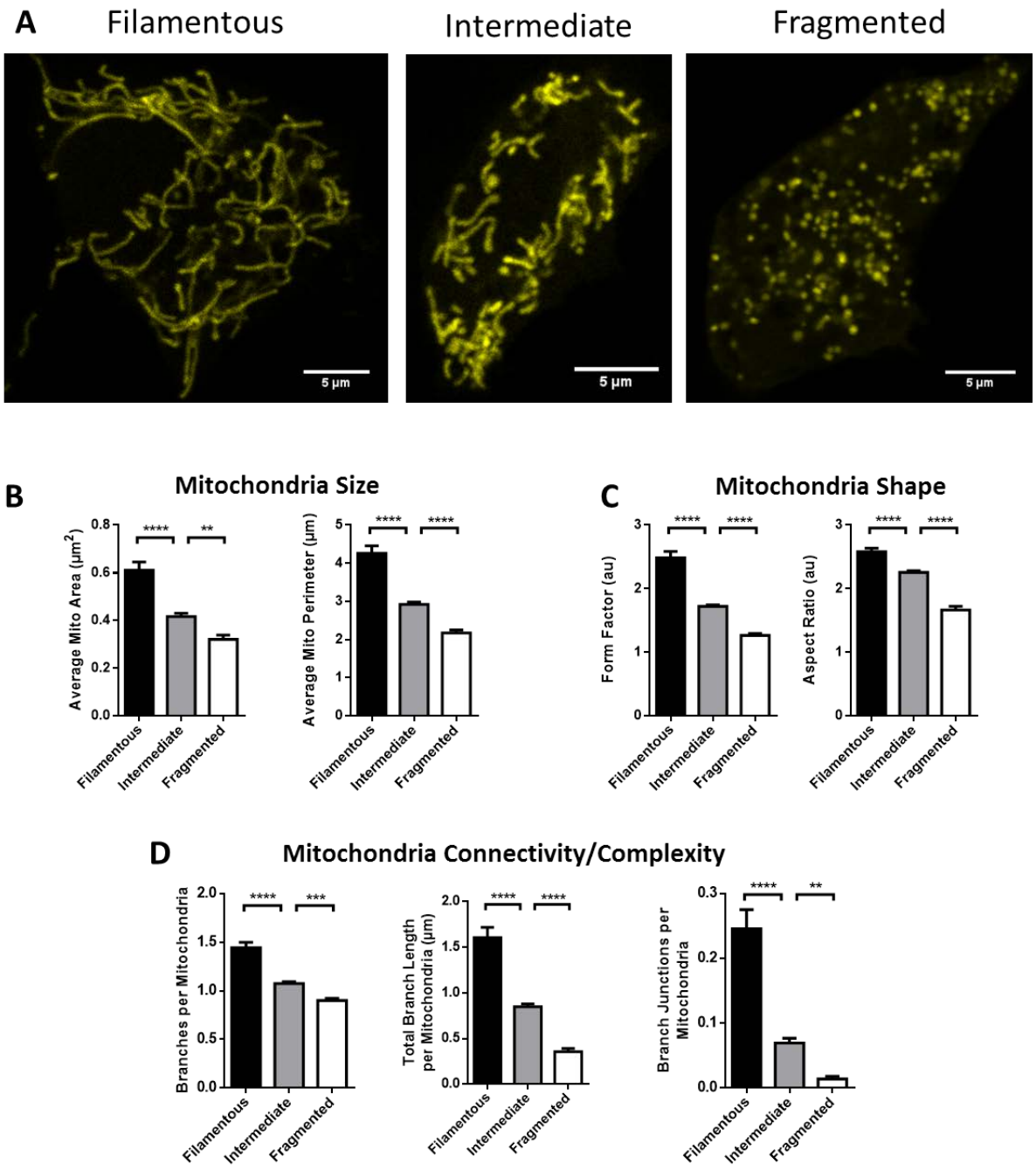

Figure 4. Demonstration of ability to distinguish various mitochondrial morphology types. An image set (84 images) of MIN6 cells that were transfected with Mito-YFP plasmid were manually categorized by visual inspection into 3 morphology types: filamentous, intermediate, and fragmented. (A) Representative images from each morphological category. (B-D) Mitochondria were identified using the combination threshold approach and their morphological parameters quantified and compared between the three morphological groups. (B) Comparison of mitochondrion size parameters (area and perimeter). (C) Comparison of shape parameters (form factor and aspect ratio). (D) Comparison of connectivity/complexity parameters (number of branches, branch length, and branch junctions). (All data are represented by mean ± SEM; *p<0.05, **p<0.01, ***p<0.001, ****p<0.0001 as determined by One-way ANOVA with Sidak post-hoc test; n=84 images total)

3.1.4 Validation of morphometric classifications by unsupervised clustering

To further validate our pipeline for 2D analysis of mitochondrial morphology and structure, we used Spanning-tree Progression Analysis of Density-normalized Events (SPADE) (134) to automatically classify morphology independent of potential human bias (See Chapter 2.11 for additional details). SPADE is an analysis tool often used in flow cytometry to visualize, cluster, and differentiate cell types based on cell markers (134). Rather than using cell type-specific markers, we aimed to cluster and differentiate cells based on their quantified mitochondrial features. A SPADE tree was constructed based on the morphological parameters we derived from the full test set of MIN6 cell images used previously (Figure 5A). Each node in the tree represents a single image in the set (84 images resulting in 84 nodes), and branching in the tree represents the relative resemblance of images based on their morphological parameters. We asked the program to divide these images into 3 groups based on the morphological parameters. Mitochondria in the 3 groups that SPADE distinguished appeared noticeably dissimilar upon visual inspection (Figure 5B). Comparative analysis revealed that the 3 SPADE-identified groups were significantly different from each other in all the morphological parameters (Figure 5C-E). These results suggest that SPADE Subgroups 1, 2 and 3 corresponded to cells with filamentous, intermediate and fragmented mitochondrial morphology, respectively, and this was also evident from the output images (Figure 5B). When comparing the automated SPADE categorization to our manual categorization of the 84 images there was 86% match, and this close agreement is also evident when comparing the results in Figures 4B-D with those in Figures 5C-E. The ability of SPADE to distinguish different morphologies based on our analysis results further supports the validity of our pipeline for 2D analysis of mitochondrial network structure and complexity in pancreatic β-cells.

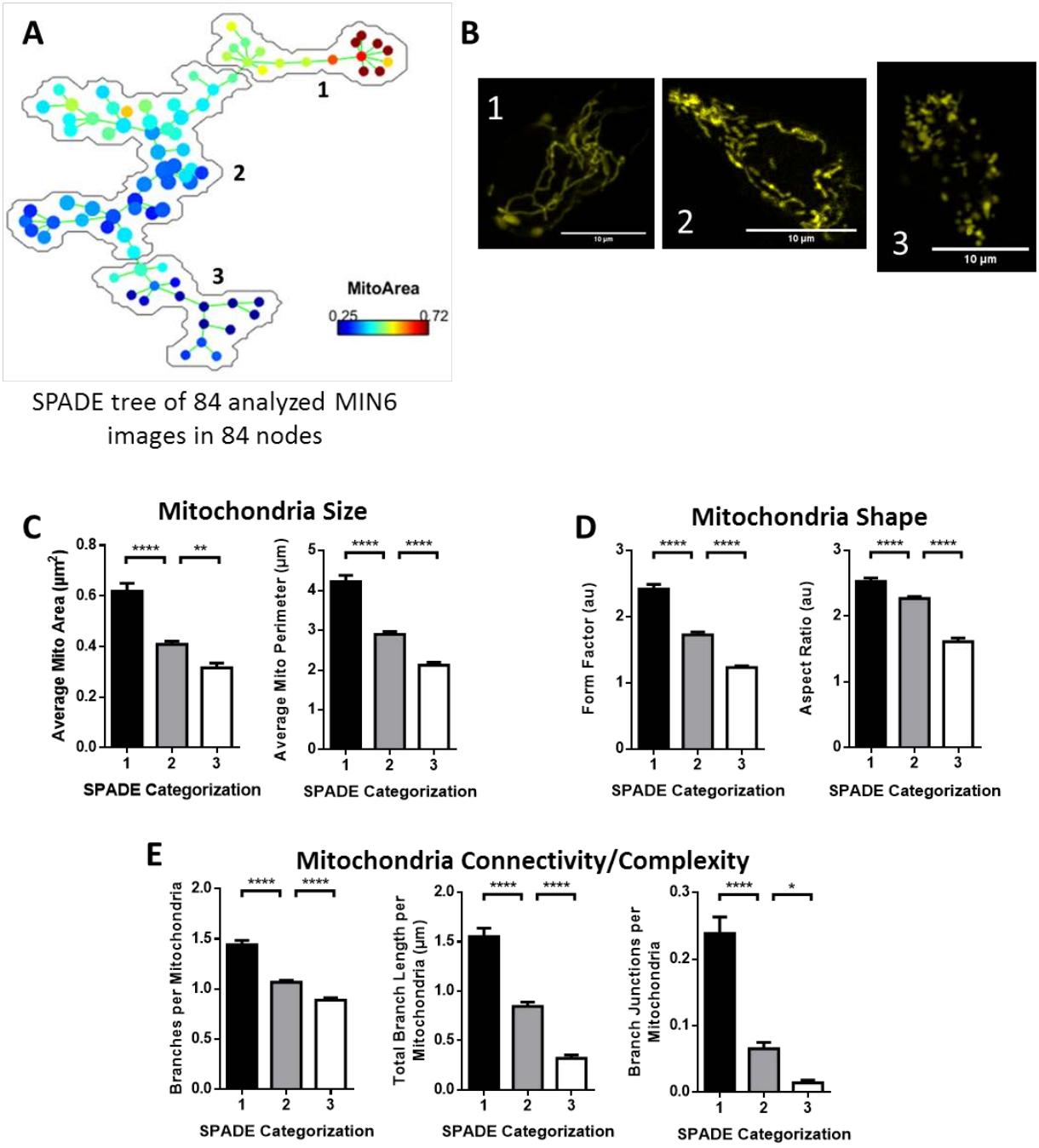

Figure 5. Unsupervised categorization of mitochondrial morphology using SPADE. Spanning-tree Progression Analysis of Density-normalized Events (SPADE) was used to automatically classify mitochondrial images based on their calculated morphological parameters. (A) A SPADE tree was generated using the same image set as in Figure 4 and automatically categorized into 3 groups. Each node in the tree represents a single image (84 images and 84 nodes). Nodes are colour-coded based on the average mitochondrion area. (B) Representative images from each group. (C-E) Comparison of morphological parameters between the 3 SPADE-identified groups: (C) Comparison of mitochondrion size parameters (area and perimeter), (D) Comparison of shape parameters (form factor and aspect ratio). (E) Comparison of connectivity/complexity parameters (branches, branch length, and branch junctions). (All data are represented by mean ± SEM; *p<0.05, **p<0.01, ***p<0.001, ****p<0.0001 as determined by One-way ANOVA with Sidak post-hoc test; n=84 images total)

3.1.5 Physiological glucose stimulation is associated with mitochondrial hyperpolarization and mitochondrial fission in primary islet cells

After validating our ability to detect morphological differences in MIN6 cell mitochondria, we tested if we could detect more subtle changes in the morphology and function (measured simultaneously) in primary islet cells. Dispersed islet cells from male BclxWT control mice (3-6 months old) were cultured in either basal 3mM glucose (3G) or physiologically stimulatory 17mM glucose (17G) for 1 hour. To simultaneously detect changes in mitochondrial morphology and function on a *per mitochondrion* basis we subsequently stained mitochondria with the fluorescent indicators MTG (membrane potential-insensitive) and TMRE (membrane potential-sensitive) for 30 min before imaging (see Section 2.9 for details). Using our mitochondrial analysis pipeline, we used the MTG signal to measure morphology, and as a mask for measuring TMRE intensity (Figure 6A). As expected, cells cultured in 17G had mitochondria with higher TMRE to MTG intensity ratio than 3G (Figure 6B), demonstrating that they are more active and hyperpolarized. Visual inspection of the images (represented by Figure 6A) did not reveal any obvious morphological differences between the cells in low and high glucose. However, our analysis pipeline was able to detect a number of changes. Despite no change in total mitochondrial area, the number of mitochondria increased following glucose stimulation (Figure 6C), suggesting an increase in mitochondrial fission. Accordingly, mitochondria in cells cultured in 17G were significantly smaller (decreased average area and perimeter; Figure 6D), more round (decreased form factor; Figure 6E), and had reduced network complexity (decreased *per mitochondria* branch number, branch points and branch lengths; Figure 6F). Consequently, our analysis pipeline was able to detect subtle physiological changes to mitochondrial morphology and function in primary

islet cells that were not evident by visual inspection. This establishes that it is sufficiently sensitive to be used for quantitative comparison of β-cell mitochondria in physiology and pathophysiology.

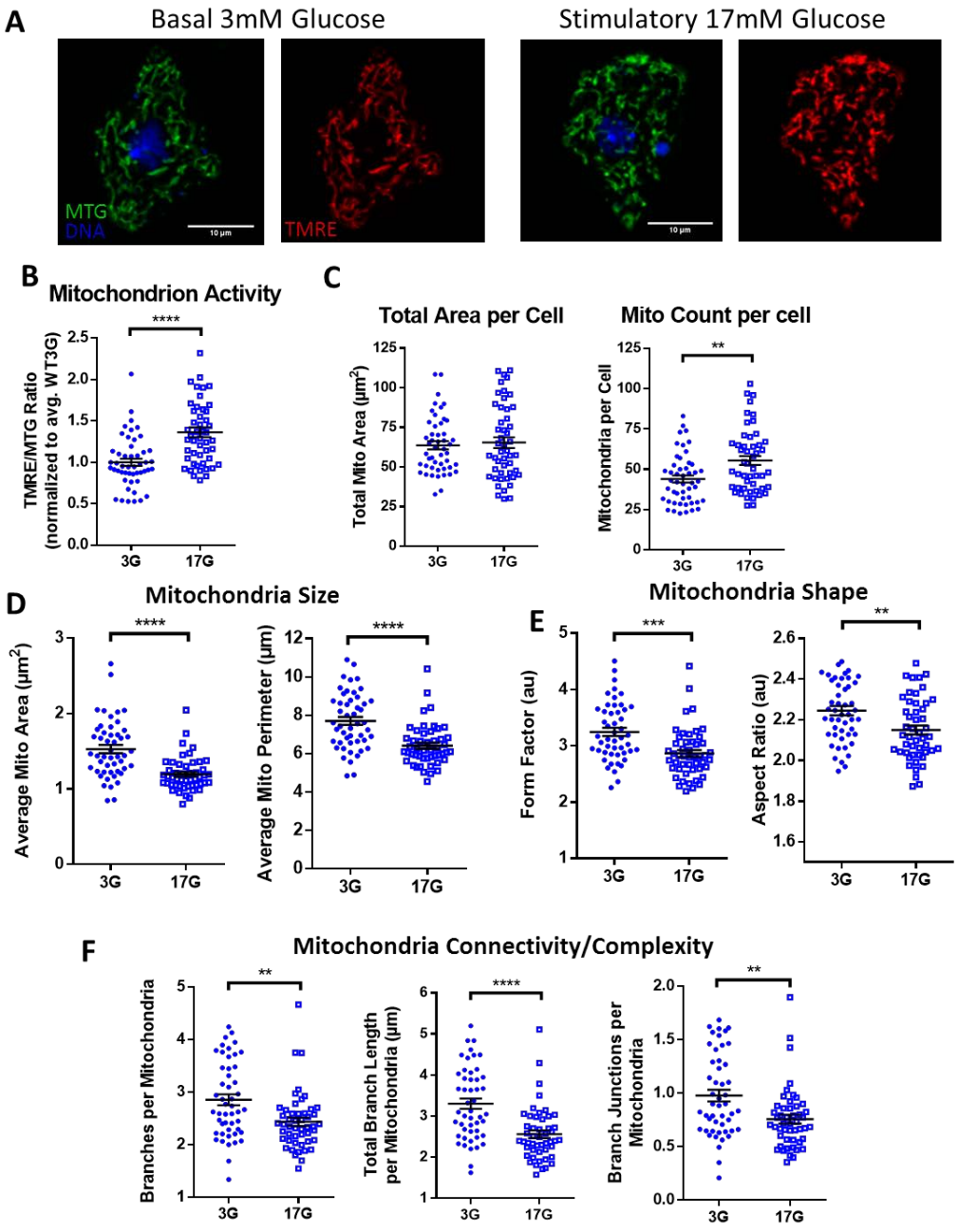

Figure 6. Glucose stimulation is associated with mitochondrial fission in pancreatic islet cells. Primary islet cells isolated from male BclxWT mice were dispersed on coverslips and cultured for 4 days in 11mM glucose. The cells were then treated in either 3mM glucose (3G) or 17mM glucose (17G) for 60 mins. Cells were stained with 0.1μg/mL Hoescht 33342, 50nM MitoTracker Green FM (MTG), and 25nM TMRE for 30 min before imaging. Mitochondrial morphology and polarization were quantified as described in Chapter 2.9. (A) Representative images of MTG and TMRE stained islet cell in 3G and 17G. (B-F) Quantification of confocal images was done in FIJI/ImageJ for the following parameters: (B) Normalized TMRE/MTG ratio (normalized to 3G), (C) Total mitochondrial area and mitochondria count per cell, (D) average mitochondrion size, (E) mitochondrion shape, (F) mitochondrial connectivity/complexity. (All data are represented by mean ± SEM; **p<0.01, ***p<0.001, ****p<0.0001 as determined by Student's t-test; n=49 cells total in each glucose treatment. Cells were obtained from 4 mice and imaged in 4 separate experiments)

3.1.6 Establishing an approach for mitochondrial network analysis in 3D

While our 2D analysis reliably measures mitochondrial morphology in a cross-section, it does not provide a complete picture of the complexity and interconnectedness of the whole network, or allow for direct quantitation of total mitochondrial mass. Total mitochondrial area has been used to estimate mitochondrial mass in neurons and fibroblasts (145, 146), but β-cells are comparatively less flat and therefore more likely to have a distributed 3 dimensional mitochondrial network that spans several mitochondrial layers. To allow precise quantification of total mitochondrial volume and network structure we therefore established another analysis pipeline for 3D. For this, 2D serial sections were acquired at different focal planes through entire cells, with spacing between planes set according to the Nyquist standard (131). To maximize z-resolution, pinhole size was reduced to 0.5AU (for details, see Chapter 2.9). However, even with optimized confocal image acquisition settings each optical slice contains out of focus light from adjacent sections, which compromises accurate 3D rendering of the mitochondrial network. This inherent limitation of raw confocal images can be mitigated by deconvolution; a mathematical process which helps remove background signal and noise (e.g. out-of-focus light). Figure 6A shows a representative comparison of the mitochondrial network in a mito-YFP-expressing MIN6 cell following 3D reconstruction of the raw (left) and deconvolved (right) confocal image stacks. Analysis of the raw 3D reconstruction identified only 6 separate mitochondrial units within the network, while 25 units were identified following deconvolution (Figure 6A). This suggests that elimination of noise and out of focus signal by deconvolution is critical for the software to be able to distinguish individual mitochondrial units.

We next assessed our ability to distinguish and quantify different mitochondrial network morphologies in 3D. We obtained image stacks of Mito-YFP expressing MIN6 cells, and similar

to our 2D analysis, we manually categorized the cells into 3 groups based on their mitochondrial morphology: “fragmented”, “filamentous”, and “intermediate” (Figure 7B). Mitochondria were identified in each slice of the image stack and the “3D Object Counter” function was then used to mathematically map each mitochondrion in 3D space. Quantification by “3D Object Counter” revealed that even if the number of mitochondria per cell differed significantly, the total mitochondrial volume of each cell was constant between the 3 groups (Figure 7C). This indicates that significant morphological heterogeneity can occur independent of changes to mitochondrial mass. As in our 2D analysis, the number of mitochondria per cell progressively increased from filamentous to intermediate to fragmented morphologies (Figure 7C), while the average mitochondrial volume decreased (Figure 7D). Skeletonization of the 3D network revealed that the number of branches and branch junctions also decreased, illustrating that mitochondrial fragmentation, not surprisingly, is associated with a reduction in overall network complexity (Figure 7E). Together, this demonstrates that we are able to measure mitochondrial volume and classify differences in 3D mitochondrial network morphology based on the acquisition and deconvolution of an optimized image stack, followed by reconstruction and analysis of the entire mitochondrial network.

In summary, we have established robust pipelines for confocal imaging and analysis of mitochondrial structure in pancreatic β-cells in both 2D and 3D. These analysis pipelines were next used to study if Bcl-x_L has potential roles in regulating mitochondrial morphogenesis and mass in β-cells.

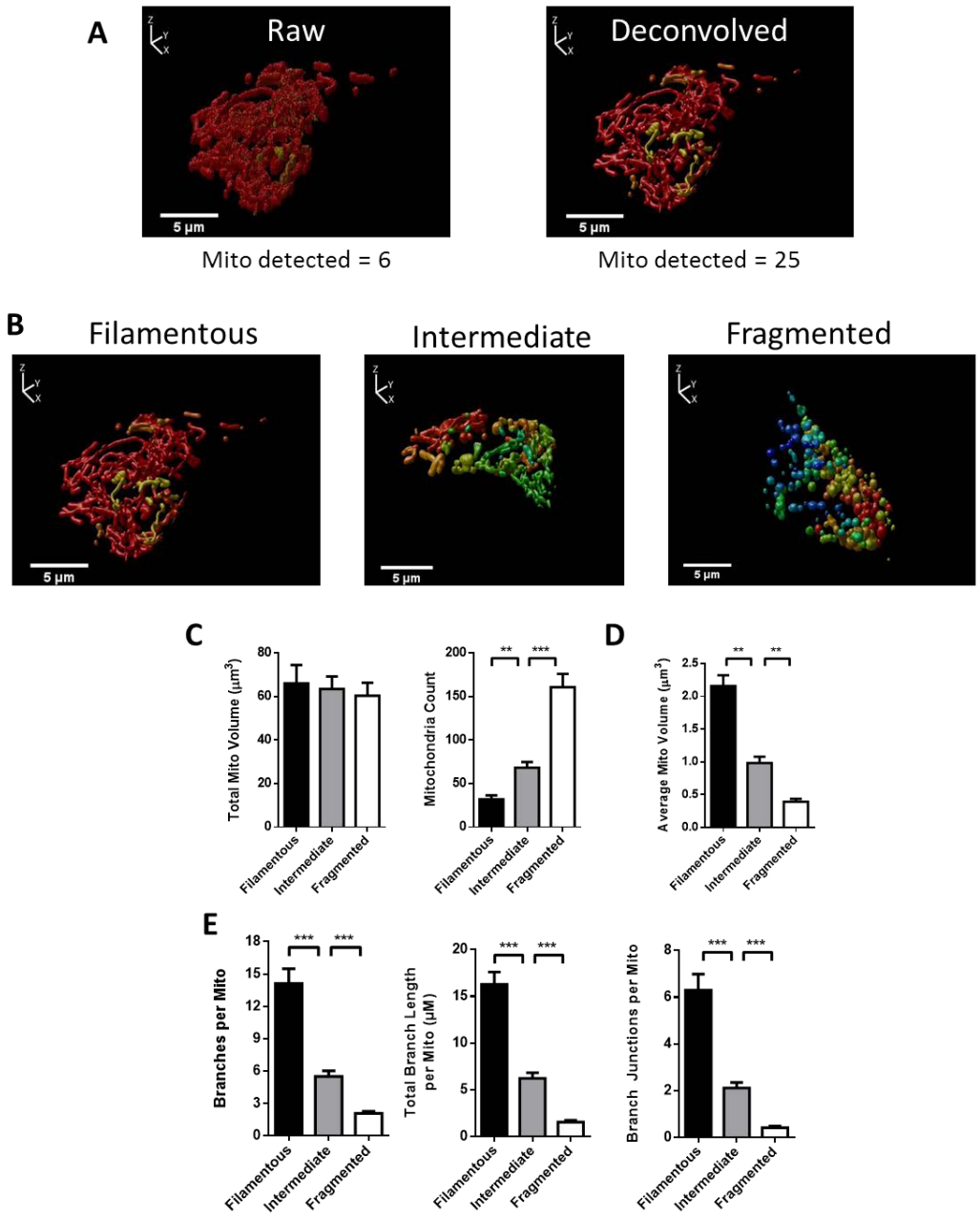

Figure 7. Importance of deconvolution and verification of 3D analysis. MIN6 cells transfected with Mito-YFP plasmid were imaged under optimal Nyquist criterion over several z-planes to form image stacks of the full mitochondrial network. (A) Side-by-side comparison of 3D reconstruction based on the raw image stack prior to deconvolution versus the same image stack after deconvolution. Deconvolution was performed using Huygens Essential software. (B) Representative 3D reconstructions of mitochondrial networks with 3 manually-identified morphological types: filamentous, intermediate, and fragmented. Each mitochondrial network is represented by a different colour. (C-E) The mitochondria in these image stacks were quantified with FIJI/ImageJ (see Chapter 2.10 for details) and compared between morphological groups for the following 3D parameters: (C) total mitochondrial volume and mitochondria count, (D) average mitochondrion volume, and (E) mitochondrial connectivity/complexity (branches, branch length, and branch junctions). (All data are represented by mean ± SEM; **p<0.01, ***p<0.001, ****p<0.0001 as determined by One-way ANOVA with Sidak post-hoc test; n=9-10 cells in each group; imaged from 2 independent experiments)

3.2 Role of Bcl-x_L in mitochondrial morphology and function in islet cells

3.2.1 Overexpression of Bcl-x_L alters the morphology, reduces the volume and impairs the function of β-cell mitochondria

To study the roles of Bcl-x_L in β-cell mitochondrial physiology and morphology, we first tested the effects of Bcl-x_L gain-of-function (GOF). We overexpressed eYFP-tagged Bcl-x_L (Bcl-x_L-YFP) under the CMV promoter using an adenovirus vector (Ad.Bcl-x_L-YFP) at MOI of 10 in MIN6 cells, which resulted in Bcl-x_L mRNA levels that were ~190 fold higher than the control cells transduced with Ad.GFP (Figure 8A). We compared the mitochondrial morphology in transfected cells expressing Bcl-x_L-YFP to cells expressing a mitochondria-targeted eYFP (Mito-YFP) control, and observed that 24 hours following Bcl-x_L overexpression the mitochondrial network had lost its normal tubular structure and converged into a single clump (Figure 8B). This effect was also seen in primary islet cells following transduction with Ad.Bcl-x_L-YFP (MOI=10) and mitochondrial co-staining revealed that Bcl-x_L-YFP strongly co-localizes with the mitochondrial aggregates (Figure 8C). We further explored this phenomenon by tracking Bcl-x_L overexpressing MIN6 cells for 24 hours following transfection using a high-content imaging system. As exemplified in Figure 8D, the Bcl-x_L overexpressing cells maintained normal dispersed mitochondrial structures 5 hours after transfection. However, as time went on, the mitochondria progressively aggregated until the entire mitochondrial network consisted of one or two immobile clusters after approximately 10-12 hours (Figure 8D). To determine if this striking change in morphology is associated with changes to mitochondrial mass, we performed stack confocal imaging, reconstructed the mitochondrial network in 3D, and measured its volume. Interestingly, Bcl-x_L overexpression significantly decreased the total mitochondrial volume compared to Mito-YFP (Figure 8E). To further investigate this, we used western blot to probe for protein translocase

of outer membrane 20 (TOM20), an often used surrogate marker of mitochondrial mass (Figure 8F). Semi-quantitative analysis of band densities showed that Bcl-x_L-YFP overexpression was associated with a very strong trend toward decreased TOM20 protein levels (Figure 8G, p=0.061). Finally, mitochondrial function was assessed using the Seahorse MitoStress Assay. Bcl-x_L overexpression resulted in decreased oxygen consumption rate in response to glucose stimulation (25mM), as well as a decrease in the maximum respiratory capacity achieved following mitochondrial uncoupling with FCCP (Figure 8H). Together, these results demonstrate that high levels of Bcl-x_L induce metabolic β-cell dysfunction that is associated with drastic perturbations of mitochondrial morphology and a reduction in total mitochondrial volume. Our findings agree with previous reports that transgenic overexpression of Bcl-x_L impairs β-cell function and glucose metabolism in mice (120), and provide new insights into the underlying sub-cellular defects.

To further characterize the effects of Bcl-x_L overexpression on mitochondrial physiology and dynamics, we analyzed the expression of genes involved with mitochondrial fission, fusion, biogenesis, and stress. Specifically, we examined the levels of *Drp1* and *Fis1* that control mitochondrial fission (Figure 9A), *Mfn1/2* and *Opa1* that control mitochondrial fusion (Figure 9B), *Pgc-1α* and *Tfam* that regulate mitochondrial biogenesis (Figure 9C), and lastly *Nfe2l2*, *Ucp2*, *Hmox1* and *MnSod* that are all part of the cellular anti-oxidant response (Figure 9D). Following Bcl-x_L overexpression in MIN6 cells (Ad.Bcl-xL-YFP; MOI=10), *Fis1* was significantly increased compared to control (p=0.003 Figure 9A), *Opa1* trended towards increased levels (p=0.08 Figure 9B) and *Hmox1* expression was significantly decreased (p=0.02 Figure 8D). Overall, these gene expression results suggest that either Bcl-x_L and/or the mitochondrial consequences of Bcl-x_L overexpression may alter the transcription of genes involved with mitochondrial fusion, fission, and antioxidant response.

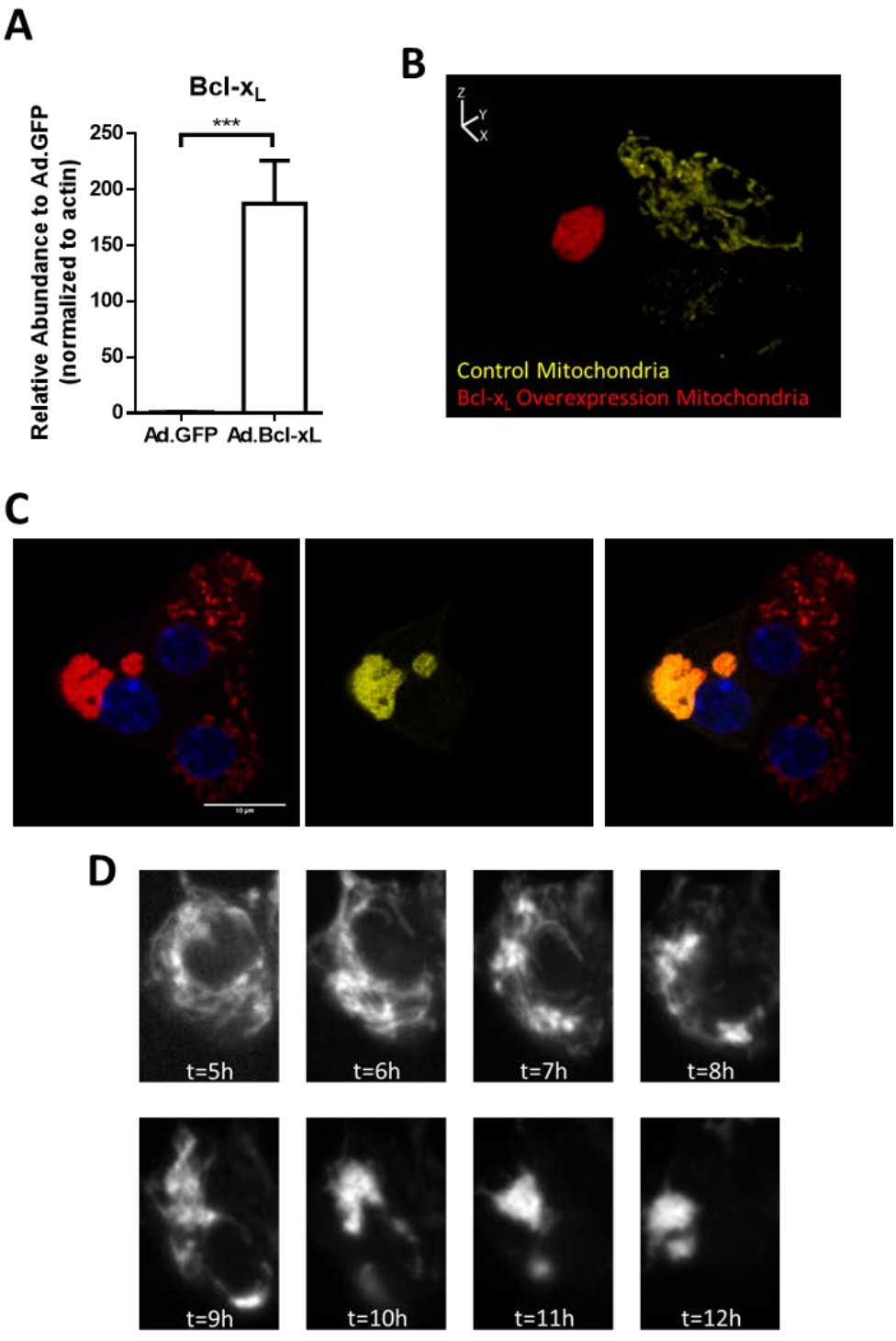
A
Bcl-x$_L$
***
Relative Abundance to Ad.GFP (normalized to actin)
250
200
150
100
50
0
Ad.GFP
Ad.Bcl-xL
B
Z
Y
X
Control Mitochondria
Bcl-x$_L$ Overexpression Mitochondria
C
D
t=5h
t=6h
t=7h
t=8h
t=9h
t=10h
t=11h
t=12h

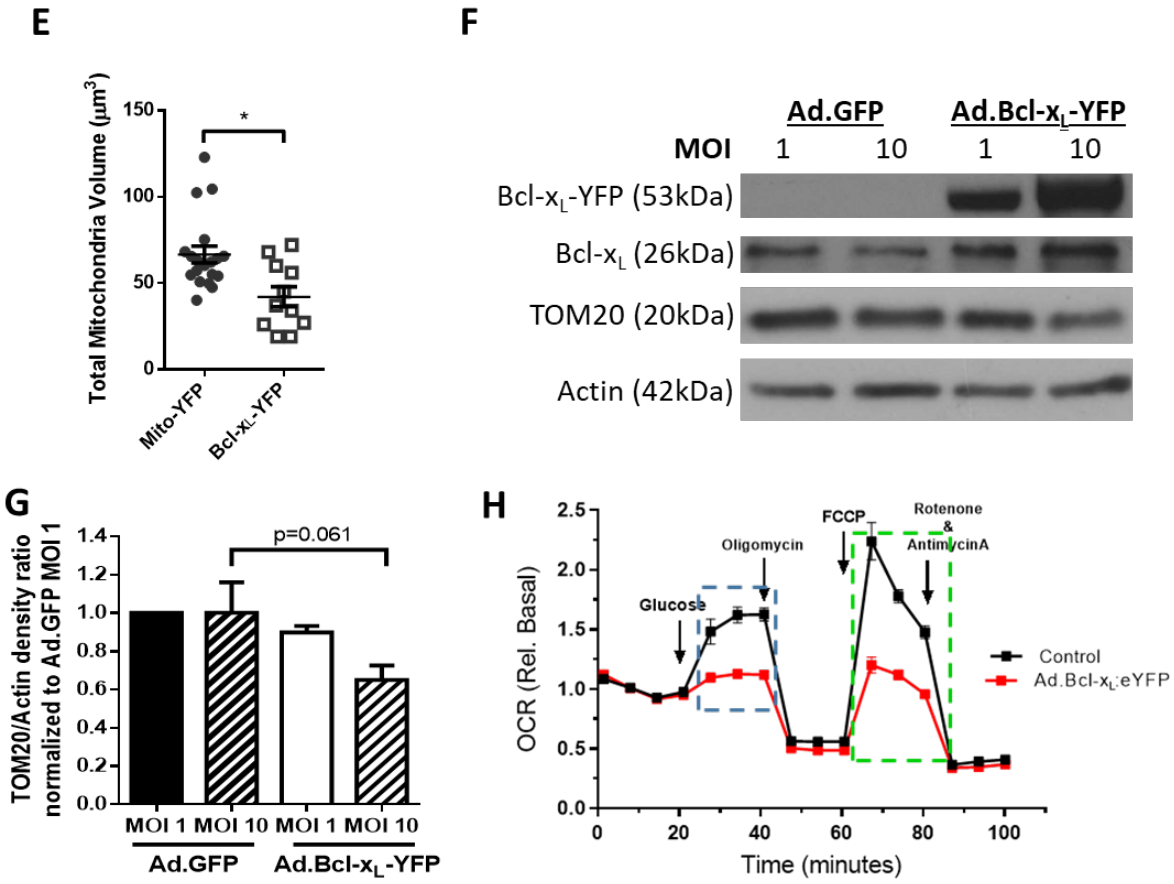

Figure 8. Effects of Bcl-x_L overexpression on mitochondrial morphology, volume, and function in β-cells. (A) *Bcl-x_L* mRNA levels in MIN6 cells transduced with either Ad.Bcl-x_L-YFP (MOI=10) or control Ad.GFP (MOI=10) for 24 hours. (***p<0.001 as determined with Ratio Paired t-test; n=7 experiments). Beta-actin was used as the housekeeping gene. (B) Representative 3D image of aggregated mitochondria structure in a MIN6 cell following Bcl-x_L overexpression (red) and a neighbouring control cell with the normal tubular mitochondrial structure (yellow). Images were taken 24 hours after transfection. (C) Representative image of a cluster of 3 primary cells; one transduced with Ad.Bcl-x_L-YFP (MOI=10) and two neighbouring un-transduced cells. Mitochondria were visualized by MitoTracker Deep Red staining. (D) Representative time-lapse images of mitochondrial structure in MIN6 cells following Bcl-x_L overexpression (4 hours to 12 hours post transfection). Image brightness and contrast were enhanced to highlight the mitochondrial structure at earlier time points. (E) Quantification and comparison of total mitochondrial volume in Bcl-x_L-YFP and mito-YFP expressing MIN6 cells 24 hours after transfection (* p<0.05 as determined with Student's t-test; n=12-16 cells). (F) Representative western blot for Bcl-x_L and TOM20 levels in MIN6 transduced with Ad.GFP and Ad.Bcl-x_L-YFP (MOI=1 and 10). Beta-actin was used as the loading control. Note that due to large differences in expression, exposure times for Bcl-x_L-YFP and endogenous Bcl-x_L were adjusted separately and band densities cannot be directly compared. (G) Quantification of western blot TOM20 density relative to actin. Band densitometry was analysed with FIJI/ImageJ (p-values were calculated using Ratio-Paired t-test; n=4). (H) Preliminary Seahorse MitoStress Assay analysis of mitochondrial respiration in primary dispersed islet cells 24 hours following transduction with Ad.Bcl-x_L-YFP. Oxygen consumption rate (OCR) following 25mM glucose stimulation (blue box) and the maximal respiratory capacity (green box) induced by FCCP treatment were decreased in Bcl-x_L overexpressing cells compared to the control. (All data are represented by mean ± SEM)

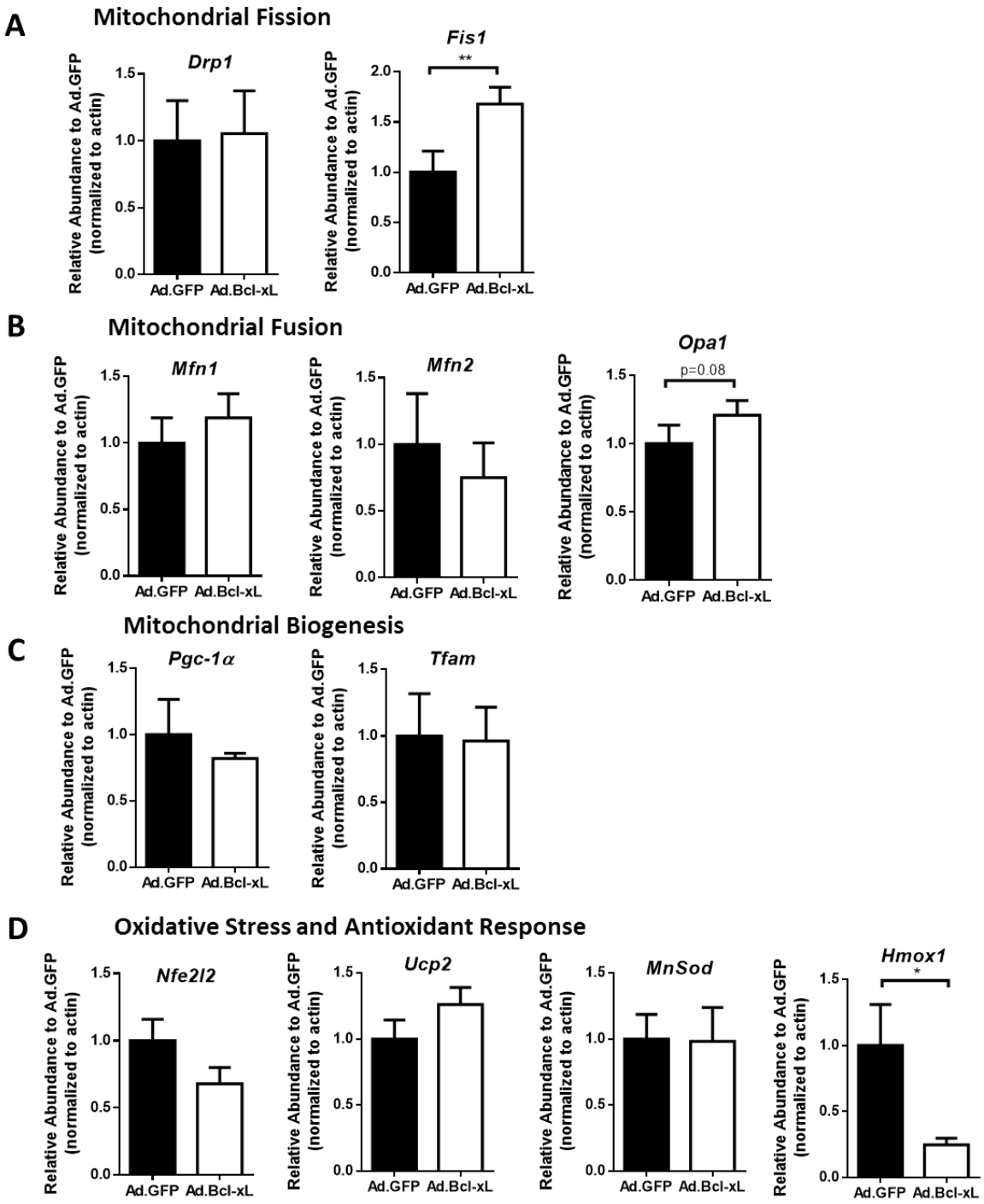

Figure 9. Effect of Bcl-x_L overexpression on the expression of genes involved with mitochondrial fission, fusion, biogenesis, and oxidative stress in MIN6 cells. MIN6 cells were transduced with Ad.Bcl-x_L-YFP (MOI=10) or control Ad.GFP (MOI=10) and relative mRNA levels compared by qPCR. Beta-actin was used as the housekeeping gene. (A-D) Relative expression levels of selected genes involved with (A) mitochondrial fission (*Drp1* and *Fis1*), (B) mitochondrial fusion (*Mfn1*, *Mfn2*, and *Opa1*), (C) mitochondrial biogenesis (*Pgc-1α* and *Tfam*), and (D) oxidative stress and antioxidant response (*Nfe2l2*, *Ucp2*, *MnSod*, and *Hmox1*). (All data are represented by mean ± SEM; **p<0.01 as calculated using Ratio Paired t-test; n=7 experimental replicates)

3.2.2 Pharmacological Bcl-2/Bcl-x_L inhibition fragments β-cell mitochondria

Because the outcome of Bcl-x_L overexpression does not necessarily reflect the normal roles of the endogenous protein, we next studied the effects of Bcl-x_L loss-of-function (LOF) on mitochondrial morphology. As a first step, we pharmacologically inhibited endogenous Bcl-x_L in Mito-YFP expressing MIN6 cells using Compound 6 (C6); a small molecule that antagonizes both Bcl-2 and Bcl-x_L (147). We have previously shown that Bcl inhibition with C6 acutely (within minutes) increases mitochondrial activity and activate K_{ATP}-dependent Ca^{2+} influx in β-cells (121). In contrast to these rapid physiological effects, more sustained Bcl inhibition (> 1 hour) initiates ROS-dependent β-cell apoptosis (121, 136). Using our mitochondrial analysis pipeline, we now found that mitochondria of C6-treated β-cells became increasingly fragmented over time (Figure 10A). After 4 hours C6 treatment they had decreased sharply in size as represented by a decrease in average area and perimeter (Figure 10C); were rounder with a decrease in form factor (FF) and aspect ratio (AR) (Figure 10D); and were less morphologically complex with significantly fewer branches, reduced branch length and fewer branch junctions (Figure 10E). These overall effects suggest that combined inhibition of Bcl-x_L and Bcl-2 function relatively quickly promotes a mitochondrial fragmentation morphology (refer to Section 3.1.3).

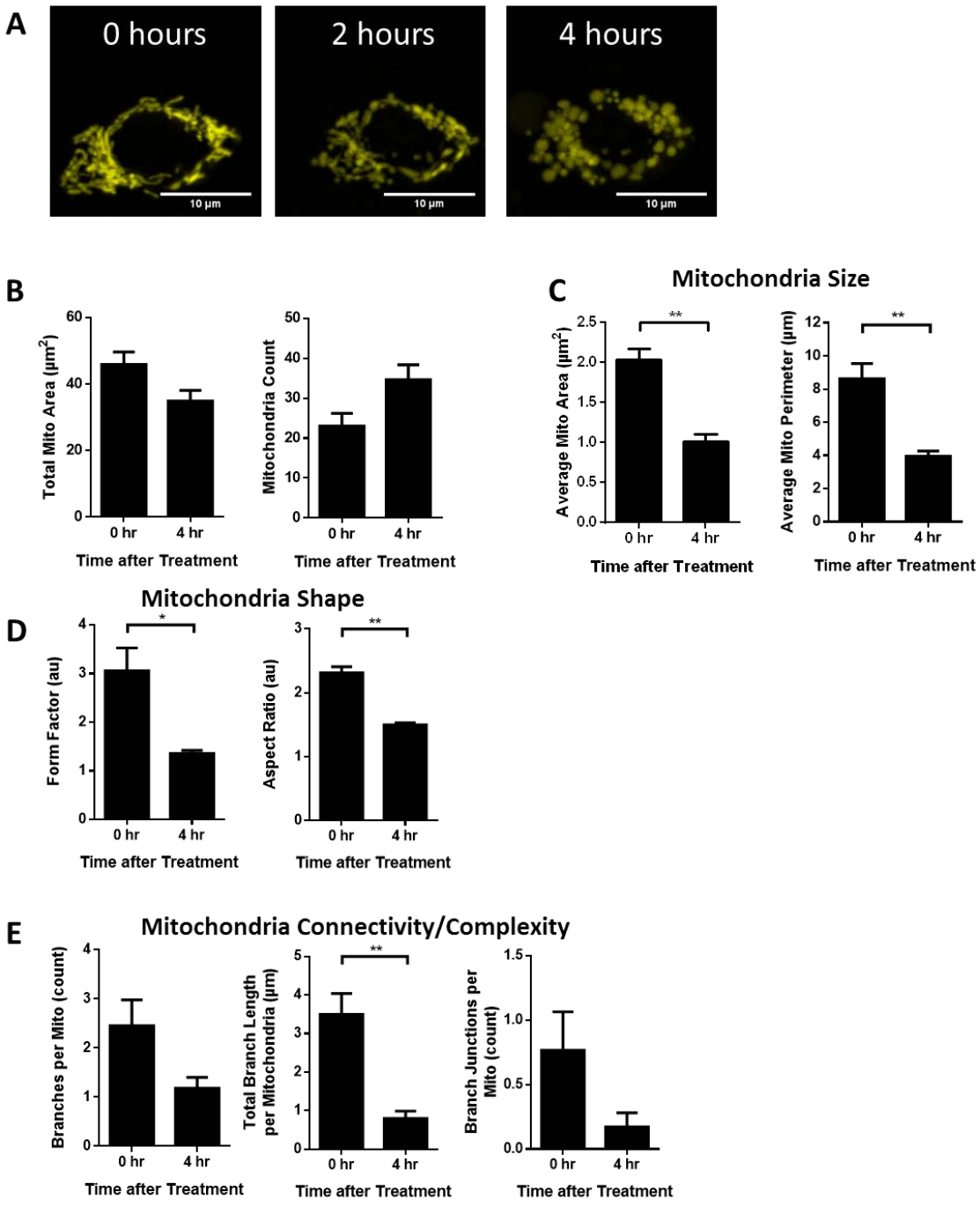

Figure 10. Bcl-x_L inhibition by Compound 6 (C6) alters mitochondrial morphology in MIN6 cells. (A) Representative images showing progressive mitochondrial fragmentation in a mito-YFP-expressing MIN6 cell treated with 40µM C6 for 0, 2, or 4 hours. (B) Total mitochondrial area and count, (C) mitochondrial size, (D) mitochondrial shape, and (E) mitochondrial connectivity/complexity were quantified and compared between 0 and 4 hours C6 treatment. (All data are represented by mean ± SEM; *p<0.05, **p<0.01 as calculated by Student's t-test; n=3 cells)

3.2.3 Loss of Bcl-x_L alters mitochondrial morphology and function in islet cells from aged female mice

To more specifically study the effect of Bcl-x_L LOF, we examined our previously-established mice with tamoxifen-inducible conditional deletion of Bcl-x_L in their β-cells (BclxβKO) (121). In all experiments the expected deletion of Bcl-x_L was confirmed by qPCR analysis of aliquots from the islet preparations (data not shown).

The effect of Bcl-x_L knockout on mitochondrial morphology and function was first studied in islets cells from aged female BclxβKO and BclxWT mice (12-14 months old). Using our combined MTG-TMRE assay (refer to Section 3.1.5), we again found that islet cells responded to stimulatory glucose with mitochondrial hyperpolarization, combined with a fragmentation that was morphologically characterized by smaller size, increased rounding and reduced network complexity (Figure 11). In these aged mice, Bcl-x_L knockout did not affect total mitochondrial count and network area (Figure 11B&C). Notably, however, BclxβKO cells had mitochondria that on average were significantly smaller and more active in basal (3mM) glucose, but in stimulatory glucose (17mM) the polarization and size of BclxβkO and BclxWT mitochondria were no different (Figures 11D&E). Loss of Bcl-x_L thus promotes more basally active mitochondria, with a morphological profile that possibly resembles the response to a modest glucose stimulation. This effect was even more evident when we quantified the difference in mitochondrial responses between 3mM and 17mM glucose (Δ3G→17G). As shown in Figures 11D,E&G deletion of Bcl-x_L resulted in significantly lower values of this 'stimulation index' for mitochondrial activity (ΔTMRE/MTG), size (ΔMean mito area), and network complexity (ΔBranches per mito). Glucose-induced changes in mitochondrial shape (ΔFF), however, did not differ significantly between the two genotypes (Figure 11F, right).

Quantitative PCR analysis of islets from these mice revealed no genotype-dependent differences in the expression of genes involved with mitochondrial fission, fusion, and oxidative stress (Figure 12A,B&D). However, *Pgc-1a* mRNA levels were significantly increased in BclxβKO islets, suggesting that loss of Bcl-x_L may affect pathways that regulate mitochondrial biogenesis (Figure 12C). To further investigate this possibility, we performed additional 3D analysis of mitochondrial structure and volume in islet cells from these mice. 3D network reconstruction and quantification did not reveal significant differences in their mitochondria (Figure 13), but there was very notable trend toward a decrease in total mitochondrial volume in BclxβKO islet cells (Figure 13B, p=0.052), which hints at possible effects on mitochondrial biomass.

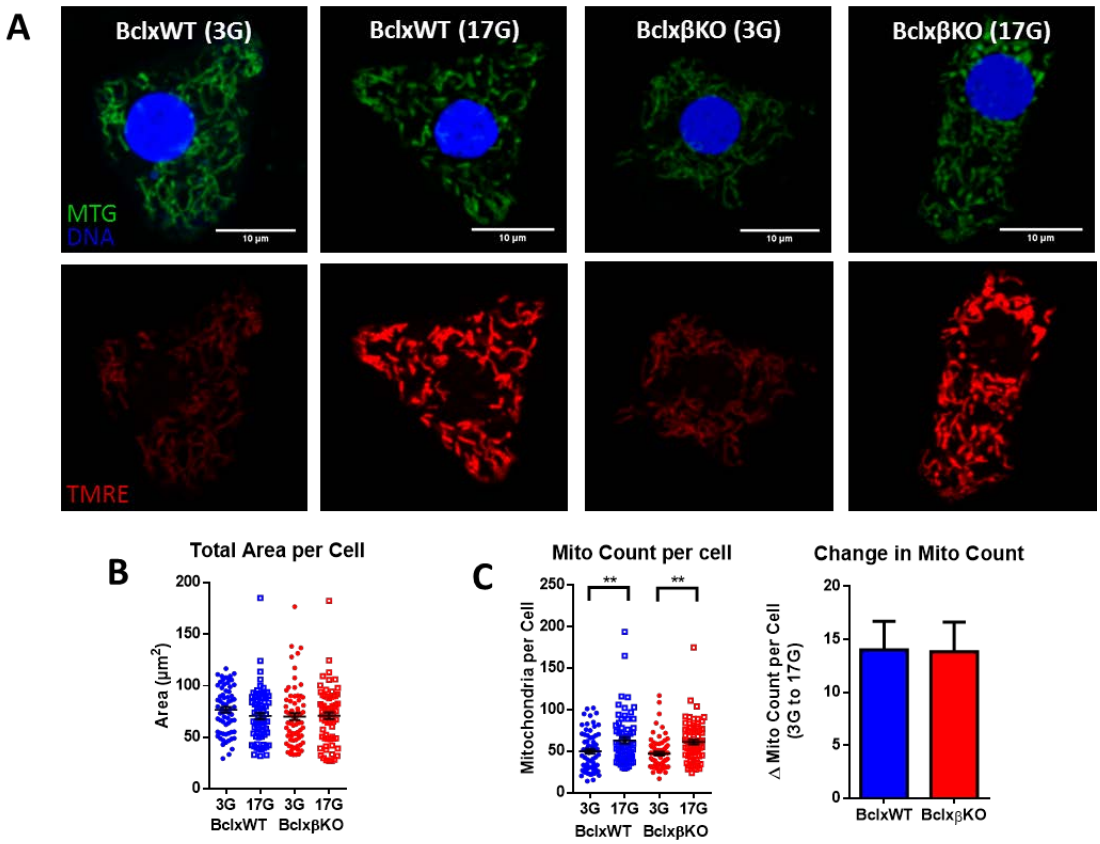

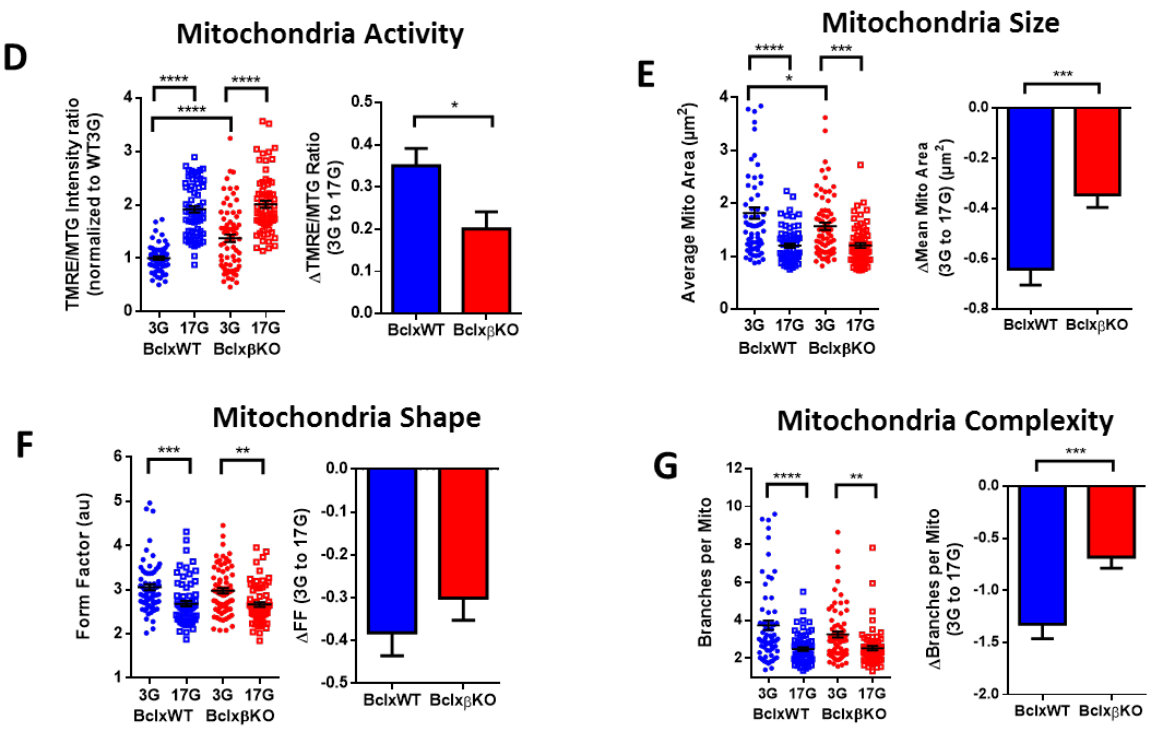

Figure 11 Comparison of mitochondrial morphology and function in BclxWT and BclxβKO β-cells from aged mice. Primary islet cells from 12-14 months old female BclxWT and BclxβKO mice were seeded on coverslips and cultured for 4 days in 11mM glucose. Cells were stained with 0.1µg/mL Hoescht 33342, 50nM MitoTracker Green FM (MTG), and 25nM TMRE for 30 min before imaging. (A) Representative images of mitochondrial morphology and TMRE staining in BclxWT and BclxβKO islet cells treated with either 3mM glucose (3G) or 17mM glucose (17G) for 1 hour. Quantification and Δ3G→17G analysis of confocal images were performed in FIJI/ImageJ for the following parameters: (B) Total mitochondrial area per cell, (C) mitochondria count per cell, (D) normalized TMRE/MTG ratio (normalized to 3G), (E) average mitochondrion area, (F) form factor, and (G) branch number. (All data are represented by mean ± SEM; *p<0.05, **p<0.01, ***p<0.001, ****p<0.0001 as determined by One-way ANOVA with Sidak post-hoc test; n=66-72 images total in each glucose treatment. Cell were obtained from 5 mice of each genotype and imaged in 5 separate experiments)

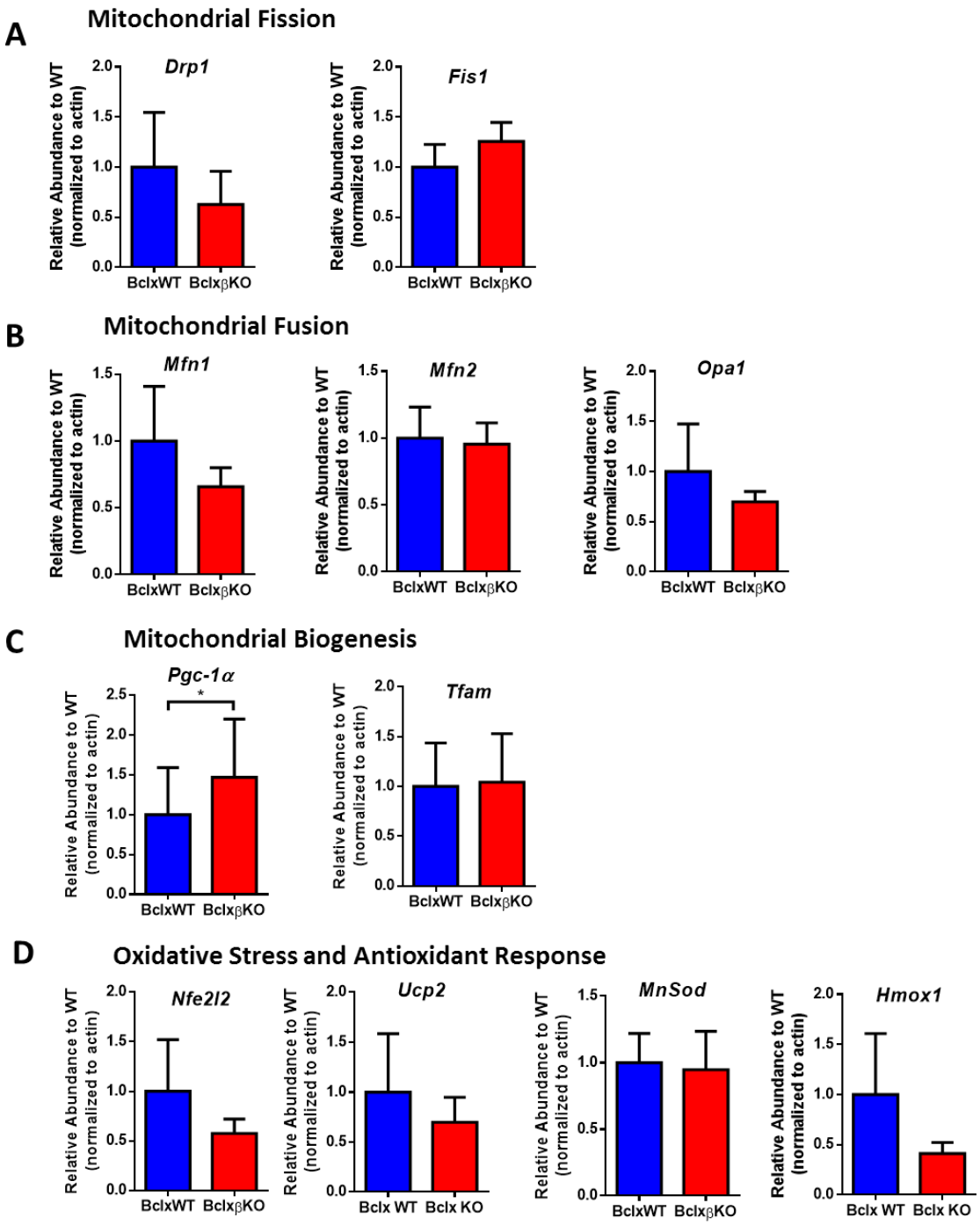

Figure 12. Effect of Bcl-x_L knockout on the expression of genes involved with mitochondrial fission, fusion, biogenesis, and oxidative stress in primary islet cells from aged mice. Islets from 12-14 months old female BclxWT and BclxβKO mice were compared by qPCR for the relative expression of selected genes involved with (A) mitochondrial fission (*Drp1* and *Fis1*), (B) mitochondrial fusion (*Mfn1*, *Mfn2*, and *Opa1*), (C) mitochondrial biogenesis (*Pgc-1α* and *Tfam*), and (D) oxidative stress and antioxidant response (*Nfe2l2*, *Ucp2*, *MnSod*, and *Hmox1*). RNA was extracted 24 hours after isolation. (All data are represented by mean ± SEM; *p<0.05 as determined by Ratio Paired t-test; n=7 experimental replicates)

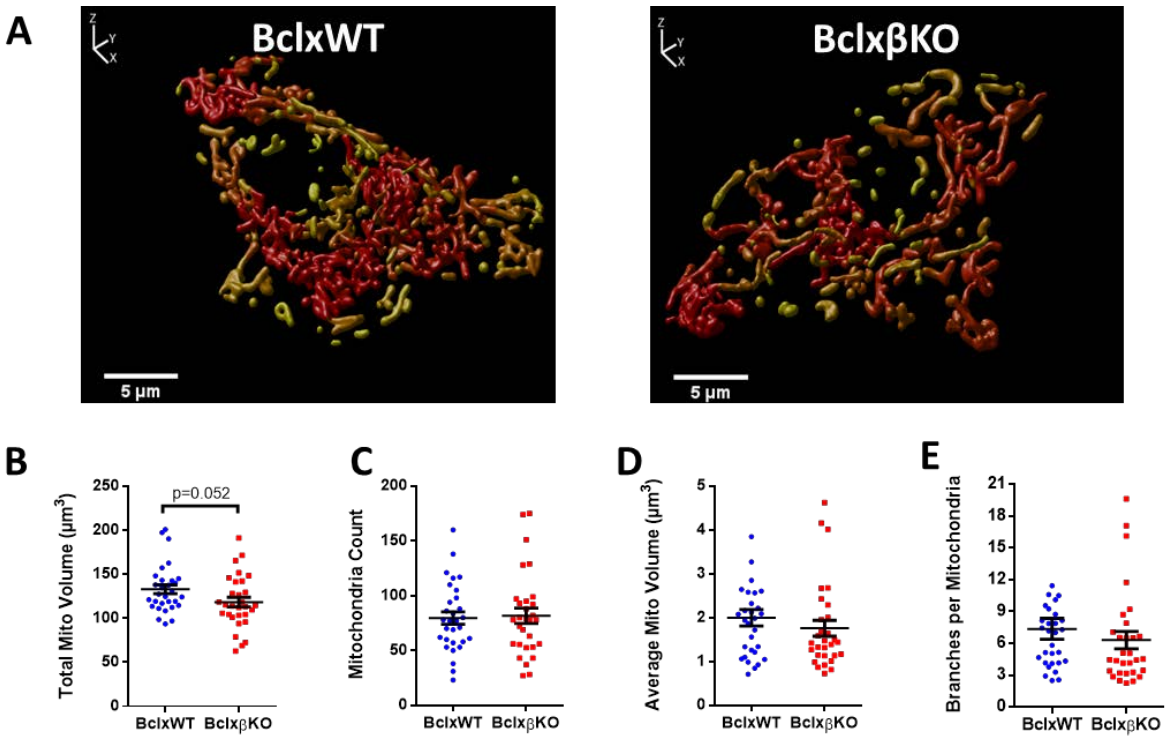

Figure 13. Effect of Bcl-x_L knockout total mitochondrial volume and 3D structure in islet cells from aged mice. Pancreatic islet cells from 12-14 months old female BclxWT and BclxβKO mice were dispersed onto coverslips and cultured for 4 days. The cells were then stained with 0.1µg/mL Hoescht 33342 and 50nM MitoTracker Deep Red FM for 30 min prior to imaging. Mitochondrial volume and structure were quantified as described previously. Deconvolution was performed in Huygens Essential software. (A) Representative 3D reconstruction images of the mitochondrial network in BclxWT and BclxβKO islet cells. Each mitochondria in the network is represented by a different colour. (B-E) Quantification of 3D reconstructed image stacks using FIJI/ImageJ for the following parameters: (B) Total mitochondrial volume, (C) mitochondria count per cell, (D) average mitochondrion volume, and (E) average mitochondrial branch number. (All data are represented by mean ± SEM; p-values were calculated using One-way ANOVA with Sidak post-hoc test; n=30 image stacks from 3 mice of each genotype)

3.3 Role of Bcl-x_L in islet cell adaptation to prolonged high glucose challenge

3.3.1 Loss of Bcl-x_L and prolonged exposure to high glucose alter the activity, morphology, and morphological plasticity of islet cell mitochondria

Prolonged *in vitro* exposure to high glucose has been shown to increase basal cytosolic calcium levels and insulin secretion from rodent islets (45, 148, 149), and similar functional changes are seen in β-cells from pre-diabetic *ob/ob* mice (150). Both *in vitro* and *ex vivo*, this was associated with enhanced β-cell metabolism and sensitivity to glucose (45, 149, 150). In our lab, it was also previously observed that islets cultured for 6 days in 25mM glucose did not yet demonstrate signs of overt glucotoxicity (148), in which insulin secretion and expression of key transcription factors are lost (151); rather, the islets showed elevated Ca^{2+} levels basally and were unable to return to baseline levels after a glucose stimulation, which would be compatible with enhanced metabolic activity. To further clarify the effects of prolonged high glucose exposure on β-cell mitochondrial function and dynamics, and to determine the importance of Bcl-x_L under these conditions, we now pre-cultured islets cells from male BclxβKO and BclxWT mice (4-6 month old) in normal glucose (NG, 11mM glucose) or high glucose (HG, 25mM glucose) for 6 days. After NG/HG pre-culture, we exposed islets cells short-term to 3mM (3G) and 17mM (17G) glucose and performed simultaneous 2D *per mitochondria* analysis of morphology and function. In BclxWT islet cells, HG pre-culture increased basal mitochondrial activity in low glucose, but had no effect on mitochondrial polarization in stimulatory glucose (Figure 14A). Interestingly, the basal mitochondrial polarization of BclxβKO islet cells pre-cultured in NG was as high as in BclxWT cells challenged with HG pre-culture (Figure 14A), and this basal hyperactivity of BclxβKO mitochondria was not further increased by HG pre-culture. Rather, BclxβKO cells responded to HG pre-culture with impaired mitochondrial polarization in 17G (Figure 14A). This

suggests that loss of Bcl-x_L in itself may induce basal islet cell mitochondrial hyper-activity, similar to what is normally seen following a prolonged glucose challenge. Metabolically pushing these already hyper-metabolic Bcl-x_L-deficient islet cells may possibly induce a faster progression from mitochondrial adaptation toward mitochondrial dysfunction.

Along with the above effects on mitochondrial activity, 6 days HG pre-culture induced significant increases in total mitochondria area, average mitochondrial size, form factor, and complexity in both BclxWT and BclxβKO islet cells, suggesting that the challenge of a HG pre-culture promotes a larger and more connected mitochondrial network (Fig 14B-E). In partial agreement with our results in Figure 11, the NG pre-cultured cells showed notable trends toward a fragmented morphology (decreased average area, form factor and complexity) in 17G compared to 3G, and there was a trend toward a basal fragmentation morphology in BclxβKO cells compared to BclxWT (Figure 14C-E). Here, however, none of these differences reached statistical significance, which we believe may be due to the increased cell culture time. Of note, these morphological differences between 3G and 17G were reduced even further in BclxWT cells after HG pre-culture, and were almost completely absent in the HG pre-cultured BclxβKO cells. This is most evident from the calculated Δ values (Figure 14C-E, right panels). Together, these results agree with previous reports that prolonged exposure of β-cells to elevated glucose increases their basal metabolic activity and dampens metabolic responsiveness to subsequent short-term glucose stimulation (45, 149). Our data further reveal that this is associated with significant changes to the mitochondrial network; including larger and more branched mitochondrial units, as well as a reduction in acute glucose-induced morphological plasticity that is further impaired in the absence of Bcl-x_L.

Probing at the mechanisms underlying these effects, we analyzed gene expression in NG and HG cultured islets from the same mice (Figure 15). Bcl-x_L expression levels were significantly decreased in BclxβKO islets, but were not significantly changed following HG pre-culture (Figure 15A). The expression of genes involved with mitochondrial fission, fusion, biogenesis, and oxidative stress were not significantly changed in response to HG pre-culture or Bcl-x_L knockout (Figure 15B-E). Overall, this suggests that HG pre-culture and/or Bcl-x_L knockout do not induce significant oxidative stress, and that the observed effects on mitochondrial morphology and function were not instigated by transcriptional means.

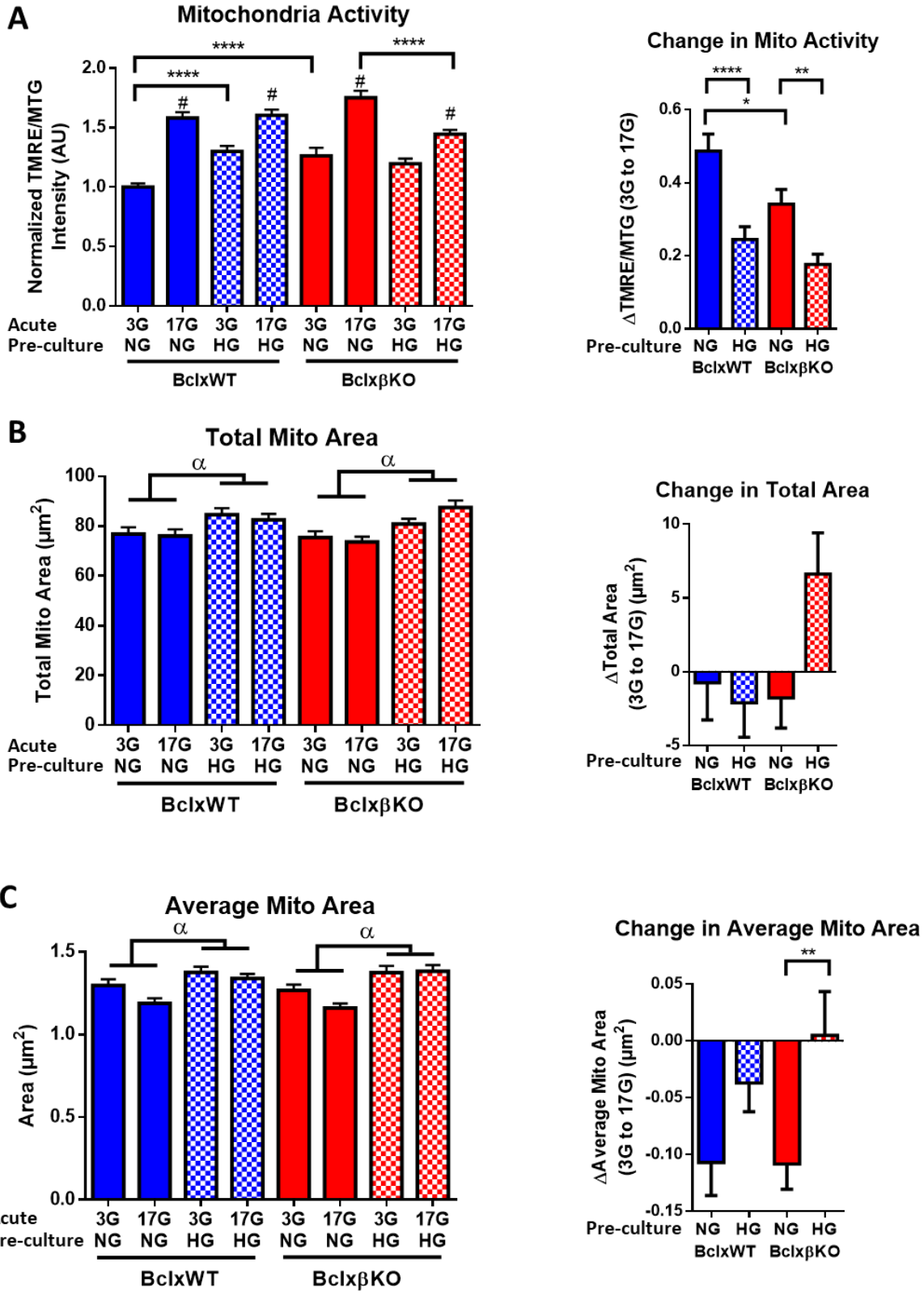
A
Mitochondria Activity
Normalized TMRE/MTG Intensity (AU)
2.0
1.5
1.0
0.5
0.0
****
****
****
#
#
#
#
Acute
Pre-culture
3G NG
17G NG
3G HG
17G HG
3G NG
17G NG
3G HG
17G HG
BclxWT
BclxβKO
Change in Mito Activity
ΔTMRE/MTG (3G to 17G)
0.6
0.4
0.2
0.0
****
**
*
Pre-culture
NG HG NG HG
BclxWT BclxβKO
B
Total Mito Area
Total Mito Area (μm2)
100
80
60
40
20
0
α
α
Acute
Pre-culture
3G NG
17G NG
3G HG
17G HG
3G NG
17G NG
3G HG
17G HG
BclxWT
BclxβKO
Change in Total Area
ΔTotal Area (3G to 17G) (μm2)
10
5
0
-5
Pre-culture
NG HG NG HG
BclxWT BclxβKO
C
Average Mito Area
Area (μm2)
1.5
1.0
0.5
0.0
α
α
Acute
Pre-culture
3G NG
17G NG
3G HG
17G HG
3G NG
17G NG
3G HG
17G HG
BclxWT
BclxβKO
Change in Average Mito Area
ΔAverage Mito Area (3G to 17G) (μm2)
0.05
0.00
-0.05
-0.10
-0.15
**
Pre-culture
NG HG NG HG
BclxWT BclxβKO

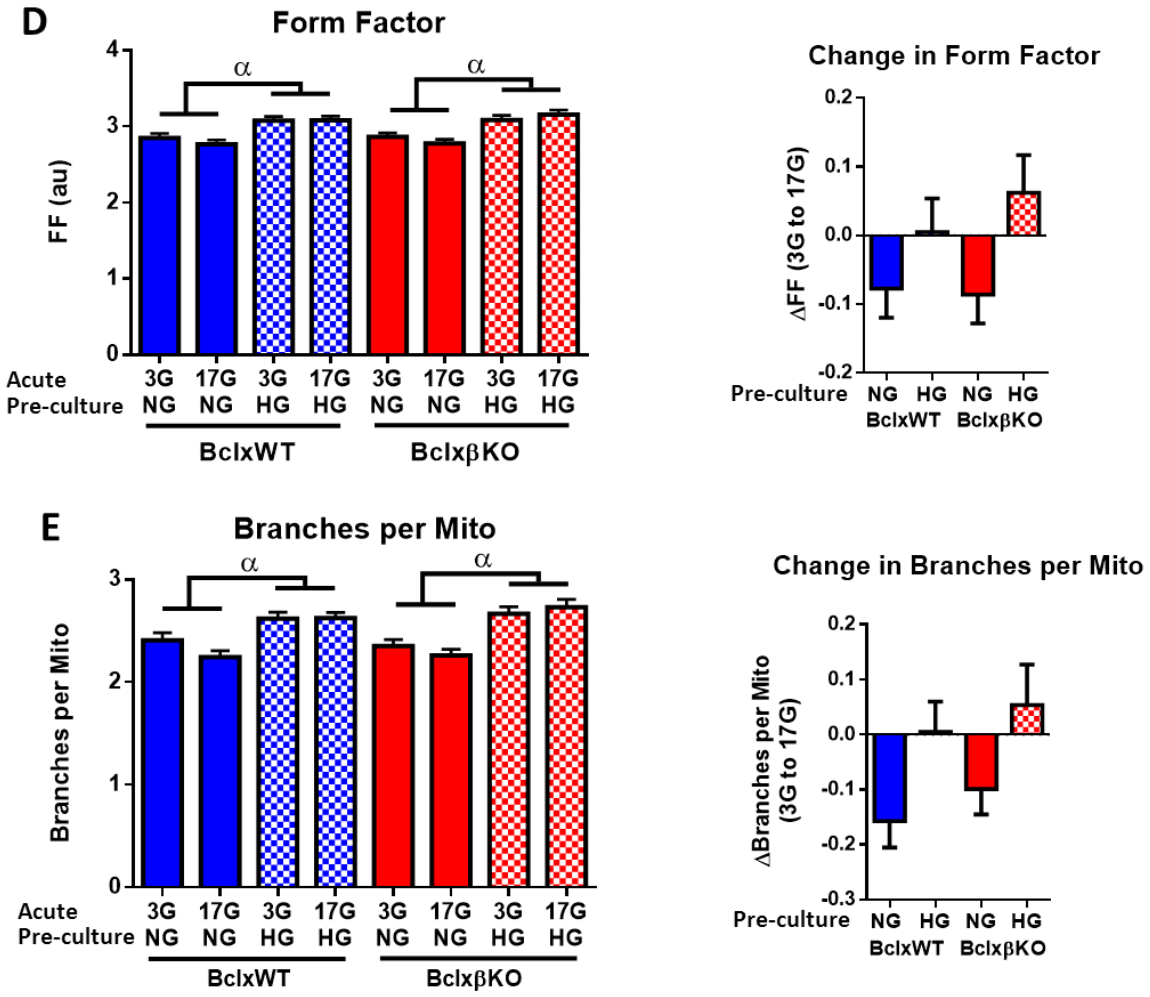

Figure 14. Comparison of mitochondrial morphology and function in BclxWT and BclxβKO β-cells after prolonged (6 day) high glucose culture. Dispersed islet cells from 4-6 months old male BclxWT and BclxβKO mice were seeded on coverslips and cultured for 6 days in either 11mM glucose (NG) or 25mM glucose (HG). The cells were then treated acutely with either 3mM glucose (3G) or 17mM glucose (17G) for 60 mins. Cells were stained with 0.1µg/mL Hoescht 33342, 50nM MitoTracker Green FM (MTG), and 25nM TMRE for 30 min before imaging. (A-E) Quantification and Δ3G→17G analysis of confocal images were performed in FIJI/ImageJ for the following parameters: (A) normalized TMRE/MTG ratio (normalized to WT-NG-3G) (#p<0.001 for difference between 3G and 17G of genotype and pre-culture; *p<0.05, **p<0.01, ***p<0.001, ****p<0.0001 as determined by One-way ANOVA with Sidak post-hoc test), (B) total mitochondria area, (C) average mitochondrion area, (D) form factor, and (E) branch number (α p<0.001 for the effect of HG pre-culture, as determined by Two-way ANOVA). (All data are represented by mean ± SEM; n=87-91 images total in each pre-culture condition and acute glucose treatment. Cells were obtained from 7 mice of each genotype and imaged in 7 separate experiments)

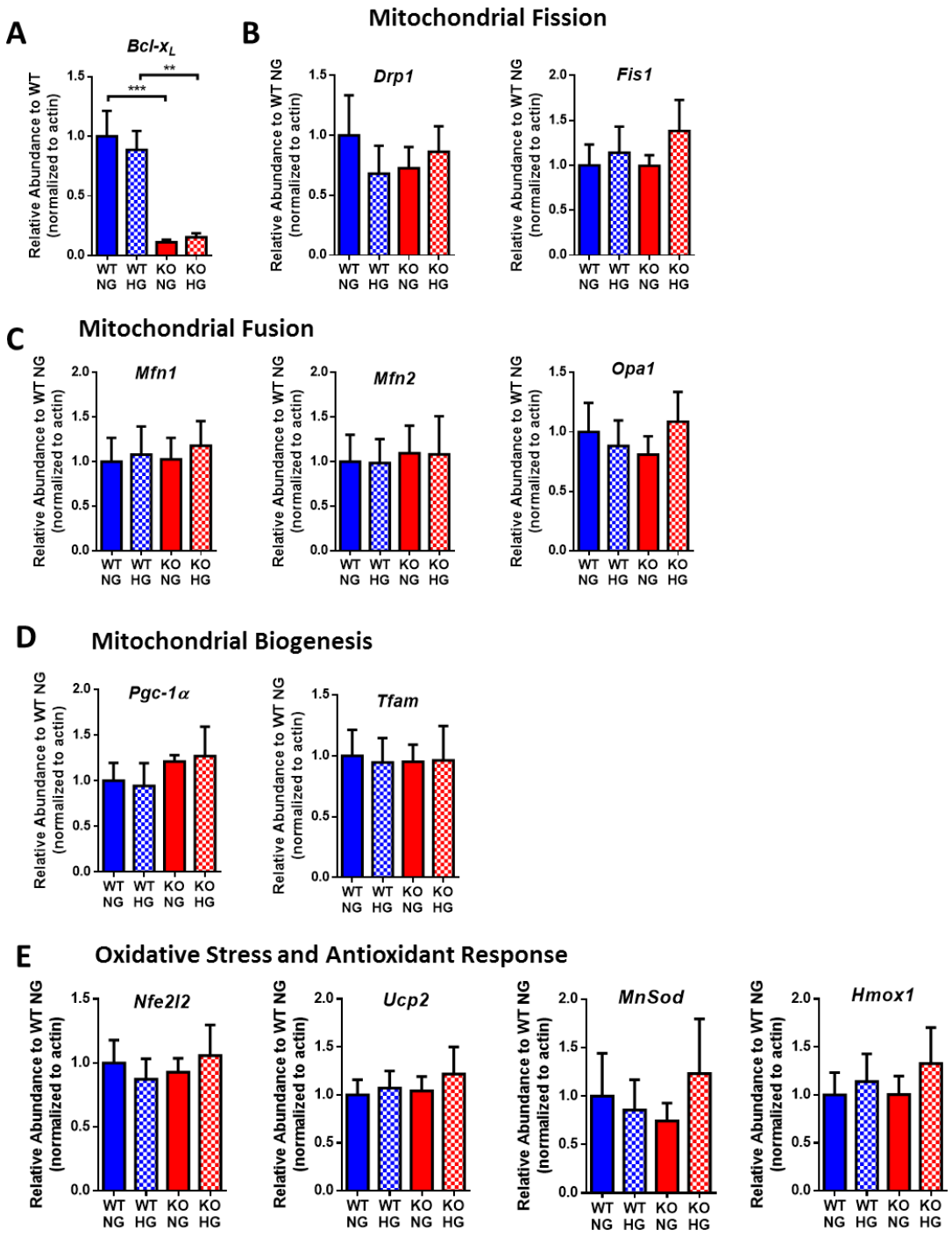

Figure 15. Effect of prolonged high glucose culture on the expression of genes involved with mitochondrial fission, fusion, biogenesis, and oxidative stress in BclxWT and BclxβKO islets. Islets from 4-6 months old male BclxWT and BclxβKO mice were cultured for 6 days in either 11mM glucose (NG) or 25mM glucose (HG) and compared by qPCR for the relative expression levels of selected genes involved with; (A) *Bcl-x*$_L$ (B) mitochondrial fission (*Drp1* and *Fis1*), (D) mitochondrial fusion (*Mfn1*, *Mfn2*, and *Opa1*), (E) mitochondrial biogenesis (*Pgc-1α* and *Tfam*), and (E) oxidative stress and antioxidant response (*Nfe2l2*, *Ucp2*, *MnSod*, and *Hmox1*). (All data are represented by mean ± SEM, Stats analysis was performed using multiple Paired Ratio t-test; n=8 experimental replicates)

3.3.2 Loss of Bcl-x_L amplifies mitochondrial volume and network complexity under high glucose culture

To further characterize the alterations in mitochondrial structure following prolonged high glucose culture and Bcl-x_L knockout, we performed 3D analysis on the mitochondrial network. In BclxWT cells, HG pre-culture did not significantly change mitochondria count, average mitochondria volume, or branch numbers (Figure 16B-D), but trended notably towards increasing total volume ($p=0.0568$, Figure 16A). In contrast, BclxβKO cells responded to prolonged HG pre-culture with marked increases in total mitochondrial volume, average mitochondrial volume, and mitochondrial branching, but not in mitochondria count. These data suggest that prolonged exposure of islet cells to high glucose stimulates growth of mitochondrial biomass along with a more fused network structure, and that these mitochondrial adaptations are normally dampened by the presence of Bcl-x_L.

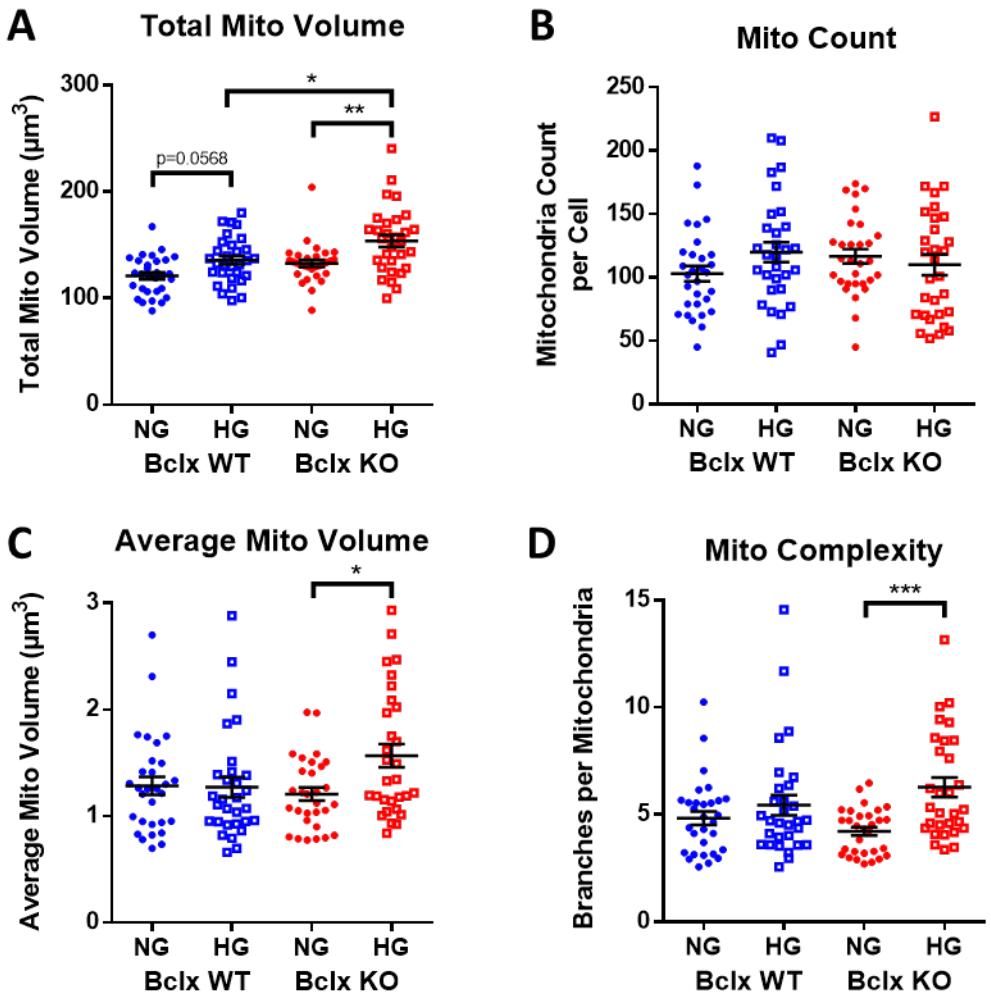

Figure 16. Effect of prolonged high glucose culture on total mitochondrial volume and 3D structure in BclxWT and BclxβKO islet cells. Dispersed islet cells from 4-6 months old male BclxWT and BclxβKO mice were seeded on coverslips and cultured for 6 days in either 11mM glucose (NG) or 25mM glucose (HG). The cells were then stained with 0.1µg/mL Hoescht 33342 and 50nM MitoTracker Deep Red FM for 30 min prior to imaging. Mitochondrial volume and structure were quantified as described previously. Deconvolution was performed in Huygens Essential software. 3D image stacks were quantified for the following parameters: (A) Total mitochondrial volume, (B) mitochondria count per cell, (C) average mitochondrion volume, and (D) average mitochondrial network branch number. (All data are represented by mean ± SEM; *p<0.05, **p<0.01, ***p<0.001 as calculated using One-way ANOVA with Sidak post-hoc test; n=30 image stacks total in each pre-culture condition. Cells were obtained from 3 mice of each genotype and imaged in 3 separate experiments)

Chapter 4: Discussion and Summary

4.1 Quantitative analysis of mitochondrial structure in pancreatic β-cells

The overall objective of this thesis was to clarify the mechanisms that regulate mitochondrial physiology and health in β-cells, with focus on potential roles for anti-apoptotic Bcl-x_L in β-cell mitochondrial morphology. Mitochondrial dynamics and network morphology can be assessed through a variety of imaging approaches such as widefield microscopy, confocal microscopy and electron microscopy (152-154). For the work in this thesis, we chose to use laser-scanning confocal microscopy as it is widely available, and compared to traditional widefield microscopy it has improved resolution and optical sectioning, which facilitates more accurate 3D reconstruction (145). Moreover, it also readily permits live cell imaging, in contrast to for instance, electron microscopy. Mitochondrial analysis in other cell types, such as fibroblast, have successfully used global threshold methods to identify fluorescently labelled mitochondria within images (144, 145). When applying similar approaches to pancreatic β-cells, we were unable to distinguish mitochondria with the accuracy and detail we believe is needed to accurately quantify subtle, physiologically relevant, changes. This is likely because most of the mitochondria in fibroblasts lie in a single plane without much overlap, whereas pancreatic β-cells are more 3 dimensional and more densely populated with mitochondria, which causes significant challenges in separating one mitochondria from another within the network. As a result, the first major aim of this project became to establish an image acquisition and analysis pipeline that was optimized for accurate confocal analysis of mitochondrial structure and morphology in β-cells.

In addition to implementing several steps for initial image processing, we overcame the critical weaknesses of global thresholding, and improved the identification of mitochondria, by using a sequential combination of global and local threshold algorithms. The superiority of this

approach was demonstrated by our mito-PAGFP experiments, which allowed photo-painting of individual mitochondria (Section 3.1.2). There is, however, one important limitation with the combined threshold approach; because a local threshold depends on relative pixel intensity in a local region, scaling of image sizes changes the number of pixels mitochondria occupy, resulting in changes to the identification. To help mitigate this, we optimized the analysis for images of sizes 200 – 500 pixel^2 and acquired images within this optimal size-range. In the future, we will further improve our method for identifying mitochondria and evaluate other approaches for local-based thresholding.

While 2D analysis can conveniently be used to study and quantify changes to mitochondrial morphology in pancreatic β-cells, it is not clear that optical cross-sections will accurately capture the true complexity and interconnectedness of the mitochondrial network in a given cell. Likely, this is best done by a full 3D reconstruction of the mitochondrial network. Moreover, quantitative assessment of total mitochondrial mass requires 3D approaches. A recent study utilized super-resolution 4π-microscopy to quantify β-cell mitochondrial structure in 3D (153), but to our knowledge no study has yet provided a detailed 3D analysis method using the more widely used and accessible confocal microscopy. Establishing the pipeline for 3D analysis of mitochondria in β-cells required us to optimize the image acquisition conditions, and we further found that image deconvolution was essential for accurate 3D reconstruction and quantification; both of these important steps are often overlooked (155, 156). These optimized conditions allowed for robust identification of mitochondria in 3D and accurate measurement of 3D characteristics.

Modern advances in the analysis of large-scale data sets in biological sciences have offered numerous novel approaches to studying complex data associated with single-cell RNA sequencing and mass cytometry (157, 158). Only recently have these tools been applied to the analysis of

imaging data (159). Here, we used SPADE (Spanning-tree Progression Analysis of Density-normalized Events) to categorize and differentiate mitochondrial morphologies in an unbiased manner, and to our knowledge we are first to do so. While our image set was comparatively small, we believe that Big Data analysis tools such as SPADE may in the future be applied with success on large-scale image sets, for instance obtained using High-Content Imaging systems.

In summary, we have established robust and sensitive pipelines for accurate confocal imaging and analysis of mitochondrial morphology in both 2D and 3D. These pipelines were then used to study effects of Bcl-x_L on mitochondria in pancreatic β-cells, and we expect that they will be used to answer other interesting questions regarding β-cell mitochondrial physiology and pathophysiology in the future.

4.2 Role of mitochondrial dynamics in β-cell glucose metabolism

We used our 2D pipeline to simultaneously measure mitochondrial morphology and function by co-staining mitochondria with a polarization-insensitive dye, MTG, and a polarization sensitive dye, TMRE. The MTG signal was then used as baseline signal for measuring mitochondrial morphology, and provided a mask for measuring TMRE intensity on a *per mitochondrion* basis. When applying this assay, we observed that physiological short-term glucose stimulation is associated with a more fragmented mitochondrial morphology, suggestive of mitochondrial fission. Our results agrees with recently published findings where mitochondrial fission, more specifically the activity of DRP1, was linked with cell glucose stimulation in INS1 cells and suggested to be necessary for optimal glucose-induced insulin secretion (91, 92). As far as we know, we are first to demonstrate this connection between glucose stimulation and mitochondrial morphometry in primary islet cells, and quantify this on a *per mitochondrion* basis.

The reciprocal interrelations of mitochondrial morphology and metabolism is complex, and remain to be fully understood (76). Studies on nutrient starvation and cells in S phase have demonstrated that fused mitochondria are more efficient at ATP production (160, 161). Moreover, work by Wikstrom *et al.* on brown adipose tissue has suggested that increased DRP1 activity and mitochondrial fission is associated with mitochondrial uncoupling and depolarization, thus decreasing the efficiency of OXPHOS and ATP production (87). These findings seem to contradict our results in islet cells, which indicate that mitochondrial fission is associated with increased mitochondrial hyperpolarization, a strong indicator of increased ATP production. Possibly these differences can be explained by differences in cell type and substrate used; Wikstrom *et al.* treated brown adipocytes with norepinephrine and palmitate (87) whereas we used glucose on pancreatic islet cells. The general question of whether fused complex mitochondria or smaller fragmented mitochondria are more efficient at ATP production therefore remains to be answered, but most likely depends on the specific cell type and treatment conditions studied.

The mechanism by which mitochondria fission in β-cells is coupled with glucose-stimulated insulin secretion is also not yet fully understood. Kabra *et al.* found that they were able to bypass the requirement of DRP1, and by extension mitochondrial fission, by directly feeding β-cells with mitochondrial substrates, suggesting that the coupling of mitochondrial fission and glucose stimulation occurs upstream of oxidative phosphorylation, likely in the glycolysis pathway (92). Another possibility is that glucose stimulation can be coupled with mitochondrial fission via an increase in hydrogen peroxide. Glucose stimulation induces an increase in β-cell H_2O_2 levels, and physiological levels of ROS have been suggested as important signals for glucose-stimulated insulin secretion (65, 66, 136). When liver cells were treated acutely with high (25mM) glucose, Yu *et al.* saw a reversible increase in H_2O_2 levels that was associated with a mitochondrial

fragmentation morphology (162). Other studies in muscle cells determined that H_2O_2 is able to induce mitochondrial fragmentation (163, 164). This suggests hydrogen peroxide may potentially link glucose stimulation to mitochondrial fission in β-cells. However, the studies in H_2O_2-treated muscle cells observed a decrease in mitochondrial polarization, which suggests the fission may be due to excessive oxidative stress rather than a physiological response (163, 164). It has also been suggested that increasing levels of H_2O_2 arise from fragmented mitochondria and requires mitochondrial fission (162) rather than inducing it, adding additional complexity to the question.

Overall, our results link glucose stimulation and mitochondrial hyperpolarization to physiological mitochondrial fission in pancreatic islet cells. While the mechanism by which the fragmentation morphology occurs remains to be determined, the putative importance of mitochondrial fission is further highlighted by our findings. Future studies involving the measurement of ROS levels and glycolysis inhibitors may help elucidate the underlying mechanisms.

4.3 Effects of Bcl-x_L on β-cell mitochondrial morphology and function

Previous publications have demonstrated that both transgenic overexpression (120) and knockout (121) of Bcl-x_L have consequences for β-cell glucose metabolism that suggest changes to their mitochondrial physiology. Here, we investigated this possibility further, and found that both gain- and loss-of-function of Bcl-x_L had significant effects on mitochondrial structure and function in β-cells. *In vitro* overexpression of Bcl-x_L in MIN6 and primary islet cells induced a striking aggregation of Bcl-x_L. We observed that overexpressed Bcl-x_L strongly co-localized with mitochondria, which agrees with previous reports of its sub-cellular distribution in β-cells (121, 165), and the fact that Bcl-x_L contains a trans-membrane domain that targets it to the mitochondrial

outer membrane (166). Accordingly, we found that the aggregation of Bcl-x_L reflected an aggregation of all the cell's mitochondria, and that this severe morphological change corresponded with a decrease in total mitochondrial mass and impaired respiratory capacity. Together this suggests that the metabolic defect in β-cell-specific Bcl-x_L overexpressing transgenic mice (120), may in fact result from defects in mitochondrial structure and loss of mitochondrial mass.

Using two Bcl-x_L loss-of-function models we obtained further evidence to suggest Bcl-x_L has effects on both mitochondrial structure and function. When we pharmacologically inhibited Bcl-x_L with C6, we observed fragmentation of the mitochondrial network. Notably, the mitochondrial fission associated with C6 treatment was more severe than the subtle mitochondrial fragmentation effect associated with short-term glucose stimulation. Quantification of the morphology reveal that treatment by C6 lowered the average mitochondrial form factor by 56%, while stimulation with glucose only lowered the form factor by 12%. Knowing that prolonged C6 treatment induces β-cell apoptosis, this does suggest that C6-induced fission is, at least partly, due to increased oxidative stress, whereas acute glucose-induced mitochondrial fission is a physiological response. As such, these data may provide an interesting morphological comparison of mitochondrial fission associated with β-cell physiology and pathophysiology.

Our β-cell specific Bcl-x_L knockout mouse model provided additional loss-of-function evidence to support that Bcl-x_L has effects on β-cell mitochondrial function that are linked to changes in mitochondrial morphology. Deletion of Bcl-x_L resulted in smaller and more hyperpolarized mitochondria in un-stimulated islet cells, which seems to agree with our previous demonstration of increased islet NAD(P)H levels following Bcl-x_L knockout (121), and studies in neurons where Bcl-x_L knockout produced shorter mitochondria (146). The basal changes in mitochondrial morphology in Bcl-x_L knockout islet cells were less severe than the response to C6,

which may partly be due to the fact that C6 antagonizes both Bcl-2 and Bcl-x_L and thereby exposes the cell to additional stress. Somewhat surprisingly, we did not observe any differences in mitochondrial morphology and membrane potential between BclxWT and BclxβKO islet cells stimulated with 17mM glucose. Conceivably, this can be explained if the effects of Bcl-x_L deletion on mitochondrial morphology and function are relatively minor and overshadowed by the effects of a glucose stimulus. Alternatively, it may reflect an inherent limit to the physiological glucose-induced changes in mitochondrial polarization and morphology (i.e. a saturation effect), or a limitation in our ability to detect these. Due to the increase in basal mitochondrial activity, Bcl-x_L knockout β-cells seem to have less dynamic range than BclxWT cells in regards to both their functional and morphological responsiveness to stimulatory glucose. Although this could be interpreted as a functional defect, we believe it more likely reflects an overall metabolic sensitization of the Bcl-x_L knockout β-cells. Future work to characterize the morphological and functional responses to a range of glucose concentrations could help clarify this.

4.3.1 Potential mechanisms linking Bcl-x_L to mitochondrial morphogenesis

Both our Bcl-x_L GOF and LOF studies suggest a role for Bcl-x_L in shaping mitochondrial morphology and dynamics, but the mechanism remains unclear. When considering the mitochondrial aggregation associated with Bcl-x_L overexpression, we believe it represents one of two things; 1) a cluster of fragmented mitochondria, or 2) a cluster of hyper-fused mitochondria. Each of these would be formed on a different basis. A recent paper (167) showed that overexpressing the mitochondrial outer membrane protein MitoNEET in β-cells increased mitochondrial fission but inhibited mitophagy, resulting in an aggregation of mitochondrial fragments inside autophagosomes. As Bcl-x_L has been reported to inhibit mitophagy (126), it is

possible that its overexpression may have a similar outcome. Bcl-x_L would then affect morphogenesis primarily via changes to mitophagy. Alternatively, Bcl-x_L may actually alter the relative rates of normal mitochondrial fission and fusion. Indeed, the mitochondrial structure after Bcl-x_L overexpression appears very similar to mitochondria in INS1 cells following MFN1 overexpression (168). The possibility that Bcl-x_L overexpression promotes fusion also seems to be supported by our time-lapse imaging (Figure 8D). Rather than fragmentation, we saw the mitochondria "swirl inwards", forming several clumps before finally forming the larger aggregates. This is also consistent with findings in neurons where Bcl-x_L overexpression pushes the mitochondria to be morphologically elongated (146). Moreover, we found that Bcl-x_L inhibition and knockout both promoted fragmentation, suggesting that Bcl-x_L LOF conversely shifts mitochondrial dynamics towards fission.

Regulation of mitochondrial fission and fusion by Bcl-x_L could be through direct effects on the fission and fusion machinery. Studies in *C. elegans* suggest that CED-9, a homolog of Bcl-x_L and Bcl-2, promotes mitochondrial fusion by directly interacting with, and increasing the activity of, both FZO-1 and EAT-3, which are homologs of MFN1/2 and OPA1, respectively (124). Bcl-x_L has also been demonstrated to bind and increase the activity of DRP1 in neurons (122). Our gene expression analysis showed only minor effects of Bcl-x_L on the transcription of genes involved with fission and fusion. Expression of the fission receptor, *Fis1*, was significantly increased following Bcl-x_L overexpression, which we speculate may be a compensatory mechanism to increase mitochondrial dynamics and counter the mitochondrial aggregation and loss of mobility. The lack of significant changes to the expression of other important facilitators of fission and fusion suggests the effects may be occurring mainly post-translation, but western

blot analysis will be required to determine the effects of Bcl-x_L on the phosphorylation of DRP1 and MFN1/2 at their various activity-regulating sites.

Alternatively, Bcl-x_L may control mitochondrial morphology by regulating mitochondrial ROS. Previous work in our lab suggested that Bcl-x_L conferred protection against high ribose treatment by lowering superoxide levels (148). Consistent with this, we now show that overexpression of Bcl-x_L in MIN6 cells lowered expression levels of *Hmox1,* which mediates the production of two antioxidants, biliverdin and bilirubin, and is activated as part of the anti-oxidant response (169). This decrease in *Hmox1* expression suggests that Bcl-x_L may help reduce oxidative stress. Moreover, our lab previously reported that H_2O_2 levels increased in β-cells when Bcl-2 was pharmacologically inhibited or knocked out, and the same was seen in response to combined Bcl-2/Bcl-x_L inhibition with C6 (136). Taken together, these results suggest that loss of Bcl-x_L might also produce increased levels of β-cell ROS, which may in turn promote a mitochondrial fragmentation morphology, as has been demonstrated in other systems (162-164). Since Bcl-x_L knockout islets do not show significant changes in the expression of genes involved with oxidative stress and antioxidant responses (Figure 12), any additional ROS the knockout β-cells may produce would likely be within the physiological range needed for normal β-cell function (63-66). In all, it is an intriguing possibility for future study that Bcl-x_L may regulate mitochondrial morphology and function indirectly via ROS-dependent mechanisms.

Finally, it is possible Bcl-x_L may indirectly regulate mitochondrial morphology through its interaction with other members of the Bcl-2 protein family. Inhibition or loss of Bcl-x_L may free BAX and BAK, thereby activating them and initiating apoptosis. The connection between apoptosis and mitochondrial fission has been established in numerous studies (81, 82, 170) and BAX and BAK has been shown to have pro-fission activities (171-173). Combined Bcl-2/Bcl-x_L

inhibition eventually triggers β-cell apoptosis, and after 4 hours treatment it is therefore possible that C6 promotes fission via activation of BAX/BAK and/or apoptosis (121). However, dispersed Bcl-x_L KO islet cells do not undergo increased cell death under normal culture conditions (148). It is therefore unlikely that the increased mitochondrial activity and fission we observe in Bcl-x_L KO islet cells is the result of apoptosis activation, but it remains possible that BAX and BAK promote mitochondrial fission independent of their apoptotic roles, as demonstrated previously (174). We also speculate that Bcl-x_L knockout could free the BH3-only protein BAD and thereby allow increased BAD phosphorylated at serine 155 (BADp155), which causes it to bind and allosterically activate glucokinase (175, 176). Glucokinase functions to connect glycolysis and mitochondrial metabolism in β-cells (177), which in turn may promote mitochondrial fission. Indeed, BclxβKO islets have 58% increased levels of BADp155 (121). It therefore seems possible that Bcl-x_L, via BAD, can indirectly act as a metabolic check to glycolytic pathways, and the mitochondrial morphological changes are consequence of the changes in glucose metabolism.

In summary, we have demonstrated that Bcl-x_L is able to regulate mitochondrial morphology and function in islet cells. The previously reported effects of Bcl-x_L on β-cell metabolism may be partly due to its effect on mitochondrial fission-fusion dynamics. How Bcl-x_L affects β-cell mitochondrial morphology remains unclear, but it is possible that it involves a complex combination of the mechanisms discussed above. Future studies of β-cell mitophagy, time-lapse ROS detection, and the involvement of other members of the Bcl-2 protein family may help further elucidate this.

4.4 Role of Bcl-x_L in β-cell mitochondrial biomass

In addition to affecting mitochondrial morphology, our gain- and loss-of-function experiments revealed that Bcl-x_L has an impact on mitochondrial mass, and suggest this is particularly prominent when the β-cells are chronically under a high metabolic workload. Both Bcl-x_L overexpression in MIN6 cells and knockout in primary islet cells appeared to decrease mitochondrial volume. This seems contradictory, but it remains to be determined if the volume of the mitochondrial aggregates in Bcl-x_L overexpressing primary cells is also reduced. Conceivably, MIN6 cells and primary islet cells may in some ways respond differently to changes in Bcl-x_L. As an example, transformed cells (i.e. MIN6 cells) may have decreased levels of tumor-suppressor, p53, activity (178), which is known to interact with Bcl-x_L (179) and has been demonstrated to inhibit mitophagy in β-cells (110). It is, therefore, possible that MIN6 cell respond differently than primary cells via changes to mitophagy. This would be consistent with work in primary neurons where overexpression of Bcl-x_L increased mitochondrial biomass (146).

To better understand how Bcl-x_L overexpression and knockout may reduce mitochondrial mass, we investigated the expression of genes responsible for mitochondrial biogenesis. *Pgc-1α* was significantly increased following Bcl-x_L knockout, but not following Bcl-x_L overexpression, which does not correlate with the results of our mitochondrial volume analysis. Possibly, the increase in *Pgc-1α* could be a compensatory mechanism due to decreased mitochondrial biomass. However, this hypothesis is challenged by the fact that there is no compensatory increase in *Pgc-1α* in response to the decreased mitochondrial volume in Bcl-x_L overexpressing cells. Alternatively, PGC-1α alone may not dictate β-cell mitochondrial biogenesis and biomass to the extent previously believed. A recent study did not detect altered mitochondrial mass in PGC-1 knockout β-cells, instead fatty acid metabolism was disrupted (104). Lastly, Bcl-x_L may

predominantly affect mitochondrial biogenesis at the protein level. Luciferase assays and western blot analysis of the phosphorylation states can be used to better study the effect of Bcl-x_L overexpression on PGC1α and TFAM activity in the future. Opposite to mitochondrial biogenesis is mitophagy, which also controls mitochondrial mass by eliminating mitochondria from the cell. Bcl-x_L has been reported to interact directly with key mitophagy-regulating proteins (180), and this could also be investigated in the future to clarify Bcl-x_L's effects on mitochondrial structure and mass.

4.5 Effects of Bcl-x_L on β-cell mitochondria during a prolonged glucose challenge

The *in vitro* model of prolonged HG pre-culture aims to model the condition underlying prediabetes, where β-cells are chronically exposed to elevated glucose levels due to insulin resistance (181). While β-cells in the pre-diabetic stage do not experience severe glucotoxicity, as defined by the loss of insulin secretion and key transcription factors (151), they have increased insulin, and expand in mass to maintain glucose homeostasis (181). Mouse models have further demonstrated that β-cells in prediabetes respond with elevated mitochondrial metabolism to meet the heightened insulin demand (150). In our islet cells, basal mitochondrial activity was elevated following 6 days HG pre-culture (Figure 14A), which is consistent with such metabolic amplification, and with previous reports that HG pre-culture increases basal intracellular calcium level and basal insulin secretion (45, 148). We have now demonstrated, that these HG-induced adaptations are associated with an increase in the average size and morphological complexity of β-cell mitochondria, implying a more fused and connected network. Along with this, there was a decreased morphological responsiveness of the mitochondria to acute glucose stimulation. The fact that fused mitochondria following HG culture have increased basal activity, whereas acute

glucose stimulation induces a physiological fragmentation (Figure 10), suggests that neither a fragmented nor a fused mitochondrial morphology, per se, implies higher metabolic activity of the individual mitochondria.

In our BclxβKO islet cells the metabolic challenge of prolonged HG culture did not further increase the already elevated basal mitochondrial activity. Rather, the response to short-term 17mM glucose was reduced, suggesting the onset of mitochondrial dysfunction (Figure 14). Interestingly, these BclxβKO mitochondria also had the most severe loss of the morphological (fragmentation) response to the short term glucose stimulus. This suggests that acute morphological responsiveness, specifically the capacity for rapid fission, may be a feature of healthy mitochondria. Overall, these indications of impaired mitochondrial responsiveness in HG pre-cultured BclxβKO islet cells seem at odds with our lab's previous observation that HG pre-cultured BclxβKO islets had normal size calcium responses to 15mM glucose (148). However, based on our new 3D mitochondrial characterization (Figure 16), we now believe that an adaptive increase in total mitochondrial mass may be compensating for the reduced functionality of the individual mitochondrial units in response to stimulatory glucose.

Mitochondria were on average larger and more connected after the HG challenge, particularly in BclxβKO islet cells. This may reflect either an increase in mitochondrial fusion or a reduction in mitochondrial fission. The latter might be suggested by the reduced physiological glucose-induced fragmentation response we discussed above. Possibly, the increase in overall mitochondrial network connectivity is an adaptive response to increased mitochondrial stress (81). Mechanistically, such mitochondrial adaptations may involve changes in ROS, as oxidized glutathione has been shown to be a strong inducer of mitochondrial fusion (79). Moreover, low/transient increases in ROS are believed to be important for long-term mitochondrial health

through the process of mitochondrial hormesis (mitohormesis), which involves upregulation of antioxidant defenses and mitochondrial biogenesis (182). This would be consistent with the HG-induced increase in total mitochondrial area, and even more strikingly by the increase in total mitochondrial volume in BclxβKO cells. The fact that our gene expression analysis did not indicate the presence of oxidative stress or significant antioxidant responses might indicate that the morphologically fused mitochondria successfully prevent the formation of *excessive* ROS, and by extension also mitochondrial damage. Also here, future experiments comparing mitochondrial and total cellular ROS between our genotypes and treatment groups may help shed light on the mechanisms.

Overall, these results demonstrate that prolonged exposure of islet cells to high glucose induces significant changes to mitochondrial function and structure. They support the idea that endogenous Bcl-x_L normally dampens basal mitochondrial activity, and further reveal that Bcl-x_L helps limit the functional and structural alterations to islet cell mitochondria under chronic elevated glucose. This function of Bcl-x_L may potentially help delay the onset of glucotoxicity-associated "metabolic overload" (12, 151). Further extension of this work may provide new knowledge regarding the processes of metabolic adaptation and maladaptation in the progression from prediabetes to T2D.

4.6 Overall Summary

Using a combination of line scanning confocal microscopy and the open source image analysis software ImageJ/FIJI, we have established a robust pipeline that can accurately identify mitochondria and quantify their morphology, volume and network complexity in pancreatic β-cells. The ability to distinguish different mitochondrial morphologies was confirmed by comparing

manual image categorization to an unbiased grouping based on high-dimensional SPADE analysis of the calculated mitochondrial parameters. Using this pipeline, we imaged and analyzed mouse islet cells and found that glucose-induced mitochondrial hyperpolarization was associated with physiological mitochondrial fission. We further applied this approach to determine the mitochondrial effects of overexpressing, pharmacologically inhibiting, and genetically deleting Bcl-x_L in β-cells. Overexpression of Bcl-x_L induced mitochondrial dysfunction that was characterized by severe mitochondrial aggregation (seemingly hyper-fusion) and a reduction in total mitochondrial mass. On the other hand, knocking out Bcl-x_L induced subtle mitochondrial fission and increased basal mitochondrial hyperpolarization, suggesting elevated metabolic activity at the level of the individual mitochondria. Finally, we found that islet cells respond to a prolonged period of high glucose exposure with an increase in the size and overall connectivity of their mitochondrial network. In Bcl-x_L-deficient β-cells this increase in mitochondrial mass and networking was significantly amplified, and this possibly compensated for an associated loss of morphological and functional responsiveness of their individual mitochondria to acute glucose simulation. Taken together, these results provide additional evidence for our previous observation that endogenous Bcl-x_L dampens β-cell mitochondrial metabolism, and support the hypothesis that Bcl-x_L is important for β-cell adaptation to metabolic stress by affecting mitochondrial dynamics.

References

1. International Diabetes Federation. IDF Diabetes Atlas Poster Seventh Edition Brussels, Belgium: International Diabetes Federation; 2015 [cited 2016 October 11]. Available from: http://www.idf.org/sites/default/files/Atlas7e-poster.pdf.

2. Mathers CD, Loncar D. Projections of global mortality and burden of disease from 2002 to 2030. PLoS medicine. 2006;3(11):e442.

3. American Diabetes Association. Diagnosis and classification of diabetes mellitus. Diabetes care. 2011;34 Suppl 1:S62-9.

4. Muoio DM, Newgard CB. Mechanisms of disease:Molecular and metabolic mechanisms of insulin resistance and beta-cell failure in type 2 diabetes. Nature reviews Molecular cell biology. 2008;9(3):193-205.

5. Xie Z, Chang C, Zhou Z. Molecular mechanisms in autoimmune type 1 diabetes: a critical review. Clinical reviews in allergy & immunology. 2014;47(2):174-92.

6. Poretsky L. Principles of diabetes mellitus. 2nd ed. New York: Springer; 2010. xviii, 887 p. p.

7. Canadian Diabetes Association Clinical Practice Guidelines Expert C, Goldenberg R, Punthakee Z. Definition, classification and diagnosis of diabetes, prediabetes and metabolic syndrome. Canadian journal of diabetes. 2013;37 Suppl 1:S8-11.

8. Kleinberger JW, Pollin TI. Personalized medicine in diabetes mellitus: current opportunities and future prospects. Annals of the New York Academy of Sciences. 2015;1346(1):45-56.

9. von Herrath MG, Korsgren O, Atkinson MA. Factors impeding the discovery of an intervention-based treatment for type 1 diabetes. Clinical and experimental immunology. 2016;183(1):1-7.

10. Wallberg M, Cooke A. Immune mechanisms in type 1 diabetes. Trends in immunology. 2013;34(12):583-91.

11. Steck AK, Rewers MJ. Genetics of type 1 diabetes. Clinical chemistry. 2011;57(2):176-85.

12. Kahn SE, Cooper ME, Del Prato S. Pathophysiology and treatment of type 2 diabetes: perspectives on the past, present, and future. The Lancet. 2014;383(9922):1068-83.

13. Templeman NM, Skovso S, Page MM, Lim GE, Johnson JD. A causal role for hyperinsulinemia in obesity. The Journal of endocrinology. 2017;232(3):R173-R83.

14. Shanik MH, Xu Y, Skrha J, Dankner R, Zick Y, Roth J. Insulin resistance and hyperinsulinemia: is hyperinsulinemia the cart or the horse? Diabetes care. 2008;31 Suppl 2:S262-8.

15. Scott RA, Scott LJ, Magi R, Marullo L, Gaulton KJ, Kaakinen M, et al. An Expanded Genome-Wide Association Study of Type 2 Diabetes in Europeans. Diabetes. 2017;66(11):2888-902.

16. Bonnefond A, Froguel P. Rare and common genetic events in type 2 diabetes: what should biologists know? Cell metabolism. 2015;21(3):357-68.

17. Shrayyef MZ, Gerich JE. Normal Glucose Homeostasis. In: Poretsky L, editor. Principles of Diabetes Mellitus. 2 ed. New York, NY, USA: Springer; 2010. p. 17-35.

18. Mitrakou A, Ryan C, Veneman T, Mokan M, Jenssen T, Kiss I, et al. Hierarchy of glycemic thresholds for counterregulatory hormone secretion, symptoms, and cerebral dysfunction. The American journal of physiology. 1991;260(1 Pt 1):E67-74.

19. Saltiel AR. Insulin Signaling in the Control of Glucose and Lipid Homeostasis. Handbook of experimental pharmacology. 2016;233:51-71.

20. Jones BJ, Tan T, Bloom SR. Minireview: Glucagon in stress and energy homeostasis. Endocrinology. 2012;153(3):1049-54.

21. Hauge-Evans AC, King AJ, Carmignac D, Richardson CC, Robinson IC, Low MJ, et al. Somatostatin secreted by islet delta-cells fulfills multiple roles as a paracrine regulator of islet function. Diabetes. 2009;58(2):403-11.

22. Khandekar N, Berning BA, Sainsbury A, Lin S. The role of pancreatic polypeptide in the regulation of energy homeostasis. Molecular and cellular endocrinology. 2015;418 Pt 1:33-41.

23. Yada T, Damdindorj B, Rita RS, Kurashina T, Ando A, Taguchi M, et al. Ghrelin signalling in beta-cells regulates insulin secretion and blood glucose. Diabetes, obesity & metabolism. 2014;16 Suppl 1:111-7.

24. Schwartz MW, Seeley RJ, Tschop MH, Woods SC, Morton GJ, Myers MG, et al. Cooperation between brain and islet in glucose homeostasis and diabetes. Nature. 2013;503(7474):59-66.

25. Mingrone G, Castagneto-Gissey L. Type 2 diabetes mellitus in 2013: A central role of the gut in glucose homeostasis. Nature reviews Endocrinology. 2014;10(2):73-4.

26. Grunberger G. The need for better insulin therapy. Diabetes, obesity & metabolism. 2013;15 Suppl 1:1-5.

27. Rigby MR, Harris KM, Pinckney A, DiMeglio LA, Rendell MS, Felner EI, et al. Alefacept provides sustained clinical and immunological effects in new-onset type 1 diabetes patients. The Journal of clinical investigation. 2015;125(8):3285-96.

28. Vieira A, Courtney M, Druelle N, Avolio F, Napolitano T, Hadzic B, et al. beta-Cell replacement as a treatment for type 1 diabetes: an overview of possible cell sources and current axes of research. Diabetes, obesity & metabolism. 2016;18 Suppl 1:137-43.

29. Peyser T, Dassau E, Breton M, Skyler JS. The artificial pancreas: current status and future prospects in the management of diabetes. Annals of the New York Academy of Sciences. 2014;1311:102-23.

30. Maruthur NM, Tseng E, Hutfless S, Wilson LM, Suarez-Cuervo C, Berger Z, et al. Diabetes Medications as Monotherapy or Metformin-Based Combination Therapy for Type 2 Diabetes: A Systematic Review and Meta-analysis. Annals of internal medicine. 2016;164(11):740-51.

31. Palmer SC, Mavridis D, Nicolucci A, Johnson DW, Tonelli M, Craig JC, et al. Comparison of Clinical Outcomes and Adverse Events Associated With Glucose-Lowering Drugs in Patients With Type 2 Diabetes: A Meta-analysis. Jama. 2016;316(3):313-24.

32. Pernicova I, Korbonits M. Metformin--mode of action and clinical implications for diabetes and cancer. Nature reviews Endocrinology. 2014;10(3):143-56.

33. Hattersley AT, Thorens B. Type 2 Diabetes, SGLT2 Inhibitors, and Glucose Secretion. The New England journal of medicine. 2015;373(10):974-6.

34. Hollander P, Maggs DG, Ruggles JA, Fineman M, Shen L, Kolterman OG, et al. Effect of pramlintide on weight in overweight and obese insulin-treated type 2 diabetes patients. Obesity research. 2004;12(4):661-8.

35. Liang W, Gao L, Li N, Wang B, Wang L, Wang Y, et al. Efficacy and Safety of Bromocriptine-QR in Type 2 Diabetes: A Systematic Review and Meta-Analysis. Hormone and metabolic research = Hormon- und Stoffwechselforschung = Hormones et metabolisme. 2015;47(11):805-12.

36. Knowler WC, Barrett-Connor E, Fowler SE, Hamman RF, Lachin JM, Walker EA, et al. Reduction in the incidence of type 2 diabetes with lifestyle intervention or metformin. The New England journal of medicine. 2002;346(6):393-403.

37. Schellenberg ES, Dryden DM, Vandermeer B, Ha C, Korownyk C. Lifestyle interventions for patients with and at risk for type 2 diabetes: a systematic review and meta-analysis. Annals of internal medicine. 2013;159(8):543-51.

38. Wallia A, Molitch ME. Insulin therapy for type 2 diabetes mellitus. Jama. 2014;311(22):2315-25.

39. Conrad E, Stein R, Hunter CS. Revealing transcription factors during human pancreatic beta cell development. Trends in endocrinology and metabolism: TEM. 2014;25(8):407-14.

40. Gerace D, Martiniello-Wilks R, O'Brien BA, Simpson AM. The use of beta-cell transcription factors in engineering artificial beta cells from non-pancreatic tissue. Gene therapy. 2015;22(1):1-8.

41. Roder PV, Wong X, Hong W, Han W. Molecular regulation of insulin granule biogenesis and exocytosis. The Biochemical journal. 2016;473(18):2737-56.

42. Maechler P, Li N, Casimir M, Vetterli L, Frigerio F, Brun T. Role of mitochondria in beta-cell function and dysfunction. Advances in experimental medicine and biology. 2010;654:193-216.

43. Maechler P, Wollheim CB. Mitochondrial function in normal and diabetic beta-cells. Nature. 2001;414(6865):807-12.

44. Prentki M, Matschinsky FM, Madiraju SR. Metabolic signaling in fuel-induced insulin secretion. Cell metabolism. 2013;18(2):162-85.

45. Khaldi MZ, Guiot Y, Gilon P, Henquin JC, Jonas JC. Increased glucose sensitivity of both triggering and amplifying pathways of insulin secretion in rat islets cultured for 1 wk in high glucose. American journal of physiology Endocrinology and metabolism. 2004;287(2):E207-17.

46. Prentki M, Joly E, El-Assaad W, Roduit R. Malonyl-CoA signaling, lipid partitioning, and glucolipotoxicity: role in beta-cell adaptation and failure in the etiology of diabetes. Diabetes. 2002;51 Suppl 3:S405-13.

47. Cnop M, Toivonen S, Igoillo-Esteve M, Salpea P. Endoplasmic reticulum stress and eIF2alpha phosphorylation: The Achilles heel of pancreatic beta cells. Molecular metabolism. 2017;6(9):1024-39.

48. Hasnain SZ, Prins JB, McGuckin MA. Oxidative and endoplasmic reticulum stress in beta-cell dysfunction in diabetes. Journal of molecular endocrinology. 2016;56(2):R33-54.

49. Wang J, Yang X, Zhang J. Bridges between mitochondrial oxidative stress, ER stress and mTOR signaling in pancreatic beta cells. Cellular signalling. 2016;28(8):1099-104.

50. Lenzen S. Oxidative stress: the vulnerable beta-cell. Biochemical Society transactions. 2008;36(Pt 3):343-7.

51. Maechler P, Jornot L, Wollheim CB. Hydrogen peroxide alters mitochondrial activation and insulin secretion in pancreatic beta cells. The Journal of biological chemistry. 1999;274(39):27905-13.

52. Tiedge M, Lortz S, Drinkgern J, Lenzen S. Relation between antioxidant enzyme gene expression and antioxidative defense status of insulin-producing cells. Diabetes. 1997;46(11):1733-42.

53. Poitout V, Amyot J, Semache M, Zarrouki B, Hagman D, Fontes G. Glucolipotoxicity of the pancreatic beta cell. Biochimica et biophysica acta. 2010;1801(3):289-98.

54. Agrawal A, Mabalirajan U. Rejuvenating cellular respiration for optimizing respiratory function: targeting mitochondria. American journal of physiology Lung cellular and molecular physiology. 2016;310(2):L103-13.

55. Kluge MA, Fetterman JL, Vita JA. Mitochondria and endothelial function. Circulation research. 2013;112(8):1171-88.

56. Haran M, Gross A. Balancing glycolysis and mitochondrial OXPHOS: lessons from the hematopoietic system and exercising muscles. Mitochondrion. 2014;19 Pt A:3-7.

57. Papa S, Martino PL, Capitanio G, Gaballo A, De Rasmo D, Signorile A, et al. The Oxidative Phosphorylation System in Mammalian Mitochondria. In: Scatena R, Bottoni P, Giardina B, editors. Advances in Mitochondrial Medicine. Dordrecht: Springer Netherlands; 2012. p. 3-37.

58. MacDonald PE, Joseph JW, Rorsman P. Glucose-sensing mechanisms in pancreatic beta-cells. Philosophical transactions of the Royal Society of London Series B, Biological sciences. 2005;360(1464):2211-25.

59. Sekine N, Cirulli V, Regazzi R, Brown LJ, Gine E, Tamarit-Rodriguez J, et al. Low lactate dehydrogenase and high mitochondrial glycerol phosphate dehydrogenase in pancreatic beta-cells. Potential role in nutrient sensing. The Journal of biological chemistry. 1994;269(7):4895-902.

60. Zhao C, Wilson MC, Schuit F, Halestrap AP, Rutter GA. Expression and distribution of lactate/monocarboxylate transporter isoforms in pancreatic islets and the exocrine pancreas. Diabetes. 2001;50(2):361-6.

61. Ainscow EK, Zhao C, Rutter GA. Acute overexpression of lactate dehydrogenase-A perturbs beta-cell mitochondrial metabolism and insulin secretion. Diabetes. 2000;49(7):1149-55.

62. Chen WW, Freinkman E, Wang T, Birsoy K, Sabatini DM. Absolute Quantification of Matrix Metabolites Reveals the Dynamics of Mitochondrial Metabolism. Cell. 2016;166(5):1324-37 e11.

63. Droge W. Free radicals in the physiological control of cell function. Physiological reviews. 2002;82(1):47-95.

64. Zorov DB, Juhaszova M, Sollott SJ. Mitochondrial reactive oxygen species (ROS) and ROS-induced ROS release. Physiological reviews. 2014;94(3):909-50.

65. Leloup C, Tourrel-Cuzin C, Magnan C, Karaca M, Castel J, Carneiro L, et al. Mitochondrial reactive oxygen species are obligatory signals for glucose-induced insulin secretion. Diabetes. 2009;58(3):673-81.

66. Pi J, Bai Y, Zhang Q, Wong V, Floering LM, Daniel K, et al. Reactive oxygen species as a signal in glucose-stimulated insulin secretion. Diabetes. 2007;56(7):1783-91.

67. Pizzo P, Drago I, Filadi R, Pozzan T. Mitochondrial Ca(2)(+) homeostasis: mechanism, role, and tissue specificities. Pflugers Archiv : European journal of physiology. 2012;464(1):3-17.

68. Rutter GA, Hodson DJ, Chabosseau P, Haythorne E, Pullen TJ, Leclerc I. Local and regional control of calcium dynamics in the pancreatic islet. Diabetes, obesity & metabolism. 2017;19 Suppl 1:30-41.

69. Giorgi C, Agnoletto C, Bononi A, Bonora M, De Marchi E, Marchi S, et al. Mitochondrial calcium homeostasis as potential target for mitochondrial medicine. Mitochondrion. 2012;12(1):77-85.

70. Dorn GW, 2nd, Kitsis RN. The mitochondrial dynamism-mitophagy-cell death interactome: multiple roles performed by members of a mitochondrial molecular ensemble. Circulation research. 2015;116(1):167-82.

71. Tait SW, Green DR. Mitochondria and cell death: outer membrane permeabilization and beyond. Nature reviews Molecular cell biology. 2010;11(9):621-32.

72. Boldogh IR, Pon LA. Mitochondria on the move. Trends in cell biology. 2007;17(10):502-10.

73. Hollenbeck PJ, Saxton WM. The axonal transport of mitochondria. Journal of cell science. 2005;118(Pt 23):5411-9.

74. Mishra P, Chan DC. Mitochondrial dynamics and inheritance during cell division, development and disease. Nature reviews Molecular cell biology. 2014;15(10):634-46.

75. Dorn GW, 2nd. Mitochondrial dynamism and heart disease: changing shape and shaping change. EMBO molecular medicine. 2015;7(7):865-77.

76. Mishra P, Chan DC. Metabolic regulation of mitochondrial dynamics. The Journal of cell biology. 2016;212(4):379-87.

77. Youle RJ, van der Bliek AM. Mitochondrial fission, fusion, and stress. Science. 2012;337(6098):1062-5.

78. Mishra P, Carelli V, Manfredi G, Chan DC. Proteolytic cleavage of Opa1 stimulates mitochondrial inner membrane fusion and couples fusion to oxidative phosphorylation. Cell metabolism. 2014;19(4):630-41.

79. Shutt T, Geoffrion M, Milne R, McBride HM. The intracellular redox state is a core determinant of mitochondrial fusion. EMBO reports. 2012;13(10):909-15.

80. Schon EA, Gilkerson RW. Functional complementation of mitochondrial DNAs: mobilizing mitochondrial genetics against dysfunction. Biochimica et biophysica acta. 2010;1800(3):245-9.

81. Molina AJ, Wikstrom JD, Stiles L, Las G, Mohamed H, Elorza A, et al. Mitochondrial networking protects beta-cells from nutrient-induced apoptosis. Diabetes. 2009;58(10):2303-15.

82. Rambold AS, Kostelecky B, Elia N, Lippincott-Schwartz J. Tubular network formation protects mitochondria from autophagosomal degradation during nutrient starvation. Proceedings of the National Academy of Sciences of the United States of America. 2011;108(25):10190-5.

83. Lee JE, Westrate LM, Wu H, Page C, Voeltz GK. Multiple dynamin family members collaborate to drive mitochondrial division. Nature. 2016;540(7631):139-43.

84. Parone PA, Da Cruz S, Tondera D, Mattenberger Y, James DI, Maechler P, et al. Preventing mitochondrial fission impairs mitochondrial function and leads to loss of mitochondrial DNA. PloS one. 2008;3(9):e3257.

85. Shen Q, Yamano K, Head BP, Kawajiri S, Cheung JT, Wang C, et al. Mutations in Fis1 disrupt orderly disposal of defective mitochondria. Molecular biology of the cell. 2014;25(1):145-59.

86. Uo T, Dworzak J, Kinoshita C, Inman DM, Kinoshita Y, Horner PJ, et al. Drp1 levels constitutively regulate mitochondrial dynamics and cell survival in cortical neurons. Experimental neurology. 2009;218(2):274-85.

87. Wikstrom JD, Mahdaviani K, Liesa M, Sereda SB, Si Y, Las G, et al. Hormone-induced mitochondrial fission is utilized by brown adipocytes as an amplification pathway for energy expenditure. The EMBO journal. 2014;33(5):418-36.

88. Toyama EQ, Herzig S, Courchet J, Lewis TL, Jr., Loson OC, Hellberg K, et al. Metabolism. AMP-activated protein kinase mediates mitochondrial fission in response to energy stress. Science. 2016;351(6270):275-81.

89. Bindokas VP, Kuznetsov A, Sreenan S, Polonsky KS, Roe MW, Philipson LH. Visualizing superoxide production in normal and diabetic rat islets of Langerhans. The Journal of biological chemistry. 2003;278(11):9796-801.

90. Anello M, Lupi R, Spampinato D, Piro S, Masini M, Boggi U, et al. Functional and morphological alterations of mitochondria in pancreatic beta cells from type 2 diabetic patients. Diabetologia. 2005;48(2):282-9.

91. Jhun BS, Lee H, Jin ZG, Yoon Y. Glucose stimulation induces dynamic change of mitochondrial morphology to promote insulin secretion in the insulinoma cell line INS-1E. PloS one. 2013;8(4):e60810.

92. Kabra UD, Pfuhlmann K, Migliorini A, Keipert S, Lamp D, Korsgren O, et al. Direct Substrate Delivery Into Mitochondrial Fission-Deficient Pancreatic Islets Rescues Insulin Secretion. Diabetes. 2017;66(5):1247-57.

93. Twig G, Elorza A, Molina AJ, Mohamed H, Wikstrom JD, Walzer G, et al. Fission and selective fusion govern mitochondrial segregation and elimination by autophagy. The EMBO journal. 2008;27(2):433-46.

94. Park KS, Wiederkehr A, Kirkpatrick C, Mattenberger Y, Martinou JC, Marchetti P, et al. Selective actions of mitochondrial fission/fusion genes on metabolism-secretion coupling in insulin-releasing cells. The Journal of biological chemistry. 2008;283(48):33347-56.

95. Diaz F, Moraes CT. Mitochondrial biogenesis and turnover. Cell calcium. 2008;44(1):24-35.

96. Dorn GW, 2nd, Vega RB, Kelly DP. Mitochondrial biogenesis and dynamics in the developing and diseased heart. Genes & development. 2015;29(19):1981-91.

97. Zhu J, Wang KZ, Chu CT. After the banquet: mitochondrial biogenesis, mitophagy, and cell survival. Autophagy. 2013;9(11):1663-76.

98. Picca A, Lezza AM. Regulation of mitochondrial biogenesis through TFAM-mitochondrial DNA interactions: Useful insights from aging and calorie restriction studies. Mitochondrion. 2015;25:67-75.

99. Whitaker RM, Corum D, Beeson CC, Schnellmann RG. Mitochondrial Biogenesis as a Pharmacological Target: A New Approach to Acute and Chronic Diseases. Annual review of pharmacology and toxicology. 2016;56:229-49.

100. Hamacher-Brady A, Brady NR. Mitophagy programs: mechanisms and physiological implications of mitochondrial targeting by autophagy. Cellular and molecular life sciences : CMLS. 2016;73(4):775-95.

101. Melser S, Lavie J, Benard G. Mitochondrial degradation and energy metabolism. Biochimica et biophysica acta. 2015;1853(10 Pt B):2812-21.

102. Wei H, Liu L, Chen Q. Selective removal of mitochondria via mitophagy: distinct pathways for different mitochondrial stresses. Biochimica et biophysica acta. 2015;1853(10 Pt B):2784-90.

103. Liu L, Feng D, Chen G, Chen M, Zheng Q, Song P, et al. Mitochondrial outer-membrane protein FUNDC1 mediates hypoxia-induced mitophagy in mammalian cells. Nature cell biology. 2012;14(2):177-85.

104. Oropeza D, Jouvet N, Bouyakdan K, Perron G, Ringuette LJ, Philipson LH, et al. PGC-1 coactivators in beta-cells regulate lipid metabolism and are essential for insulin secretion coupled to fatty acids. Molecular metabolism. 2015;4(11):811-22.

105. De Souza CT, Gasparetti AL, Pereira-da-Silva M, Araujo EP, Carvalheira JB, Saad MJ, et al. Peroxisome proliferator-activated receptor gamma coactivator-1-dependent uncoupling protein-2 expression in pancreatic islets of rats: a novel pathway for neural control of insulin secretion. Diabetologia. 2003;46(11):1522-31.

106. Gauthier BR, Wiederkehr A, Baquie M, Dai C, Powers AC, Kerr-Conte J, et al. PDX1 deficiency causes mitochondrial dysfunction and defective insulin secretion through TFAM suppression. Cell metabolism. 2009;10(2):110-8.

107. Nile DL, Brown AE, Kumaheri MA, Blair HR, Heggie A, Miwa S, et al. Age-related mitochondrial DNA depletion and the impact on pancreatic Beta cell function. PloS one. 2014;9(12):e115433.

108. Silva JP, Kohler M, Graff C, Oldfors A, Magnuson MA, Berggren PO, et al. Impaired insulin secretion and beta-cell loss in tissue-specific knockout mice with mitochondrial diabetes. Nature genetics. 2000;26(3):336-40.

109. Spacek T, Pavluch V, Alan L, Capkova N, Engstova H, Dlaskova A, et al. Nkx6.1 decline accompanies mitochondrial DNA reduction but subtle nucleoid size decrease in pancreatic islet beta-cells of diabetic Goto Kakizaki rats. Scientific reports. 2017;7(1):15674.

110. Hoshino A, Ariyoshi M, Okawa Y, Kaimoto S, Uchihashi M, Fukai K, et al. Inhibition of p53 preserves Parkin-mediated mitophagy and pancreatic beta-cell function in diabetes. Proceedings of the National Academy of Sciences of the United States of America. 2014;111(8):3116-21.

111. Maassen JA, LM TH, Van Essen E, Heine RJ, Nijpels G, Jahangir Tafrechi RS, et al. Mitochondrial diabetes: molecular mechanisms and clinical presentation. Diabetes. 2004;53 Suppl 1:S103-9.

112. Velho G, Byrne MM, Clement K, Sturis J, Pueyo ME, Blanche H, et al. Clinical phenotypes, insulin secretion, and insulin sensitivity in kindreds with maternally inherited diabetes and deafness due to mitochondrial tRNALeu(UUR) gene mutation. Diabetes. 1996;45(4):478-87.

113. Brandle M, Lehmann R, Maly FE, Schmid C, Spinas GA. Diminished insulin secretory response to glucose but normal insulin and glucagon secretory responses to arginine in a family with maternally inherited diabetes and deafness caused by mitochondrial tRNA(LEU(UUR)) gene mutation. Diabetes care. 2001;24(7):1253-8.

114. Czabotar PE, Lessene G, Strasser A, Adams JM. Control of apoptosis by the BCL-2 protein family: implications for physiology and therapy. Nature reviews Molecular cell biology. 2014;15(1):49-63.

115. Petros AM, Olejniczak ET, Fesik SW. Structural biology of the Bcl-2 family of proteins. Biochimica et biophysica acta. 2004;1644(2-3):83-94.

116. Opferman JT. Attacking cancer's Achilles heel: antagonism of anti-apoptotic BCL-2 family members. The FEBS journal. 2016;283(14):2661-75.

117. McKenzie MD, Carrington EM, Kaufmann T, Strasser A, Huang DC, Kay TW, et al. Proapoptotic BH3-only protein Bid is essential for death receptor-induced apoptosis of pancreatic beta-cells. Diabetes. 2008;57(5):1284-92.

118. Ospina A, Lagunas-Martinez A, Pardo J, Carrodeguas JA. Protein oligomerization mediated by the transmembrane carboxyl terminal domain of Bcl-XL. FEBS letters. 2011;585(19):2935-42.

119. Carrington EM, McKenzie MD, Jansen E, Myers M, Fynch S, Kos C, et al. Islet beta-cells deficient in Bcl-xL develop but are abnormally sensitive to apoptotic stimuli. Diabetes. 2009;58(10):2316-23.

120. Zhou YP, Pena JC, Roe MW, Mittal A, Levisetti M, Baldwin AC, et al. Overexpression of Bcl-x(L) in beta-cells prevents cell death but impairs mitochondrial signal for insulin secretion. American journal of physiology Endocrinology and metabolism. 2000;278(2):E340-51.

121. Luciani DS, White SA, Widenmaier SB, Saran VV, Taghizadeh F, Hu X, et al. Bcl-2 and Bcl-xL suppress glucose signaling in pancreatic beta-cells. Diabetes. 2013;62(1):170-82.

122. Li H, Chen Y, Jones AF, Sanger RH, Collis LP, Flannery R, et al. Bcl-xL induces Drp1-dependent synapse formation in cultured hippocampal neurons. Proceedings of the National Academy of Sciences of the United States of America. 2008;105(6):2169-74.

123. Cleland MM, Norris KL, Karbowski M, Wang C, Suen DF, Jiao S, et al. Bcl-2 family interaction with the mitochondrial morphogenesis machinery. Cell death and differentiation. 2011;18(2):235-47.

124. Rolland SG, Lu Y, David CN, Conradt B. The BCL-2-like protein CED-9 of C. elegans promotes FZO-1/Mfn1,2- and EAT-3/Opa1-dependent mitochondrial fusion. The Journal of cell biology. 2009;186(4):525-40.

125. Levine B, Sinha SC, Kroemer G. Bcl-2 family members: Dual regulators of apoptosis and autophagy. Autophagy. 2008;4(5):600-6.

126. Wu H, Xue D, Chen G, Han Z, Huang L, Zhu C, et al. The BCL2L1 and PGAM5 axis defines hypoxia-induced receptor-mediated mitophagy. Autophagy. 2014;10(10):1712-25.

127. Sandebring A, Thomas KJ, Beilina A, van der Brug M, Cleland MM, Ahmad R, et al. Mitochondrial alterations in PINK1 deficient cells are influenced by calcineurin-dependent dephosphorylation of dynamin-related protein 1. PloS one. 2009;4(5):e5701.

128. Karbowski M, Arnoult D, Chen H, Chan DC, Smith CL, Youle RJ. Quantitation of mitochondrial dynamics by photolabeling of individual organelles shows that mitochondrial fusion is blocked during the Bax activation phase of apoptosis. The Journal of cell biology. 2004;164(4):493-9.

129. Schindelin J, Arganda-Carreras I, Frise E, Kaynig V, Longair M, Pietzsch T, et al. Fiji: an open-source platform for biological-image analysis. Nature methods. 2012;9(7):676-82.

130. Schmid MC, T. Sigma Filter internet: National Institute of Health; 2007 [cited 2018 February 28]. Available from: https://imagej.nih.gov/ij/plugins/sigma-filter.html.

131. Imaging SV. Microscopy Nyquist rate and PSF calculator Internet2018 [cited 2018 February 18]. Available from: https://svi.nl/NyquistCalculator.

132. Tseng Q. AdaptiveThreshold --- ImageJ plugin Internet2015 [cited 2018 February 28]. Available from: https://sites.google.com/site/qingzongtseng/adaptivethreshold.

133. Ollion J, Cochennec J, Loll F, Escude C, Boudier T. TANGO: a generic tool for high-throughput 3D image analysis for studying nuclear organization. Bioinformatics. 2013;29(14):1840-1.

134. Qiu P, Simonds EF, Bendall SC, Gibbs KD, Jr., Bruggner RV, Linderman MD, et al. Extracting a cellular hierarchy from high-dimensional cytometry data with SPADE. Nature biotechnology. 2011;29(10):886-91.

135. Qiu P. SPADE V3.0 - Spanning-tree Progression Analysis of Density-normalized Events [Internet]2017 [cited 2018 January 2]. Available from: http://pengqiu.gatech.edu/software/SPADE/.

136. Aharoni-Simon M, Shumiatcher R, Yeung A, Shih AZ, Dolinsky VW, Doucette CA, et al. Bcl-2 Regulates Reactive Oxygen Species Signaling and a Redox-Sensitive Mitochondrial Proton Leak in Mouse Pancreatic beta-Cells. Endocrinology. 2016;157(6):2270-81.

137. Brand MD, Nicholls DG. Assessing mitochondrial dysfunction in cells. The Biochemical journal. 2011;435(2):297-312.

138. Shirendeb UP, Calkins MJ, Manczak M, Anekonda V, Dufour B, McBride JL, et al. Mutant huntingtin's interaction with mitochondrial protein Drp1 impairs mitochondrial biogenesis and causes defective axonal transport and synaptic degeneration in Huntington's disease. Human molecular genetics. 2012;21(2):406-20.

139. Martorell-Riera A, Segarra-Mondejar M, Munoz JP, Ginet V, Olloquequi J, Perez-Clausell J, et al. Mfn2 downregulation in excitotoxicity causes mitochondrial dysfunction and delayed neuronal death. The EMBO journal. 2014;33(20):2388-407.

140. Davies VJ, Hollins AJ, Piechota MJ, Yip W, Davies JR, White KE, et al. Opa1 deficiency in a mouse model of autosomal dominant optic atrophy impairs mitochondrial morphology, optic nerve structure and visual function. Human molecular genetics. 2007;16(11):1307-18.

141. Li F, Wang Y, Zeller KI, Potter JJ, Wonsey DR, O'Donnell KA, et al. Myc stimulates nuclearly encoded mitochondrial genes and mitochondrial biogenesis. Molecular and cellular biology. 2005;25(14):6225-34.

142. Robson-Doucette CA, Sultan S, Allister EM, Wikstrom JD, Koshkin V, Bhattacharjee A, et al. Beta-cell uncoupling protein 2 regulates reactive oxygen species production, which influences both insulin and glucagon secretion. Diabetes. 2011;60(11):2710-9.

143. Karbowski M, Cleland MM, Roelofs BA. Photoactivatable green fluorescent protein-based visualization and quantification of mitochondrial fusion and mitochondrial network complexity in living cells. Methods in enzymology. 2014;547:57-73.

144. Koopman WJ, Visch HJ, Smeitink JA, Willems PH. Simultaneous quantitative measurement and automated analysis of mitochondrial morphology, mass, potential, and motility in living human skin fibroblasts. Cytometry Part A : the journal of the International Society for Analytical Cytology. 2006;69(1):1-12.

145. Nikolaisen J, Nilsson LI, Pettersen IK, Willems PH, Lorens JB, Koopman WJ, et al. Automated quantification and integrative analysis of 2D and 3D mitochondrial shape and network properties. PloS one. 2014;9(7):e101365.

146. Berman SB, Chen YB, Qi B, McCaffery JM, Rucker EB, 3rd, Goebbels S, et al. Bcl-x L increases mitochondrial fission, fusion, and biomass in neurons. The Journal of cell biology. 2009;184(5):707-19.

147. Enyedy IJ, Ling Y, Nacro K, Tomita Y, Wu X, Cao Y, et al. Discovery of small-molecule inhibitors of Bcl-2 through structure-based computer screening. Journal of medicinal chemistry. 2001;44(25):4313-24.

148. Shih AZ. Bcl-x_L protects pancreatic beta-cells from high glucose-induced failure by dampening mitochondrial metabolism [master's thesis]. Vancouver: University of British Columbia; 2015.

149. Svensson C, Hellerstrom C. Long-term effects of a high glucose concentration in vitro on the oxidative metabolism and insulin production of isolated rat pancreatic islets. Metabolism: clinical and experimental. 1991;40(5):513-8.

150. Irles E, Neco P, Lluesma M, Villar-Pazos S, Santos-Silva JC, Vettorazzi JF, et al. Enhanced glucose-induced intracellular signaling promotes insulin hypersecretion: pancreatic beta-cell functional adaptations in a model of genetic obesity and prediabetes. Molecular and cellular endocrinology. 2015;404:46-55.

151. Robertson RP, Harmon J, Tran PO, Tanaka Y, Takahashi H. Glucose toxicity in beta-cells: type 2 diabetes, good radicals gone bad, and the glutathione connection. Diabetes. 2003;52(3):581-7.

152. Ding WX, Li M, Biazik JM, Morgan DG, Guo F, Ni HM, et al. Electron microscopic analysis of a spherical mitochondrial structure. The Journal of biological chemistry. 2012;287(50):42373-8.

153. Dlaskova A, Spacek T, Santorova J, Plecita-Hlavata L, Berkova Z, Saudek F, et al. 4Pi microscopy reveals an impaired three-dimensional mitochondrial network of pancreatic islet beta-cells, an experimental model of type-2 diabetes. Biochimica et biophysica acta. 2010;1797(6-7):1327-41.

154. Mitra K, Lippincott-Schwartz J. Analysis of mitochondrial dynamics and functions using imaging approaches. Current protocols in cell biology. 2010;Chapter 4:Unit 4 25 1-1.

155. Biggs DS. 3D deconvolution microscopy. Current protocols in cytometry. 2010;Chapter 12:Unit 12 9 1-20.

156. North AJ. Seeing is believing? A beginners' guide to practical pitfalls in image acquisition. The Journal of cell biology. 2006;172(1):9-18.

157. Anchang B, Hart TD, Bendall SC, Qiu P, Bjornson Z, Linderman M, et al. Visualization and cellular hierarchy inference of single-cell data using SPADE. Nature protocols. 2016;11(7):1264-79.

158. Chester C, Maecker HT. Algorithmic Tools for Mining High-Dimensional Cytometry Data. Journal of immunology. 2015;195(3):773-9.

159. Caicedo JC, Cooper S, Heigwer F, Warchal S, Qiu P, Molnar C, et al. Data-analysis strategies for image-based cell profiling. Nature methods. 2017;14(9):849-63.

160. Gomes LC, Di Benedetto G, Scorrano L. During autophagy mitochondria elongate, are spared from degradation and sustain cell viability. Nature cell biology. 2011;13(5):589-98.

161. Mitra K, Wunder C, Roysam B, Lin G, Lippincott-Schwartz J. A hyperfused mitochondrial state achieved at G1-S regulates cyclin E buildup and entry into S phase. Proceedings of the National Academy of Sciences of the United States of America. 2009;106(29):11960-5.

162. Yu T, Robotham JL, Yoon Y. Increased production of reactive oxygen species in hyperglycemic conditions requires dynamic change of mitochondrial morphology. Proceedings of the National Academy of Sciences of the United States of America. 2006;103(8):2653-8.

163. Fan X, Hussien R, Brooks GA. H2O2-induced mitochondrial fragmentation in C2C12 myocytes. Free radical biology & medicine. 2010;49(11):1646-54.

164. Iqbal S, Hood DA. Oxidative stress-induced mitochondrial fragmentation and movement in skeletal muscle myoblasts. American journal of physiology Cell physiology. 2014;306(12):C1176-83.

165. Gurzov EN, Germano CM, Cunha DA, Ortis F, Vanderwinden JM, Marchetti P, et al. p53 up-regulated modulator of apoptosis (PUMA) activation contributes to pancreatic beta-cell apoptosis induced by proinflammatory cytokines and endoplasmic reticulum stress. The Journal of biological chemistry. 2010;285(26):19910-20.

166. Kaufmann T, Schlipf S, Sanz J, Neubert K, Stein R, Borner C. Characterization of the signal that directs Bcl-x(L), but not Bcl-2, to the mitochondrial outer membrane. The Journal of cell biology. 2003;160(1):53-64.

167. Kusminski CM, Chen S, Ye R, Sun K, Wang QA, Spurgin SB, et al. MitoNEET-Parkin Effects in Pancreatic alpha- and beta-Cells, Cellular Survival, and Intrainsular Cross Talk. Diabetes. 2016;65(6):1534-55.

168. Park KS, Wiederkehr A, Wollheim CB. Defective mitochondrial function and motility due to mitofusin 1 overexpression in insulin secreting cells. The Korean journal of physiology & pharmacology : official journal of the Korean Physiological Society and the Korean Society of Pharmacology. 2012;16(1):71-7.

169. Loboda A, Damulewicz M, Pyza E, Jozkowicz A, Dulak J. Role of Nrf2/HO-1 system in development, oxidative stress response and diseases: an evolutionarily conserved mechanism. Cellular and molecular life sciences : CMLS. 2016;73(17):3221-47.

170. Guo C, Wilkinson KA, Evans AJ, Rubin PP, Henley JM. SENP3-mediated deSUMOylation of Drp1 facilitates interaction with Mff to promote cell death. Scientific reports. 2017;7:43811.

171. Brooks C, Wei Q, Feng L, Dong G, Tao Y, Mei L, et al. Bak regulates mitochondrial morphology and pathology during apoptosis by interacting with mitofusins. Proceedings of the National Academy of Sciences of the United States of America. 2007;104(28):11649-54.

172. Karbowski M, Lee YJ, Gaume B, Jeong SY, Frank S, Nechushtan A, et al. Spatial and temporal association of Bax with mitochondrial fission sites, Drp1, and Mfn2 during apoptosis. The Journal of cell biology. 2002;159(6):931-8.

173. Wasiak S, Zunino R, McBride HM. Bax/Bak promote sumoylation of DRP1 and its stable association with mitochondria during apoptotic cell death. The Journal of cell biology. 2007;177(3):439-50.

174. Sheridan C, Delivani P, Cullen SP, Martin SJ. Bax- or Bak-induced mitochondrial fission can be uncoupled from cytochrome C release. Molecular cell. 2008;31(4):570-85.

175. Danial NN, Gramm CF, Scorrano L, Zhang CY, Krauss S, Ranger AM, et al. BAD and glucokinase reside in a mitochondrial complex that integrates glycolysis and apoptosis. Nature. 2003;424(6951):952-6.

176. Danial NN, Walensky LD, Zhang CY, Choi CS, Fisher JK, Molina AJ, et al. Dual role of proapoptotic BAD in insulin secretion and beta cell survival. Nature medicine. 2008;14(2):144-53.

177. Schmitt H, Lenzen S, Baltrusch S. Glucokinase mediates coupling of glycolysis to mitochondrial metabolism but not to beta cell damage at high glucose exposure levels. Diabetologia. 2011;54(7):1744-55.

178. Skelin M, Rupnik M, Cencic A. Pancreatic beta cell lines and their applications in diabetes mellitus research. Altex. 2010;27(2):105-13.

179. Bharatham N, Chi SW, Yoon HS. Molecular basis of Bcl-X(L)-p53 interaction: insights from molecular dynamics simulations. PloS one. 2011;6(10):e26014.

180. Hollville E, Carroll RG, Cullen SP, Martin SJ. Bcl-2 family proteins participate in mitochondrial quality control by regulating Parkin/PINK1-dependent mitophagy. Molecular cell. 2014;55(3):451-66.

181. Tabak AG, Herder C, Rathmann W, Brunner EJ, Kivimaki M. Prediabetes: a high-risk state for diabetes development. Lancet. 2012;379(9833):2279-90.

182. Yun J, Finkel T. Mitohormesis. Cell metabolism. 2014;19(5):757-66.